INTEGRATED GEOPHYSICAL INVESTIGATION OF THE OCCURRENCE AND STRUCTURAL EFFECTS OF BITUMEN IN AGBABU, SOUTH-WEST, NIGERIA

BY

OGUNLANA, FUNMILOLA OLUSOLA
PG/PSC1514388

UNIVERSITY OF BENIN
BENIN CITY

FEBRUARY, 2020

INTEGRATED GEOPHYSICAL INVESTIGATION OF THE OCCURRENCE AND STRUCTURAL EFFECTS OF BITUMEN IN AGBABU, SOUTH-WEST, NIGERIA

BY

OGUNLANA, FUNMILOLA OLUSOLA
B.Sc PHYSICS (UNAD)
M.Sc GEOPHYSICS (BENIN)

(MATRIC NO: PG/PSC1514388)

A THESIS SUBMITTED IN THE DEPARTMENT OF PHYSICS TO THE SCHOOL OF POSTGRADUATE STUDIES AS A PART OF THE REQUIREMENT FOR THE AWARD OF DEGREE OF DOCTOR OF PHILOSOPHY (PhD) IN GEOPHYSICS/EXPLORATION GEOPHYSICS FROM DEPARTMENT OF PHYSICS, FACULTY OF PHYSICAL SCIENCE, UNIVERSITY OF BENIN, BENIN CITY, NIGERIA

FEBRUARY, 2020

CERTIFICATION

This is to certify that this Doctorate degree (PhD) thesis was written by Ogunlana Funmilola Olusola in the Department of Physics, Faculty of Physical Sciences, University of Benin, Benin City, Nigeria, under the supervision of Prof. O. M. Alile.

…….. ……

SUPERVISOR **DATE**

PROF. O. M. ALILE

DECLARATION

UNIVERSITY OF BENIN
SCHOOL OF POSTGRADUATE STUDIES

INTEGRATED GEOPHYSICAL INVESTIGATION OF THE OCCURRENCE AND STRUCTURAL EFFECTS OF BITUMEN IN AGBABU, SOUTH-WEST, NIGERIA

BY

OGUNLANA, FUNMILOLA OLUSOLA
B.Sc PHYSICS (UNAD)
M.Sc GEOPHYSICS (BENIN)

THE BOARD OF EXAMINERS DECLARES AS FOLLOWS THAT THIS IS THE ORIGINAL WORK OF THE CANDIDATE THAT THE THESIS IS ACCEPTED IN PARTIAL FULFILMENT OF THE REQUIREMENT FOR THE AWARD OF THE DEGREE OF DOCTOR OF PHILOSOPHY (PhD) IN GEOPHYSICS/EXPLORATION GEOPHYSICS

NAME	**SIGNATURE**	**DATE**
SUPERVISOR: PROF. O. M. ALILE	_____	_____
HEAD OF DEPT: PROF. O. M. ALILE	_____	_____
EXTERNAL EXAMINER	_____	_____

DEDICATION

This thesis is dedicated to my parent, Evang. Nathaniel Olusanya Ola and Mrs. Florence Sijuola Ola; for their love and trust in me, for the foundation, for the several self denials and sacrifices they made for my sake and for going the extra mile, against all odds, in ensuring that I am schooled to their satisfactions.

To my darling husband, Engr. Ogunlana Olawole and my wonderful children (Lauretta, Benita, Festus and Stella); who had made the writing of the thesis so much easier.

To God Almighty, the owner of my life, for His grace that was always sufficient, for His strength that never failed wisdom and understanding that was unparallel. To Him alone be all the Glory and Honour.

CERTIFICATION OF THESIS/DISSERTATION ON PLAGIARISM

We the undersigned attest and declare that the thesis of Mrs. OGUNLANA FUNMILOLA OLUSOLA titled: **INTEGRATED GEOPHYSICAL INVESTIGATION**

OF THE OCCURRENCE AND STRUCTURAL EFFECTS OF BITUMEN IN AGBABU, SOUTH-WEST, NIGERIA has successfully passed the antiplagiarism test and does not violate any copyright regulations.

_____ _____

Name of Chief Supervisor/Sign & Date **Name of HOD/Sign & Date**

ACKNOWLEDGEMENT

My sincere thanks and praises are highly rendered to Almighty God (the author and the finisher of my faith) for saving my life till this present time. I am also deeply indebted and eternally grateful to my supervisor and Head of Department of Physics, University of Benin Prof. O.M. Alile, for accepting to supervise this research work despite his very busy schedule. He did not only thoroughly and

painstakingly supervise the research work but also helped in getting the resistivity meter (PASI 16GL-N Earth resistivity meter) which was used in collecting the field data in Agbabu, Ondo-State, southwest Nigeria.

To him, I say “thanks so much and may the Lord bless and reward you abundantly, Amen.

My profound gratitude goes to Dr. Chris Aigbogun also of Department of Physics for his interest in this research work and for his thorough assistance during the proposal and preliminary stage of the research, and his encouragement. Some of his comments on the research during my frequent consultations with him are quite humbling, and they are all appreciated. Special thanks go to Prof. S.O. Azi, and other staff of the Department, Prof. F.O. Ezomo Prof. J.O.A Idiodi, Dr. John Airen, Dr. Babalola, Mr J.E Ighodalo etc for their love and encouragement all through the course of this research.

My sincere thanks and appreciation also go to my parents and siblings, I say thank you all for your love, support and prayers. My husband and my children’s commitment to my success for bringing you on board at the right time, I love you all, and I will always do.

I wish to acknowledge and appreciate the assistance of Dr. S.O Ogungbemi, Dr. G.O Badmus, Mrs R. A Adeleye, Dr. (Mrs) O.O Abiola and Dr. Mrs Awodosu (ABUAD), for their relentless effort and useful suggestions towards the completion of this work.

I must not forget my people at EKSU both academic and non-academic staff of Department of Physics, Ekiti State University, Ado-Ekiti, most especially Prof. A.I Mukolu, Prof. (Mrs) F.M Ojelabi, Ass Prof. E.B. Faweya, Dr. M.O Isinkaye, Dr. A.A. Oyedele, Dr. K.A Aduloju, Mr T.H Akande, Mr G.S Agunbiade, Mr G.O. Olowomofe, Mr F.A. Adeleye, Mrs Aladesuyi, Dr. O.F Ojo (Geology) and Dr.(Mrs) K. A Adigun (Statistics). Thanks and God bless you all.

TABLE OF CONTENT

LISTS OF FIGURES

LISTS OF TABLES

LISTS OF PLATES

ABSTRACT

This study was carried out to investigate the occurrence and structural effects of bitumen in Agbabu community using integrated geophysical methods (aeromagnetic, aero-radiometric and electrical resistivity tomography (ERT). Two forms of datasets (Secondary and Primary) were used. These datasets provided useful information on the lithology and geological structures within the area. The geophysics data processing approach employed concentrated on enhancing the geophysical data quality and this aided in tracing accurate positioning of geological boundaries, the responses related to bituminous zone and geological structures that may be of vital economic importance

The digitized geological map covering the study area was obtained for lithological information. The secondary datasets consist of an aeromagnetic and aero-radiometric basically for the reconnaissance study. Aeromagnetic and aero-radiometric map was obtained from the Nigerian Geological Survey Agency (NGSA) and processed using Oasis Montaj software to depict main lithology and structural features present in the Agbabu area. The primary data was acquired within the area suspected to have high potential for bitumen deposit using the wenner-schlumberger configuration. The potential difference produced was measured with the aid of PASI 16 GL-N Earth resistivity meter. The apparent resistivity values obtained was processed using RES2DINV software which helped to automatically obtain the 2D inversion model of the subsurface.

The results of aeromagnetic study show low TMI amplitude (-201.5 – 16.8nT) and high AS amplitude (0.053 – 0.172nT) at suspected bitumen deposit regions. The low TDR amplitude (- 1.4 to - 0.4nT) confirms a concealed basement depression hosting bitumen deposit. The 3D-Euler deconvolution helps to locate the sources of magnetic anomalies, it is deeper within the sedimentary terrain (841 – 1703m) and shallower (185 – 841m) within the basement. The interpretations of radiometric datasets revealed the spatial variation of potassium (K), thorium (Th) and uranium (U) radioelement concentrations as high as (0.6 – 2.5%), (7.9 – 28.0 ppm) and (1.9 – 5.1 ppm) respectively within the basement complex, but also low as (0.0 – 0.6%), (1.8 – 9.2ppm) and (0.3 – 1.9ppm) respectively within the sedimentary terrain. The ternary image shows very

low radiometric intensity that contained the bitumen structures, moderately high around lithological boundaries and concealed linear features reveal. This research has shown that the occurrence of bitumen was found between the depth of 13.4m and 9.93m for Traverses 1,2,3 and Traverses 4,5 respectively in 2-Dimensional electrical resistivity images which corroborated by boreholes with a depth of about 18m. The results of this research indicated that bitumen has an average thickness of 11.67 m. The answers aid the exploitation of bitumen and made available for government and other relevant bodies in formulating policies for minerals development in the country. From the result of the coordinates of the airborne surveys, agreed perfectly with the values of Geophysical (ERT) traverses indicating the reliability of this type of joint geophysical investigation

CHAPTER ONE

INTRODUCTION

The bedrock of Nigeria's economy before the revealing of petroleum deposit had been the solid minerals and agricultural sectors, but currently, it is the oil and gas sector. Over 80% of the country's revenue comes from export and domestic sales of oil and gas. As the hydrocarbon potentials of the prolific Niger Delta go depleted or in the near future may be outworn due to unceasing exploitation, attention needs to be shifted to other area of revenue. The occurrence and textural settings of the Agbabu sea mangrit (bitumen) deposition have been researched due to the benefit of bitumen as a prepared alternative resource (Obiora et al., 2015).

Asphalt-impregnated sandstones otherwise referred to as smear pluck (sailor courage) and active smear-seeping appear in south-western Nigeria within the coastal pull-apart or margin-sag Dahomey (Benin) Basin. The smear pluck emerge in an E-W girth, approximately 140 km protracted and 4 – 6 km wide, expand from Edo, Ondo and Ogun State in southwest Nigeria (Adegoke *et al*., 1981). Bituminous pluck are calm of courage, heavy anoint and bole that are plentiful in minerals and aquatic. The strong oil in the bituminous grit is familiarly exhort bitumen, which is very dark in color (predicate), sticky and thick estate. Total reserve of the heavy oil is estimated to exceed 30 billion barrels (Adegoke *et al.,* 1980).

The oil is found in the coarse grained clastics within the formation in two discrete bands (the X and Y horizons), each has 30–40 m thick and separated by 6–15 m carbonaceous shale with a thin band of lignite (Ako *et al.,* 1983) and overburden thickness in excess of 50m thick at Agbabu, Ondo State, south western Nigeria (Enu, 1985).

1.1.1 Background of Study

Aeromagnetic and aero-radiometric datasets have been used to interpret the geological structural design, which attend as potential mineralization zones (Wemegah *et al*., 2015). Airborne magnetic and radiometric surveys have been used extensively in the mineral deposits around the world (Rajesh *et al.,* 2006). Magnetic properties of rocks and sediments are determined by the quantity of magnetic minerals (iron, nickel and cobalt bearing minerals), the manner and lifetime of the mature, and their thermal and geochemical historiology (Case and Sikora., 1984). Airborne magnetic and radiometric prospect have been applied widely in the ore prospect activity principally for the outline of mineralization circumference and metalliferous precipitate in most parts of the circle (Keating, 1995). In particular, the aeromagnetic order as the geophysical technique is extending for the other-deposit contains magnetite, which is a common accessory mine found in many other apatites.

Magnetic surveys can be performed on land, at sea and in air. The speed of operation and cost make airborne magnetic surveys very attractive, where the principal objective has been to assist in mineral and groundwater development through improved geologic mapping. In addition, aeromagnetic surveys have traditionally been applied at the early stage of petroleum exploration to determine depth and major structure of crystalline basement rocks underlying sedimentary basins (Paterson and Reeves, 1985). The methodology for acquiring and compiling data appears to be keeping pace with modern technology so that presently the magnetic method is by far the most widely used of all geophysical survey; both in terms of line-kilometers surveyed annually and in total line-kilometers. Thus, compared to other geophysical methods, the aeromagnetic data are always readily available and so it is important to exploit the potentialities of these data.

Similarly airborne radiometric survey is used to measure variations in the mineral composition, properties of soils and their parent geological material in order to map lateral lithological changes. This method involves the measurement of naturally occurring uranium (U), thorium (Th) and potassium (K), which could be found as trace elements that exist in rock forming minerals and soil

profiles. In the magnetic and radiometric survey, the quantity of magnetic minerals appears to be the primary variable determining magnetic-field variations (measured as magnetic susceptibility) whereas the gamma ray responds from the radioelement (K, U and Th) in the rocks can be related to the distribution of materials respectively (Wilford *et al.,* 1997).

Studies using geophysical method for sub-surface understanding of Nigeria tar sand deposit have been carried out in recent time (Odunaike *et al.,* 2010 and Akinmosin *et al.,* 2011). Other examples of the application of geophysical methods in tar sand exploration have also been reviewed in the works by Cristall *et al.,* 2004 and Bauman, 2005.

Electrical resistivity tomography (ERT) is one of the most popular methods for the shallow subsurface and is applied for hydrogeological, engineering, or agricultural questions. Applications cover a wide range of scales, from mm/cm scales at laboratory samples, decimeter to meter scale in soils, meter to decimeters for groundwater questions, but can reach several hundred meters or even kilometer for deep geological structures. Instruments have been rapidly developing in the past decades.

Variations in electrical resistivity (or conductivity) typically correlate with variations in lithology, water saturation, fluid conductivity, porosity and permeability, which may be used to map stratigraphic units, geological structure, sinkholes, fractures and groundwater. The acquisition of resistivity data involves the injection of current into the ground via a pair of electrodes and then the resulting potential field is measured by a corresponding pair of potential electrodes. The field set-up requires the deployment of an array (Wenner-Schlumberger) of regularly spaced electrodes, which are connected to a central control unit via multi-core cables. Resistivity data are then recorded via complex combinations of current and potential electrode pairs to build up a pseudo cross-section of apparent resistivity beneath the survey line. The depth of investigation depends on the electrode separation and geometry, with greater electrode separations yielding bulk resistivity measurements from greater depths.

The recorded data are transferred to a PC for processing. In order to derive a cross-sectional model of true ground resistivity, the measured data are subject to a finite-difference inversion process via RES2DINV software.

Data processing is based on an iterative routine involving determination of a two-dimensional (2D) simulated model of the subsurface. Convergence between theoretical and observed data is achieved by non-linear least squares optimization. The extent to which the observed and calculated theoretical models agree is an indication of the validity of the true resistivity model (indicated by the final root-mean-squared (RMS) error).

The true resistivity models are presented as colour contour sections revealing spatial variation in subsurface resistivity. The 2D method of presenting resistivity data is limited where highly irregular or complex geological features are present. Constraints: Readings can be affected by poor electrical contact at the surface. An increased electrode array length is required to locate increased depths of interest therefore the site layout must permit long arrays. Resolution of target features decreases with increased depth of burial.

1.1.2 Statement of Problem

The economy downturn has been fallen the prices of petroleum products in the international market made the country to experience hard economic situation leading to recession. This drastic fall has propelled the country to consider other ways of reducing the harsh economic realities by considering the exploration and exploitation of solid minerals. The need to locate, identify and classify economic mineral deposit (especially bitumen) into regions/blocks with the aim of encouraging investors to apply and develop them, inform the choice of this research. By extension, it is an effort to diversify the nation's economy and reduce over dependence on oil and gas to run the economy. Increase global awareness for bitumen in Ondo State is envisaged, through the result of this research.

1.1.3 Justification

The continued expansion in the demand for minerals of all kinds since the turn of the century have led to the development of many geophysical techniques of ever increasing sensitivity for the detection and mapping of the unseen deposits and structures (Telford *et al*., 1990). The structural control and the hydrothermal alteration of rocks and geophysical characterization of mineral deposits can be discerned from integrated interpretation of airborne magnetic and radiometric data (Airo, 2002). In addition, integrated geophysical method (ERT) offers a quick way of examining large areas, and it should prove useful in the search for mineral deposits in any part of the world (Airo and Loukola-Ruskeeniemi, 2003). It should be noted that, the Earth's magnetic field of an area is directly influenced by geological structures, geological composition and magnetic minerals, most often due to changes in the percentage of magnetite in the rock. Objects that are underground can warp the simple patterns of the Earth's magnetic field into complex shapes (Grant and Martin, 1966). These inform the use of aeromagnetic, aero-radiometric and electrical resistivity tomography (ERT) methods for this study.

1.1.4 Scope of Study

The scope of this study is to integrate aero-magnetic and aero-radiometric methods with ERT survey in order to investigate the occurrence and structural effects of bitumen deposit in Agbabu community. The results of the airborne surveys help to narrow down potential areas for bitumen deposit which were occupied with geophysical (ERT) traverses within Agbabu town. This study revealed detail geological structures and lithologies in the study area.

1.1.5 Limitation

The limitation encountered in the course of this work is that the survey area being located in the rural area with bitumen showed at the surface limit the extent to which the profile length could be extended, as the maximum electrode spread was 150 m.

1.1.6 Aim and Objectives

The purpose of this work is to use integrated geophysical methods to investigate the occurrence and the structural effects of bitumen in Agbabu community.

The objectives are to:

i. determine the principal radioelements that are contained in the rock from the aero-radiometric data;

ii identify the trend and depth to the top of geologic structures causing magnetic anomaly from the aeromagnetic data;

iii determine geoelectrical parameters of rock materials from the 2Dimensional (2D) electrical resistivity interpretation;

iv. deduce subsurface lithology and delineate basement structures that favour bitumen occurrence; and

v. correlate the ERT with aeromagnetic and radiometric studies.

1.2 Geology and Description of the Study Area

The study area is located within the geographical grids of latitude 6º 35' 16.3" N and 6º 37' 13.9" N and longitude 4º 49' 29.0" E and 4º 50' 20.7" E in Odigbo local government area of Ondo State. It falls within the sedimentary terrain in the Dahomey basin of southwestern, Nigeria.

The Dahomey basin is an Atlantic verge basin and it includes Mesozoic-Cenozoic sedimentary succession reaching a thickness of over 3000m. It extends from south-eastern Ghana to the western flank of the Niger Delta. Its stratigraphy is classified by various authors into Abeokuta Group, Imo Group, Oshosun Formation, Ilaro Formation and Coastal Plain sands and Alluvium (Jones and Hockey, 1964; Adegoke and Omatsola, 1981 and Agagu, 1985). The Agbabu area is underlain by the sediments of the Imo group.

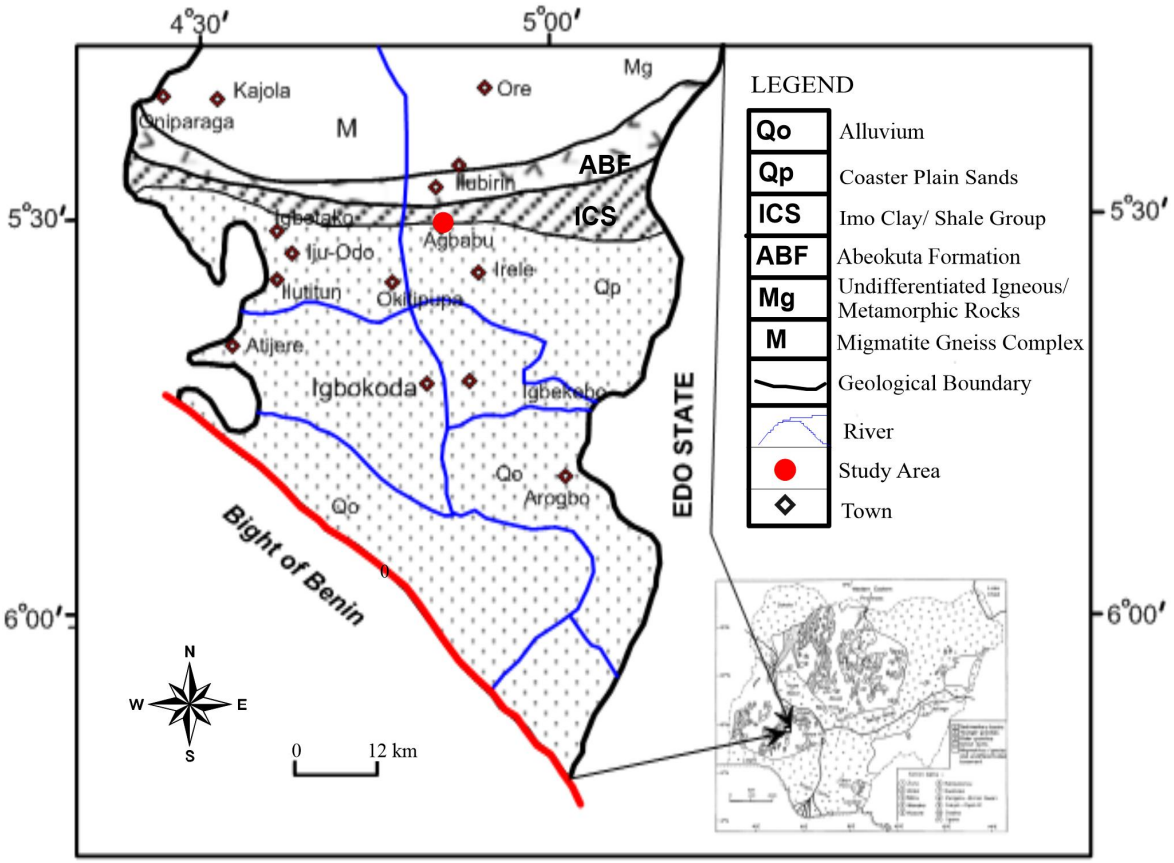

Figure 1.0: Geological map of southern part of Ondo State showing the Study Area (Modified After Amigun *et al*., 2012)

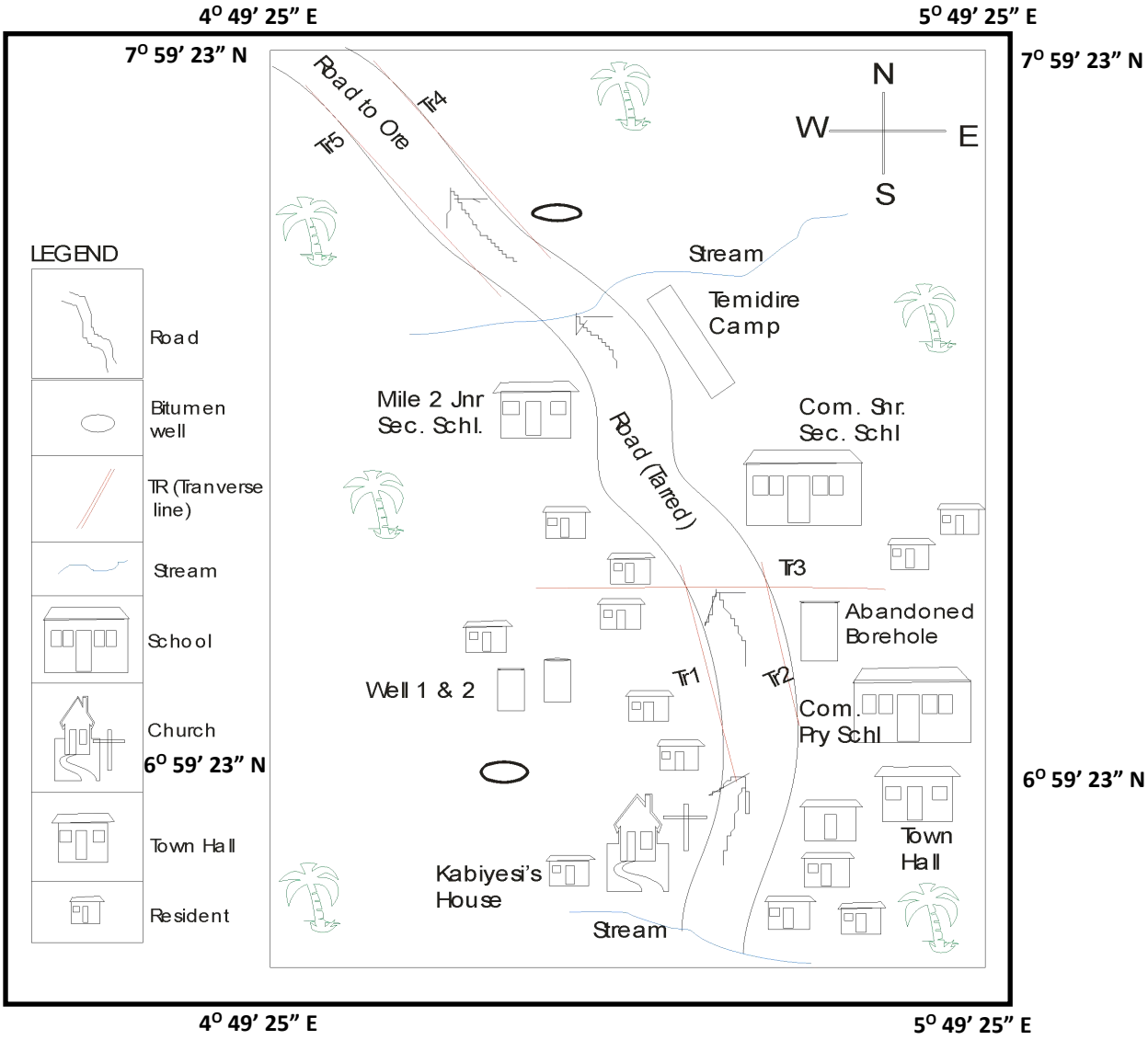

Figure 1.1: Base map of the study area

CHAPTER TWO

LITERATURE REVIEW

2.1 Magnetism of the Earth

The Earth can be divided into three parts; that is crust, mantle and core. The core of the Earth can also be divided into two parts that is the molten outer core and the solid inner core. The core of the Earth is the main provider of heat energy in the Earth (Davies and Davies, 2010). Inglis (1955) pointed out that, it is impossible at present for determine the types of convectional motion in the molten core. Reeve (2010) indicated that the movement of the charged electric particles within the molten core produces a magnetic field around the Earth after several theoretical and experimental studies. This magnetic field enveloping the Earth gives rise to the magnetic features of the various rocks found within or on the surface of the Earth. The flow of these electrical currents effectively creates a huge electromagnet (Clark and Emerson, 1991).

2.1.1 Nature of the Geomagnetic Field

The Earth's magnetic field within or at the surface of the Earth is produced from the molten outer core (Rivas, 2009). The Earth's magnetic field is made up of three parts (Telford *et al.,* 1990) namely;

1. The major field, which differ comparatively gradually and starts within the earth.
2. The minor field varies quickly and is of external origin.
3. The spatial variations of the major which are usually smaller than the main field, are nearly constant in time and place and caused by local magnetic anomalies in the near-surface crust of the Earth.

2.1.2 The Earth's Magnetic Field

If an un-magnetized needle could be hung at its centre of gravity, so that it is free to align itself in any direction, and if other magnetic fields are absent, it would take the course of the total geomagnetic field (Telford *et al.,* 1990).

At any point on the earth's surface, a freely suspended magnetic needle will assume a position in space in the direction of the ambient geomagnetic field. This will generally be at an angle to both the vertical and geographic north. The magnitude of this field, *T*, the inclination (or dip) of the needle from the horizontal, *I*, and the angle it makes with geographic north, the declination*, D;* completely define the main magnetic field. Figure 2.0 illustrates the magnetic elements (Whitham, 1960). The total magnetic field, *T* can be defined in terms of the vertical component, *Z,* which changes as one crosses the magnetic equator (Z points downwards to the magnetic equator in locations above the magnetic equator, but points upwards at locations below the magnetic equator), and the horizontal component, *H*, which is always positive. *X* and *Y* are the components of *H*, which are considered positive to the north and east respectively.

$T^2 = H^2 + Z^2 = X^2 + Y^2 + Z^2$

$H = T\cos I, \qquad X = H\cos D$

$Z = T\sin I, \qquad Y = H\sin D$

$\tan D = Y/H, \qquad \tan I = Z/H$

$T = Tt = T(\cos D\cos I\mathbf{i} + \sin D\cos I\mathbf{j} + \sin I\mathbf{k})$

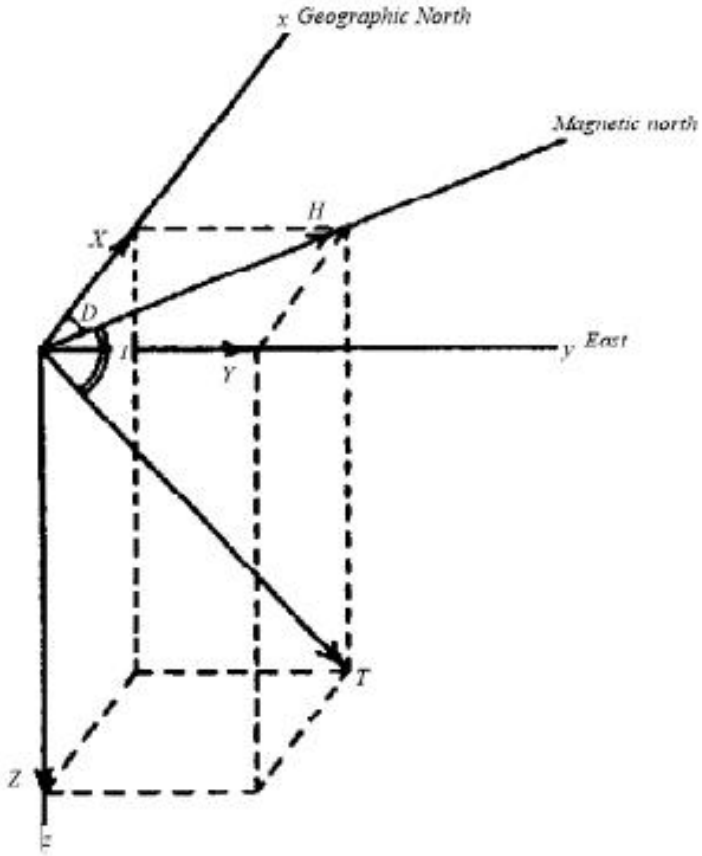

Figure 2.0: Vector representation of the geomagnetic field at any place on the Northern Hemisphere (Whitham, 1960).

These magnetic elements can be related as follows:

H = F cos I

Z = F sin I

2.2 Magnetism of Rocks and Minerals

Most rock-forming minerals are non-magnetic. Only a few magnetic minerals, that include magnetite (Fe_3O_4), ilmenite ($FeTiO_3$) and pyrrhotite (FeS), significantly affect the magnetization field of the particular area. Magnetic rocks contain these minerals in small quantities because subsurface temperatures increase with depth, substantial magnetization can occur only above certain depths.

The magnetic minerals of most sedimentary rocks are negligible. Most igneous rocks, on the other hand, have high magnetic susceptibilities, while acid igneous rocks and metamorphic rocks have

susceptibilities ranging from negligible to extremely high values (Reeves, 1989; Paterson, 1990; Reynolds, 1997).

2.2.1 Magnetic Susceptibility

Magnetic susceptibility is a physical parameter that details the degree to which a material can be magnetized in an applied external field, (Dalan, 2006). In geology, magnetic susceptibility is one characteristic of a mineral type. Its measurement gives us information about the type and quantity of minerals present in the sample. Measurement of magnetization depends on the amount and composition of the iron oxide in the rocks (Dearing, 1994; Wemegah *et al.,* 2009).

The effective magnetic susceptibility is the ratio of the magnetization effect to the applied magnetic field. It is mathematically expressed as

$$K=\chi_v = \frac{M}{H}$$

Where χ_v the volume susceptibility, H is the magnetic field and the magnetization is M and K is the magnetic susceptibility. The magnetic susceptibility is a dimensionless quantity since H and M have the same unit of Ampere/meter and for its numerical value to be compatible with the SI units, the value in c.g.s. equivalent units needs to be multiplied by 4π (Clark, 1997). Reynolds (1997) indicates that majority of the sedimentary rocks have negligible amounts of magnetic minerals, and are therefore non-magnetic. Most basic igneous rocks, on the other hand, have high magnetic susceptibilities, while acid igneous rocks and metamorphic rocks can have susceptibilities ranging from negligible to extremely high. Magnetic susceptibility is a trace parameter of rocks, because the percentage of magnetic minerals is usually one percent or less, even in basic igneous rocks (Ferreira *et al.,* 1994).

2.2.2 Remanent and Induced Magnetism

There are two components present in a rock's magnetization which is remanent magnetism and induced magnetism. Remanent magnetism known as permanent magnetism is the type which remains in the rock when the induced field is removed. Materials that belong to ferromagnetic material retain

their magnetism even when the external field is withdrawn. Rock magnetization often occurs at shallow depths due to an increment in temperature around the centre of the Earth (Clark and Emerson, 1991). Furthermore, remanent magnetization can surface when the magnetic arrangements in the domain are locked in the presence of a feeble geomagnetic field.

Primary remnant magnetization is acquired by the cooling and solidification of an igneous rock above the Curie point to normal surface temperature thermoremanent magnetization (TRM) or by detrital remnant magnetization (DRM). Secondary remnant magnetization like chemical, viscous or post-depositional remnant magnetization may be acquired in the rock's history (Reynolds, 1997). The ratio of the magnetization effect, M to the applied effect H gives the magnetic susceptibility of the rocks.

2.2.3 Magnetization at Low Magnetic Latitudes

For a small latitudes like 10º of angle of intersection, the amplitude solution for north-south drift characteristics undeservedly thicken and changes the orientation of the magnetic susceptibilities from the beginning of the magnetic sources in different directions of the visible field. There are always complexities with magnetic dataset explanations as a results of the asymmetric anomalies encountered by symmetric causative rocks mostly in anywhere on the Earth apart from areas closer to the magnetic poles (Rajagopalan, 2003).

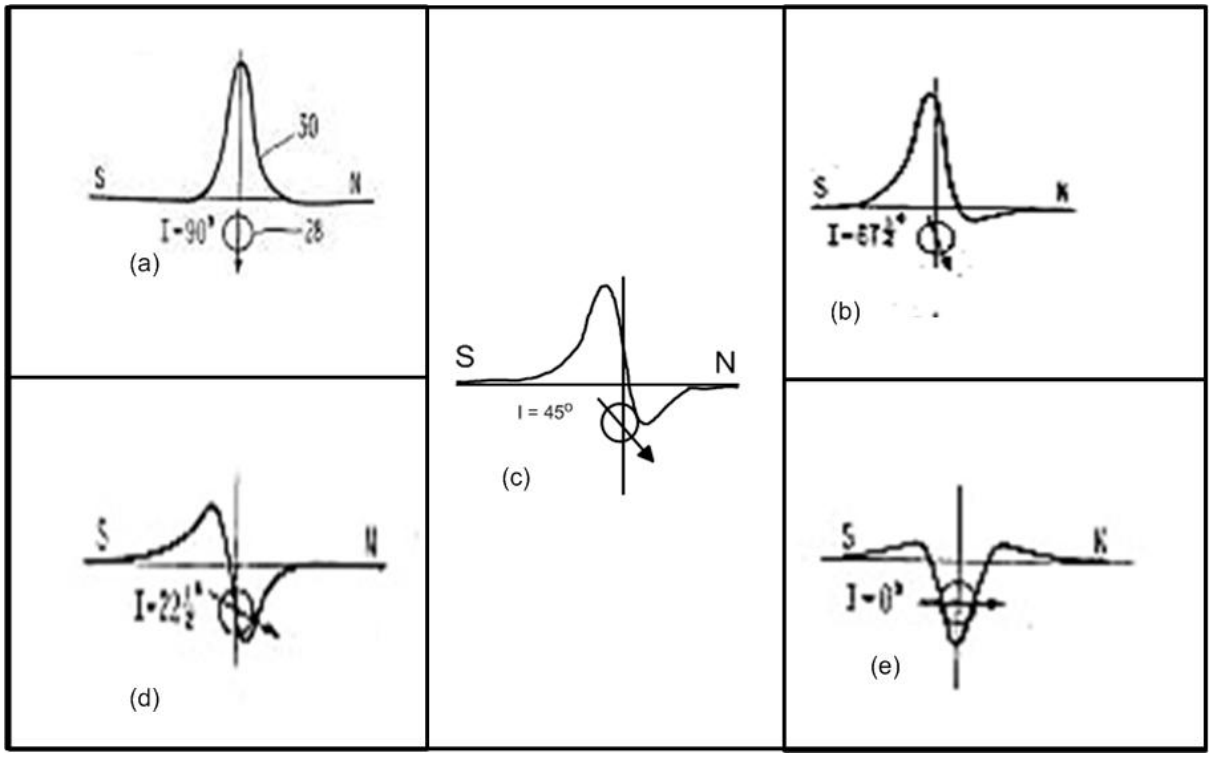

Figure 2.1: Magnetic anomaly profile at different latitude/inclination due to thin dykes of finite depth extent (Nettleton, 1971).

2.3 Rock Alteration

The deformation of rock when hot fluids moves from high pressure areas to low pressure areas is referred to as alteration. Alteration of rocks that occur during chemical weathering is called supergene alteration (Appiah, 1991). The explanations of magnetic anomalies make deformation of magnetic minerals highly significant to remember. According to Appiah, 1991, mineral deposits are mainly controlled by wall rock alteration closer to hydrothermal veins by the hot liquids. The alternation ranges from simple recrystallization to the addition, removal or rearrangement of chemical components. The nature of the alteration products rely solely upon the character of the original rock and invading fluid which explains factors like pH, vapour pressure with the degree of hydrolysis and the temperature with pressure at which the reactions took place (Studemeister, 1983).

2.4 Lithology, Structure and Magnetism

In the natural environment, magnetic minerals are pervasive and appear in every kind of rocks i.e. sediments and soils. These magnetic minerals have the magnetic dipoles locked the direction of the Earth's magnetic field during the formation of the rock (Harrison *et al.,* 2007).

Plummer *et al.,* (2001) grouped structures into two different forms which are: firstly the brittle structures which resulted in the brittle-elastic breakdown of rocks long-ago. Joints and faults formed part of this broad type of structures and secondly ductile structures which conserves the main viscoplastic alteration of rock all the way through the geological time.

Isolated magnetic anomalies, generally circular or oval in plan and several hundred meters across, and with amplitude of tens to hundreds of nanoteslas, may arise from accumulation of magnetite and pyrhotite, which may be associated with economic grades of copper, lead, zinc, silver, gold and others (Plummer *et al.,* 2001).

Grant (1985) in his paper explained that sedimentary rocks are usually non-magnetic. The analysis of geophysical data suggests that sources of magnetic bodies must be located beneath the bottom of the sedimentary rocks. Sedimentary rocks such as sandstone, dolomite and limestone have low magnetic features with extremely small magnetic anomalies.

2.5 Enhancement Techniques

Various geological techniques when applied to geophysical data appears to improve the data quality based on the employed mathematical principles. A mathematical improvement that includes analytical signal, vertical derivative, etc. are highly helpful in developing near surface geological features except that their limitations are based on the value of the data and the inclination angle between the Earth's magnetic axis and the horizontal.

2.5.1 Fourier Transform Filter

Fourier transforms are indispensable in magnetic field (Telford *et al.,* 1990) for

- Resolving specific anomalies using downward or upward continuation,
- Changing effective field angle or converting residual magnetic data to vertical-component data
- Calculation of derivatives and
- General filtering-separating anomalies from sources such as different size and depth, and modelling.

A faster algorithm developed by Cooley and Tukey, (1965) known as the Fast Fourier Transform (FFT) is a vital mathematical tool useful in calculating the Discrete Fourier Transform (DFT) and it's inverse. The FFT algorithms can be made into data processing programs in order to analyze spectral lines of the waveforms of geophysical data. Fourier transformations operate on application program such as Microsoft Excel for organizing, analyzing and storing data in the form of a table (Kearey *et al.,* 2002).

2.5.2 Analytic Signal

This analytic signal behaves in a similar manner to the reduction of the pole filter. It is the magnitude of the square root of the vertical and horizontal components of the magnetic responses (Geosoft Inc., 1996). This processing enhancement can be helpful in picturing the edges of the permanently magnetized sources and for centering anomalies over their real bodies in areas of low magnetic latitude (Ansari and Alamdar, 2009). In addition, several authors revealed that, it can be helpful in the depth estimation of magnetic bodies (Aisabokhae et al., 2018).

2.5.3 Vertical Derivative Filter

The vertical derivative filter usually removes the long wavelength properties of the magnetic responses and most importantly improves the quality of closely spaced and superposed responses (Keating, 1995). The application of the vertical derivative filter to a magnetic data is to improve the shallowest

magnetic features and suppress the deeper anomalies in the data (Geosoft Inc., 1996). The vertical derivative detailed the near surface geological features.

2.6 Principles of Radioactivity

Radioactivity is simply the emission of ionizing radiation or particles caused by the spontaneous disintegration of atomic nuclide. Geologists and geophysicists measure the gamma rays emanating from the surface of the Earth. These radiations give a lot of information about the soil and rock distribution within the Earth i.e. (lithology).

2.6.1 Basic Radioactivity

Isotopes are atoms of same element with equal number of protons but different neutron numbers. Isotopes have same chemical features, but different physical features. Unstable nuclei emit energetic ionizing radiations to become more stable.

These isotopes are called radioactive isotopes or radioisotopes. Nuclides with this feature are called radionuclide, and disintegration or nuclear decay is the breakdown of unstable nuclei (IAEA, 2003)

Table 2.1 Some Radioactive Isotopes with Medical Applications

Isotope	Use
^{32}P	cancer detection and treatment, especially in eyes and skin
^{59}Fe	anemia diagnosis
^{60}Co	gamma ray irradiation of tumors
^{99m}Tc*	brain, thyroid, liver, bone marrow, lung, heart, and intestinal scanning; blood volume determination
^{131}I	diagnosis and treatment of thyroid function
^{133}Xe	lung imaging
^{198}Au	liver disease diagnosis

Each radioactive isotope has a distinctive chance associated with the radioactive disintegration of its nuclei. This is called as the isotope half-life and is the time taken for radioactive nuclei to decay to half its initial value. Hence, after one half-life, half the original radioactive isotopes remain, and after two half-lives, one quarter of the original radioactive isotopes remain, and so on (Minty, 1996). The law of

radioactivity decay states that the reduction in the quantity of atoms of unstable nuclei with time is expressed as (IAEA, 2003).

N= $N_0 e^{-\lambda t}$

Where N is the quantity of atoms after decay with time t(s), N_o is the initial quantity of atoms and λ is the decay constant of the unstable nuclei (s-1).

The half-life $t_{1/2}$(s) of an element is defined as the time taken for N_o to decrease by half.

$$t_{1/2} = \frac{0.693}{\lambda}$$

The λ multiplied by N gives the activity of the unstable nuclei. Disintegration of unstable nucleus does not depend on additional physical factors (IAEA, 2003).

Table 2.2. Naturally occuring radioactive isotopes

Element	Isotope	Abundance (%)	Half-life (yr)	Type of radiation	Energy (MeV)
Potassium	$_{19}K^{40}$	0.012	1.3×10^9	β, K cap	1.46
Calcium	$_{20}Ca^{48}$	0.18	$> 2 \times 10^{16}$	β	0.12
Vanadium	$_{23}V^{50}$	0.24	6×10^{15}	β, K cap	0.71, 1.59
Rubidium	$_{37}Rb^{87}$	27.8	4.7×10^{10}	β	0.27
Indium	$_{49}In^{115}$	95.72	6×10^{14}	β	0.60
Lanthanum	$_{57}La^{138}$	0.089	1.1×10^{11}	β, K cap	0.54, 0.81, 1.43
Cerium	$_{58}Ce^{142}$	11.1		α	1.5

Minty (1996) indicated that radioactivity usually occurs as a sequence of the number of daughter products with a breakdown of the mother elements in order to have a stable isotope.

At this period, the behaviours of all the radioisotopes of the decay series are the same. Hence, the extent of the quantity of any daughter nuclei can be helpful in estimating the quantity of any other radio nuclei in the breakdown series. Emanations of gamma rays from the Earth surface differ with

many factors but most importantly depend on the amount of radionuclide in the top soil about 30 to 40 cm. The amount depends on the parent rock and the extent of Weathering (Elawadi *et al.,* 2004).

2.6.2 Disequilibrium

Minty (1996) indicated that the addition or removal of one or more radionuclide in a decay series completely or partly to the system is known as disequilibrium. Thorium rarely occurs out of equilibrium in nature and potassium is not affected with disequilibrium problems. Nevertheless, it is frequent in the disequilibrium of uranium decay series and can take place at numerous locations in the ^{238}U decay chain, ^{238}U can be carefully leached compare to ^{238}U, ^{230} Th and ^{226}Ra can be carefully taken out from the breakdown series and lastly ^{222}Ra (radon gas) is movable and can flee into the atmosphere from soils and rocks (Elawadi *et al.,* 2004 and IAEA, 2003).

Each member of the decay loses mass at an equal rate in equilibrium decay. In each case, the suitable constant of decay is multiplied by mass of the element. The constant of decays are hence inversely dependant on the equilibrium masses. If the required number of elements for equilibrium is exceeded or lessen, radioactivity will be faster or slower than the rate of equilibrium until equilibrium is again established.

Equilibrium can be interrupted if any gaseous or soluble intermediate products have half-lives extended enough to permit them to scatter prior to radioactivity. Approximations of the amount of uranium are then usually recorded as equivalent uranium (eU) because these approximations are calculated on the assumption of equilibrium circumstances. Thorium too is often recorded as equivalent thorium (eTh), even though the thorium decay chain is nearly constantly in equilibrium (Milsom, 2003).

2.6.3 Source-Detector Geometry

Gregory and Horwood (1961) indicated that the observed spectra are greatly influenced by the thickness of the source detector. Moreover, the Compton range which depends on the scattering in the sources increases as the thickness of the source also increases. The peaks of the photons are hence

reduced compared to the Campton background. In view of the fact that photons of low energy are simply damped than the photons of high energy, this effect is well associated with photons of lower energies. Any material between the source and the detector attenuates radiations coming from the Earth in the source. The nature of the observed spectrum is mainly influenced by the number of materials attenuating the radiations between the detector and source. For increasing damping, the photo-peaks are weaken compared to the range of energy. Measurement of spectra lines therefore depends on the amount and thickness of the source, the level of the detector above the Earth‟ surface, the size of the bedrock which is non-radioactive and the response function of the detector (Elawadi *et al.,* 2004; IAEA, 2003).

2.7 Measurement of Gamma Radiation

Natural gamma radiations vary from cosmic emissions with energies above 3 MeV to X-rays. The various peaks match the exact radioactive events, the energy of individual photon occurring anywhere within a small range determined by the nuclear kinetic energies at the decay time and by errors made during the data acquisition (Milsom, 2003).

The modern gamma ray spectrometers usually records energies of range 0 to 3 mega electron volt (MeV) using the 256 or 512 channels of information.

Every channel hence reports all gamma radiations recorded by the detector which have energies in range of 11.7 keV, weak count rates are associated with each channel. With the airborne gamma ray spectrometer, one or even zero counts in several channels of high energy are recorded for the duration of a second counting stage with sodium iodide (NaI) of 32 litres.

Figure 2.2 shows a typical spectrum from gamma ray energy distributions. ^{40}K decays with emission of gamma radiations of energy 1.46 MeV whereas uranium and thorium decays with emission of gamma radiations of energies of 1.76 MeV and 2.62 MeV respectively. Thorium portrays high peaks compared to all the three concentrations (IAEA, 2003).

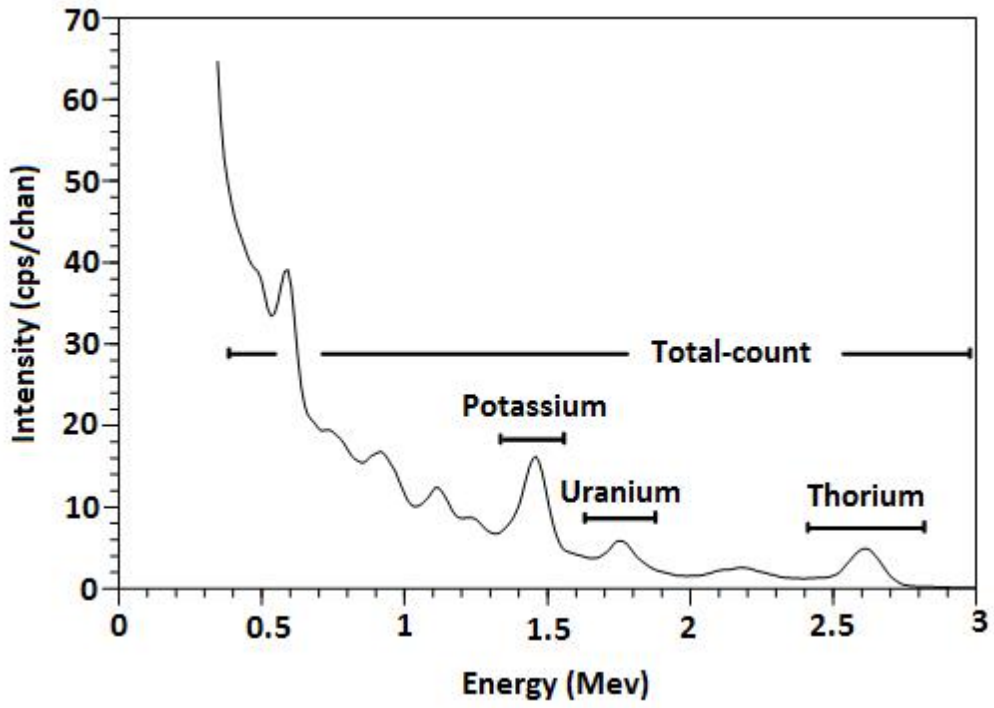

Figure 2.2: Typical spectrum of the gamma radiations showing the individual peaks (IAEA, 2003).

Granite contains sufficient amount of Potassium and Thorium and lesser portions of Uranium. The energy windows of uranium, thorium and potassium are conventionally used in the measurement of the gamma radiations. Telford et al. (1990) points it out that the totality of radioactivity produces the total-count window. Concentrations of radioactive elements in water, air and rocks with regards to nuclear geophysics and geology are expressed in percentage (%) for potassium and parts per million for both uranium and thorium (ICRU, 1994)

2.8 Mapping Natural Sources of Radiation

Naturally occurring radiation sources can be suitably classified into three groups according to their origin. The first group includes ^{40}K, ^{238}U, ^{235}U and ^{232}Th which are believed to have been produced during the creation of the universe and have half-lives of the same order as the Earth's age (Minty, 1996).

The second group comprises radioactive isotopes that are daughter products from the decay of isotopes in the first group. These have half-lives varying from small fraction of one (1) s to104 to 105 years.

The third group would include isotopes created by external causes such as the reactions of cosmic radiations with the Earth and its atmosphere. The concentration of cosmic radiation at surface of Earth is comparatively small such that all of them are absorbed in the atmosphere (Minty, 1996 and Elawadi *et al.,* 2004).

2.8.1 Geochemistry of Radioelements

2.8.1.1 Potassium

Potassium (K) is an alkali, lithophile and biophile metal. Potassium forms majority component in rock formation. Most of these rocks are the silicate minerals such as alkali feldspar, leucite, biotite, muscovite, phlogopite and some amphiboles.

Most igneous rocks have potassium being the main aggregate. The amount of potassium is used for the petrography groupings. During magmatic differentiation, potassium is gradually concentrated thus more potassium is concentrated in felsic than mafic igneous rocks.

This is observed in the variations in K concentration of basalt, normally less than 1%, and granite, which is composed of 2% to less than 6% (Elawadi *et al.,* 2004, Fertl, 1983; Wedepohl, 1978).

Dickson and Scott (1997) indicated that during weathering process, the main potassium sources will be destroyed in the order biotite-potassium-feldspar-muscovite. When weathering is taking place, the freed potassium can be used for the formation of potassium enriched minerals like illite or may be taken up in small quantities by clays (montmorillonite) under better conditions.

The magmatic and metamorphic rocks series control almost all the potassium enriched minerals such as the feldspar mainly the feldspar, thoids, leucite and nepheline, and the micas, biotite and muscovite.

2.8.1.2 Thorium

Thorium (Th) is a part of the actinide group of elements. +4 is the main oxidation state of this element and thorium-232 (^{232}Th) as the only natural occurring isotope. Thorium has an incredibly long half-life of 1.4 x 10^{10}years (Wedepohl, 1978). It is strongly lithophilic and is more abundant within the crust of

the Earth. During the decay series of thorium, the parent thorium nuclide disintegrates with emission of gamma radiations of energy 2.62 MeV and 208Ti as the daughter nuclide. Granitic rocks records higher concentration of thorium than mafic igneous rocks. The concentration of thorium normally cannot move but due to environmental conditions there can be a small movement. Th fundamentally cannot dissolve in both surface and groundwater so it is a helpful guide element in sediments of stream for finding deposits of uranium related with magmatic rocks (Chopin, 1988; Elawadi *et al.,* 2004;

Krishnaswami,(1999). Monazite and zircon are the main minerals enriched with thorium. They are immobile thus during weathering they are more stable and can be absorbed into deposits of heavy sand minerals. Thorium released during weathering (*i.e* breakdown of rocks) possibly will be preserved in iron oxides, titanium oxides and with clays (Dickson and Scott, 1997).

2.8.1.3 Uranium

Uranium (U) is an extremely heavy element and this can be considered as the most radioactive element in the world. Uranium produces the most abundant supply of concentrated energy. Uranium is contained in most soil of amount of 2 to 4 parts per million and is widespread in the crust of Earth such as tungsten, tin and molybdenum. In the crust of the Earth, most of the uranium is a combination mostly of two isotopes ^{238}U and ^{235}U. Uraninite is widespread as tiny traces in the minerals forming up the rock in granites or as bulky grains in mineralized pegmatites and granites. In addition uraninite happens in hydrothermal layer and sedimentary rocks. Zircon, monazite, apatite, allanite and sphene (accessory minerals) which are related with igneous and metamorphic rocks are the most resistant to weathering (Langmuir and Hermans, 1980; IAEA, 2003). Uranium released during weathering possibly will be preserved in authigenic iron oxides and minerals of under reducing environment forming deposits of uranium under conducive conditions (Dickson and Scott, 1997).Uranium itself does not emit gamma-rays during its decay but the most energetic gamma-rays emitted by its daughter isotopes come from ^{214}Bi which occurs late in the decay series (Dickson and Scott, 1997).

2.8.2 Distribution of the Radioelement in Rocks and Soils

For normal rocks and soils, 90% of the gamma rays measured by a spectrometer survey emanate from the uppermost 30cm to 40cm of the Earth. The content of potassium in rocks can have a range of 0 to 10% potassium but is usually 1 to 5% potassium with average of about 2% potassium. The content of Uranium and Thorium in rocks changes from near zero to several hundreds of part per million (ppm). The amount of K, U and Th depends on rock type and the geological environment. In most areas beneath the Earth, the bedrock is covered with soil. Hence, the radiation from the soil is the most essential contributor to the terrestrial radiation. The amount of the radiation from minerals in the soil depends upon the content in the original parent rocks (IAEA, 2003). Moreover potassium is extremely unable to coexist during crystallization of magma. A rock of composition of 2.5% K, 3ppm U and 15 ppm Th could be a granite, felsic intrusive or shale (Dickson and Scott, 1997).

Available data for metamorphic rocks which include gneissic rocks resulting from granite and amphibolites resulting from dolerite suggest that metamorphism does not affect radioelement content. Sedimentary rocks generally have radioelement content reflecting the parent source rock. Hence, young sediments derived from granitic sources may be expected to have quite high radioelement content, but more mature sediments, composed primarily of quartz should have very low values when specific rock types such as pegmatite, aplites, quartz, feldspar, porphyrites and mafic intrusive occur as narrow intrusions or in small areas, or are subject to faster weathering and erosion than the host country rock, it is difficult to find insitu soils (Dickson and Scott, 1997)

Granite depicts a broad array of weathering behaviour, depending on its mineralogy and the weathering system, climate e.t.c. Soils derived from granitoids generally lose around 20% of their radioelements contents during pedogenesis. Soils over radioelement-poor arenite, as over other poor radioelement-poor rocks; can show the effects of contamination by transported materials (Darnley, 1996).

Processes other than in-situ weathering can affect the radioelement content of soils. They include clay eluviations, colluvial and Aeolian transport, and soil movement. All can affect the concentration of radioelements in the thin 30cm to 40cm layer measured during aerial surveying (Wilford et al., 1997).

2.8.3 Direct Detection of Mineralization

The radiometric surveys are used extensively in many ways. This survey method was primarily used in mapping for the deposits of uranium but present day radiometric survey has diverse benefits such as delineation of lithologies. Applications of radiometric survey have been used in weak radioactive zones like sedimentary basins, volcano-sedimentary terrains, and heavily glaciated or tropical weathered areas (Elawadi *et al.,* 2004).

Analyses of geochemical and microscopic samples from rock or sediments are required to fully recognize the mineral phases that form the radioelements (Charbonneau, 1991).

Owing to the comparatively weak penetration of gamma radiations through rock and soil, the chance of detection of mineralizing of Uranium is reliant on the Uranium content in the host rock, its surface dimensions, and the positions of the measured profiles (Elawadi *et al.,* 2004).

Radiometric assay of samples in mineralized regions depicts that high percentage of potassium oxide (K_2O) content in the rock and the strong differences in the potassium oxide concentration in the rock is possible owing to the large scale deformations in the rock (Bhattacharya *et al.,* 2011).

Alteration, weathering, climatic conditions and hydrothermal processes can have effect on the concentration of the radioelements (Nicolet and Erdi-Krausz, 2003). Variations in the vegetation cover can also affect ground surveys. For example, the radioactivity of a soil covered by humus will be less than the radioactivity of the above soil. A mass equivalent to 0.08m of water will reduce the exposure rate by about 50%, because soil moisture has a similar effect and it varies as a function of time and rainfall, therefore, surveys carried out at different times of the year may not give the same estimate of

the exposure rate (IAEA, 2003). Hydrothermal processes can result in variations to the radioelement content of the host rocks.

Among the three radioelements, K is mostly affected by such processes, Th less often and U very infrequently. Potassium is often increased during alteration signature but weathering generally decreases the intensity of alteration signature (Dickson and Scott, 1997).

Potassium is generally added to the source rocks by mineralizing hydrothermal fluids. It may be hosted by K-feldspar or muscovite and potential outcropping or sub-cropping mineralization can be recognized by increase in K counts during radiometric surveying (Dickson and Scott, 1997). This could reflect the greater movement of U compared to Th during hydrothermal alteration processes and because Th is generally unaffected by alteration processes, the K/Th ratio can be a strong indicator of K alteration related with mineralisation than simply K. Thorium may be mobilized during mineralization processes for example, being partly depleted in regions of K-alteration or intense solidification, but concentrated in Th-rich materials such as laterite. The relationships between radioelement divisions and each of these types of deposit are varied and composite. A complete comprehension of the influences of solidification, K-alteration, process of weathering and local lithological differences is required to estimate the mineralization potential characterized with anomalies of radioelements.

2.9 Electrical Resistivity Tomography (ERT) Survey

The purpose of electrical surveys is to determine the subsurface resistivity distribution by making measurements on the ground surface. From these measurements, the true resistivity of the subsurface can be estimated. The ground resistivity is related to various geological parameters such as the mineral and fluid content, porosity and degree of water saturation in the rock. ERT measures resistivity in Ω·m which is the mathematical inverse of conductivity. It is a bulk physical property of materials that describes how difficult it is to pass an electrical current through the material. Resistivity measurements can be made with either a low frequency alternating current (AC) or a direct current (DC) (Christensen,

1989). As resistivity measurements are frequency dependant, care must be taken when comparing resistivity values collected using different techniques. Clay materials, metallic oxides, and sulphide minerals are some of the common sedimentary materials that can carry significant electrical current through the material itself. As such, the resistivity of most near surface sedimentary materials is primarily controlled by the quantity and chemistry of the pore fluids within the material. Any particular material can have a broad range of resistivity responses that is dependent on the level of saturation, the concentration of ions, the presence of organic fluids (such as non aqueous phase liquids, NAPLs), faulting, jointing, weathering, etc. Recent advances to field equipment and data processing procedures have made rapid 2D surveys routine and 3D surveys possible. Legacy 1D resistivity surveys are still common and are useful on many occasions, but encounter interpretation problems in areas of complex geology.

Material	Nominal resistivity (Ω m)
Sulphides:	
Chalcopyrite	1.2×10^{-5}–3×10^{-1}
Pyrite	2.9×10^{-5}–1.5
Pyrrhotite	7.5×10^{-6}–5×10^{-2}
Galena	3×10^{-5}–3×10^{2}
Sphalerite	1.5×10^{7}
Oxides:	
Hematite	3.5×10^{-3}–10^{7}
Limonite	10^{3}–10^{7}
Magnetite	5×10^{-5}–5.7×10^{3}
Ilmenite	10^{-3}–5×10
Quartz	3×10^{2}–10^{6}
Rock salt	3×10–10^{13}
Anthracite	10^{-3}–2×10^{5}
Lignite	9–2×10^{2}
Granite	3×10^{2}– $\times 10^{6}$
Granite (weathered)	3×10–5×10^{2}
Syenite	10^{2}–10^{6}
Diorite	10^{4}–10^{5}
Gabbro	10^{3}–10^{6}
Basalt	10–1.3×10^{7}
Schists (calcareous and mica)	20–10^{4}
Schist (graphite)	10–10^{2}
Slates	6×10^{2}–4×10^{7}
Marble	10^{2}–2.5×10^{8}
Consolidated shales	20–2×10^{3}
Conglomerates	2×10^{3}–10^{4}
Sandstones	1–7.4×10^{8}
Limestones	5×10–10^{7}
Dolomite	3.5×10^{2}–5×10^{3}
Marls	3–7×10
Clays	1–10^{2}
Alluvium and sand	10–8×10^{2}
Moraine	10–5×10^{3}
Sherwood sandstone	100–400
Soil (40 % clay)	8
Soil (20 % clay)	33
Top soil	250–1700
London clay	4–20
Lias clay	10–15
Boulder clay	15–35
Clay (very dry)	50–150
Mercia mudstone	20–60
Coal measures clay	50
Middle coal measures	>100
Chalk	50–150
Coke	0.2–8
Gravel (dry)	1400
Gravel (saturated)	100
Quaternary/Recent sands	50–100

Table 2.3: Ground resistivity material

2.10 Resistivity Method

Electrical resistivity studies in geophysics may be understood in the context of current flow through a subsurface medium consisting of layers of materials with different individual resistivity (Reynolds and Wiley, 1997). The resistivity ρ of a material is a measure of how well the material retards the flow of electrical current.

Resistivities vary tremendously from one material to another. For example, the resistivity of a good conductor such as copper is of the order of $10^{-8}\ \Omega\, m$, the resistivity of an intermediate conductor such as wet topsoil is$\sim$ 10 Ω m, and the resistivity of poor conductors such as sandstone is $\sim 10^{8}$ Ω m. Due to this great variation, measuring the resistivity of an unknown material has the potential for being very useful in identifying that material, given little further information. In field studies, the resistivity of a material may be combined with reasoning along geologic lines to identify the materials that constitute the various underground layers. Equation (1) below is relevant to the bodies with simple geometry e.g cylinder provided the medium is homogeneous and defined for semi-infinite medium. The resistivity appears as the material-specific constant of proportionality in the expression for the total resistance of the cylinder

$$\mathrm{R} = \rho \frac{L}{A} \qquad (1)$$

The total resistance R may be obtained experimentally through Ohm's law, $R = \frac{V}{I}$ where V is the potential difference between the ends of the cylinder and I is the total current flowing through the cylinder. The resistivity of the material, an intrinsic property of the material, is then related to experimentally measured extrinsic parameters

$$\rho = \left(\frac{V}{I}\right)\left(\frac{A}{L}\right) = \mathrm{R_{app}\,K} \qquad (2)$$

Where: ρ = resistivity, K = geometric factor, R = resistance, I = current. In equation 2, the resistivity is given by the product of the apparent resistance" R = $\frac{V}{I}$ and a ''geometric factor'' K= $\frac{A}{L}$ that carries

information about the geometry of the cylinder. This type of product of an apparent resistance and a geometric factor will appear again when the resistivity of the ground is determined. It is more difficult to arrive at an expression for the resistivity of material that is not as geometrically simple as a uniform cylinder. A good starting point is shown in Fig. 2.3, which depicts current flowing radially away from a single electrode at positive potential located on the surface of the ground. The subsurface is of uniform composition, and $V = 0$ infinitely far away from the electrode. Equipotential surfaces are indicated by solid lines, while the unit vector field shows the direction of **J** and thus **E**. The equipotential surfaces are perpendicular to the lines of current and may be understood as creating the local potential gradients or ‘‘voltage drops’’ that drive the current according to the simple scalar form of Ohm’s law given by $I = \frac{V}{R}$. The resistance of the air above the ground is assumed to be infinite so that the ground forms a Dirichlet-type boundary.

2.11 BASIC PRINCIPLE

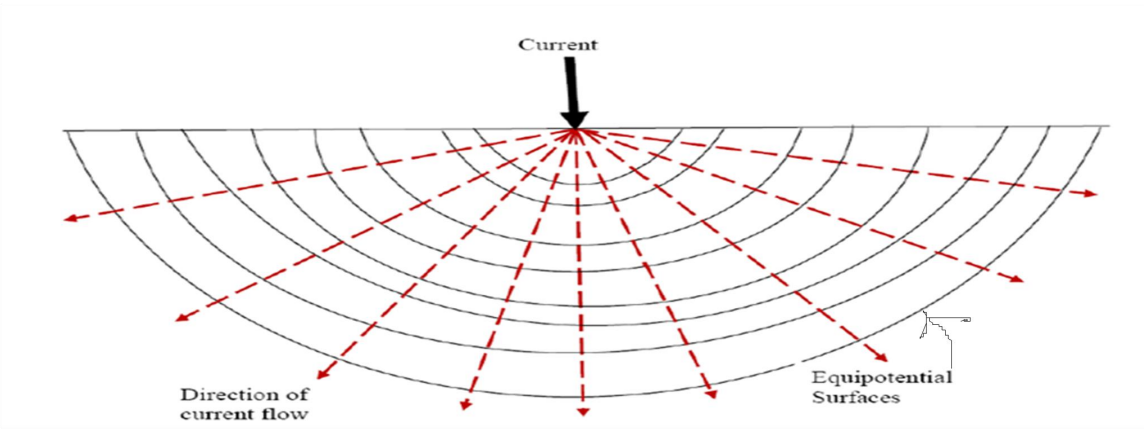

Figure 2.3: Current flow and equipotential surfaces in a level field with homogeneous subsurface structure. The unit vector field shows the directions of the current density J and thus the electric field E. (Telford et al., 1990)

Resistivity studies in geophysics may begin with the vector form of Ohm’s law, (Telford et al,. 1990)

$$J = \sigma E = \frac{1}{\rho} E = - \frac{1}{\rho} \nabla V \qquad (3)$$

In eq. (3), **J** is the current density vector, **E** is the electric field vector measured in units of volts per meter, V is the electric potential in volts, σ is the conductivity measured in $(\Omega\, m)^{-1}$, and ρ is the resistivity measured in (Ω-m). The units of the current density are A/m^2. The physical interpretation of the current density is that each component of **J** gives the amount of current flowing through each square meter of a two-dimensional surface perpendicular to the direction of flow of that component of **J**. For example, J_x indicates the number of amperes flowing in the x direction crossing each square meter of the y–z plane (Telford et, al., 1990).

Figure 2.3 shows a subsurface of uniform composition of infinite extent with one source and one sink electrode for the current. The current electrodes may be treated as point sources or sinks of spherically symmetric current flow in the half plane below the surface. The total current I flow away from or toward each electrode across the surface of a half sphere with area $\frac{1}{2}$ $(4\pi r^2)$. Ohm's law for one electrode then has the simple form

$$J = -\frac{1}{\rho}\frac{dv}{dr} \tag{4}$$

For constant ρ, this first-order differential equation is readily integrated and yields

$$V(r) = \frac{\rho I}{2\pi r} \tag{5}$$

For the potential, a distance r from the electrode in eq. (5) given as I is the total current flowing from one current flowing to the other through the ground.

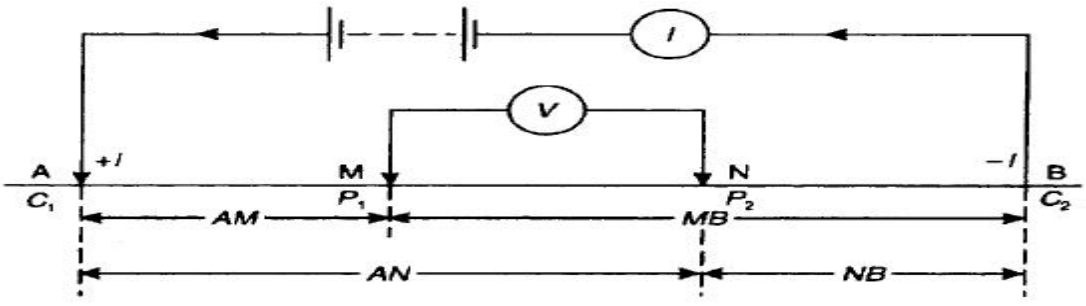

Figure 2.4: Generalised form of electrode configuration in resistivity surveys (Telford et, al., 1990)

The electric potentials measured at *M* and *N* in the general linear array of Fig. 2.4 are superposition of the potential of eq. (5) due to each of the two source electrodes located at *A* and *B*. With the distances between the electrodes given by *AM, MB*, etc., and *V* infinitely far from the current source, the potentials at *M* and *N* are given by

$$V_M = \frac{\rho I}{2\pi}\left(\frac{1}{AM} - \frac{1}{MB}\right) \quad (6)$$

And

$$V_N = \frac{\rho I}{2\pi}\left(\frac{1}{AN} - \frac{1}{NB}\right) \quad (7)$$

The total potential difference between the electrodes *M* and *N* is thus

$$V_{MN} = V_M - V_N = \frac{\rho I}{2\pi}\left[\left(\frac{1}{AM} - \frac{1}{MB}\right) - \left(\frac{1}{AN} - \frac{I}{NB}\right)\right] \quad (8)$$

This may be rearranged to yield

$$\rho = \frac{V_{MN}}{I} K \quad (9)$$

where

$$K = 2\pi\left[\left(\frac{1}{AM} - \frac{1}{MB}\right) - \left(\frac{1}{AN} - \frac{I}{NB}\right)\right] \quad (10)$$

is the ‘‘geometric factor’’ that will acquire a particular value for a given electrode spacing. For the Wenner array, all of the separations are equal to a constant value *a* and the Wenner geometric factor assumes the simple form $K = 2\pi a$

Thus, the apparent resistivity for the Wenner array is

$$\rho_{wenner} = \left(\frac{V_{MN}}{I}\right) K = \left(\frac{V_{MN}}{I}\right) 2\pi a \quad (11)$$

Equation (11) is the first of the two main mathematical results of this section. The resistivity of eq. (11) is the apparent resistivity of the ground as measured by the surface electrodes. This value depends on

the apparent resistance ($\frac{V}{I}$) and the geometric factor *K* that accounts for the electrode spacing. This is the same situation as encountered in the simple resistivity example of equation (2). The stratification of the subsurface is brought into the equation through the geometric factor *K (Telford, et, al., 1990).*

2.12 Electrode Configurations

Electrodes are generally placed at arbitrary locations however, a number of electrode configurations have been used in recording resistivity field data, each suitable for a particular geological situation. The conventional arrays most commonly used include Wenner (alpha), Schlumberger, Wenner-Schlumberger, dipole-dipole, pole-pole and pole-dipole arrays. These arrays with their corresponding geometric factor are illustrated in figure below

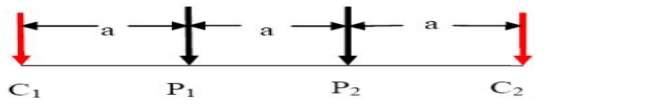

(a) Conventional Wenner (Wenner-alpha) array

$k = 2\pi a$

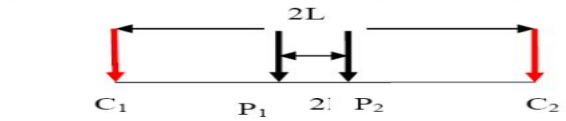

(b) Schlumberger array

$k = \frac{\pi L^2}{2l}$

$k = \pi n(n+1)(n+2)a$

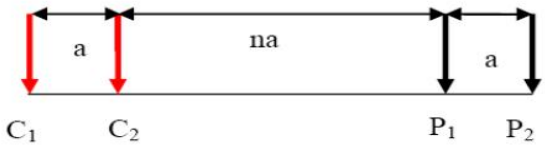

(c) Dipole-dipole array

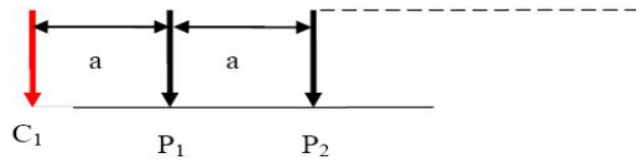

$C_2 \quad \infty$

$k = 4\pi a$

(d) Pole-dipole array

$P_2 \quad \infty$

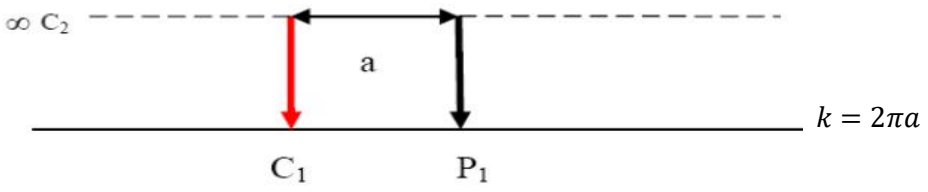

(e) Pole-pole array

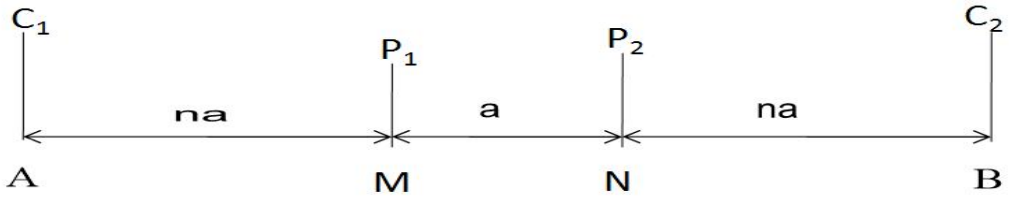

$k = n\pi(n+1)a$

(f) Wenner-Schlumberger array

Figure 2.5: Electrode configurations used in electrical resistivity surveys (Stummer et al., 2004)

2.12.1 Wenner array

This is a robust array that was popularized by the pioneering work carried out by the University of Birmingham research group (Griffiths and Turnbull 1985; Griffiths, et. al., 1990). Many of the early 2-D surveys were carried out with this array. The sensitivity plot for the Wenner array has almost horizontal contours beneath the centre of the array. Because of this property, the Wenner array is relatively sensitive to vertical changes in the subsurface resistivity below the centre of the array. However, it is less sensitive to horizontal changes in the subsurface resistivity. In general, the Wenner array is good in resolving vertical changes (i.e. horizontal structures), but relatively poor in detecting horizontal changes (i.e. narrow vertical structures) Loke, 2004. Compared to other arrays, the Wenner array has a moderate depth of investigation. The signal strength is inversely proportional to the geometric factor used to calculate the apparent resistivity value for the array (Figure 2.4). For the Wenner array, the geometric factor is $\mathbf{2\pi a}$, which is smaller than the geometric factor for other arrays.

Among the common arrays, the Wenner array has the strongest signal strength. This can be an important factor if the survey is carried out in areas with high background noise.

2.12.2 Schlumberger array

The Schlumberger array is similar to the Wenner array with respect to having a nested electrode configuration except the potential electrodes have an internal spacing of *a* and the current electrodes are spaced in an increased distance of *na* from the potential electrodes, where the integer value *n* varies dependent upon target size and depth. The geometric factor is **K = πn (n+1) a,** which can be shown to be just a modification of the Wenner array result. The Schlumberger array of electrodes provides for high signal-to-noise ratios, good resolution of horizontal layers, and good depth sensitivity. The Schlumberger technique is somewhat easier to use than the Wenner technique because only two of the four electrodes are moved between successive readings. As an example, we can conduct a Schlumberger VES survey by making the current electrodes spaced much further apart than the potential electrodes. In vertical sounding the potential electrodes remain fixed while the current-electrode spacing is expanded symmetrically about the center of the spread. For large values of *L* it may be necessary to increase *1* also in order to maintain a measurable potential. Only when the current electrodes become relatively distant does the potential electrode spacing need to be expanded in order to have measurable potentials.

2.12.3 Pole-pole array

This array is not as commonly used as the Wenner, dipole-dipole and schlumberger arrays. In practice the ideal pole-pole array, with only one current and one potential electrode, does not exist. To approximate the pole-pole array, the second current and potential electrodes *(*C_2 and P_2) must be placed at a distance which is more than 20 limes the maximum separation between C_1 and P_1 electrodes used in the survey. The effect of the C_2 (and similarly for the P_2) electrode is approximately proportional to the ratio of the C_1-P_1 distance to the C_2-P_1 distance. If the effects of the C_2 and P_2 electrodes are not taken into account, the distance of these electrodes from the survey line must be at least 20 times the largest C_1-P_1 spacing used to ensure that the error is less than 5%. In

surveys where the inter-electrode spacing along the survey line is more than a few meters, there might be practical problems in finding suitable locations for the C_2 and P_2 electrodes to satisfy this requirement. Another disadvantage of this array is that because of the large distance between the P_1 and P_2 electrodes, it can pick up large amount of telluric noise which can severely degrade the quality of the measurements. Thus this array is mainly used in surveys where relatively small electrode spacing's (less than 10 meters) are used. It has also been used for 3-D surveys (Li and Oldenburg, 1992).

2.12.4. Pole-dipole array

The pole-dipole array also has relatively good horizontal coverage, with higher signal strength compared with the dipole-dipole array. Pole-dipole is not sensitive to telluric noise unlike pole-pole. In pole-dipole array, it has asymmetrical array and over symmetrical structures. In some situations, the asymmetry in the measured apparent resistivity values could influence the model obtained after inversion. One method to eliminate the effect of this asymmetry is to repeat the measurements with the electrodes arranged in the reverse manner. By combining the measurements with the "forward" and "reverse" pole-dipole arrays, any bias in the model due to the asymmetrical nature of this array would be removed. The pole-dipole array also requires a remote electrode, the C_2 electrode, which must be placed sufficiently far from the survey line. Thus the pole-dipole array is less affected by the C_2 remote electrode compared with the pole-pole array. If the distance of the C_2 electrode is more than 5 times the largest C_1-P_1 distance used, the error caused by neglecting the effect of the C_2 electrode is less than 5% (the exact error also depends on the location of the P_2 electrode for the particular measurement and the subsurface resistivity distribution). Because it has a good horizontal coverage, this is an attractive array for multi-electrode resistivity meter systems with a relatively small number of nodes. The signal strength is lower compared with the Wenner and Wenner-Schlumberger arrays but higher than the dipole-dipole array. In short, if the survey is in a noisy area and a good vertical resolution is needed with limited survey time, the Wenner array is used. The reasonably good

horizontal and vertical resolution, the Wenner-Schlumberger array with overlapping data levels is used. When there is a system with insufficient number of electrodes, the pole-dipole array with measurements in both the forward and reverse directions might be a viable choice. For prospects, where small electrode spacing and good horizontal coverage is required, the pole-pole array might be a good choice (Loke, 2014).

2.13 2-D Electrical Imaging Prospect

The disadvantage of the resistivity sounding method is that it does not take into account horizontal changes in the subsurface resistivity In many situations, particularly for surveys over elongated geological bodies, this is a reasonable assumption. However, at the present time, 2-D surveys are the most practical economic compromise between obtaining very correct results and keeping the survey costs down (Dahlin, 1996).

In many geological situations, 2-D electrical imaging surveys can give useful results that are complementary to the information obtained by other geophysical method. For example, seismic methods can map undulating interfaces well, but will not be effective (without using advanced data processing techniques) in mapping discrete bodies such as boulders, cavities and pollution plumes. Ground radar surveys can give full pictures but have very limited depth penetration in areas with conductive unconsolidated sediments, such as clayey soils. Two-dimensional electrical surveys should be used in addition with seismic or ground-penetrating radar (GPR) surveys as they provide sufficient information about the subsurface (Stratton, 1941).

Figure 2.6 shows the typical setup for a 2-D survey with some electrodes along a straight line joined to a multi-core cable. Under a normal condition, a constant spacing between adjacent electrodes is used. One technique used to extend horizontally the area covered by the survey, particularly for a system with a limited number of electrodes, is the roll-along method. After completing the sequence of measurements, the cable is moved past one end of the line by several unit electrode spacing. All the measurements which involve the electrodes on part of the cable which do not overlap the original end

of the survey line are repeated. After reading the control file, the computer program then automatically selects the appropriate electrodes for each measurement. In a typical survey, most of the fieldwork is in laying out the cable and electrodes. After that, the measurements are taken automatically and saved in the computer (Dahlin and Loke 1998).

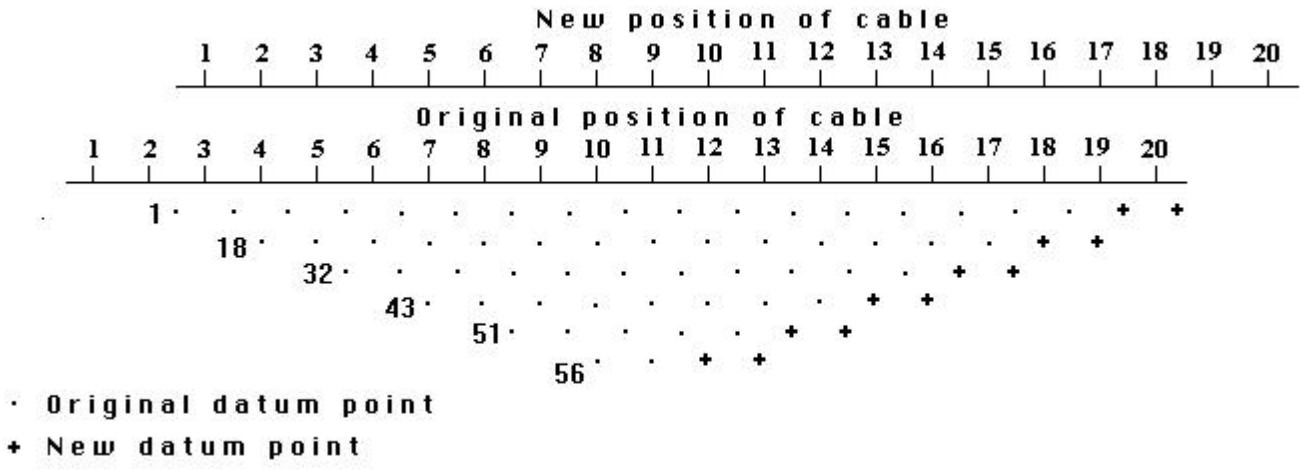

Figure 2.6: The use of the roll-along method to extend the area covered by a survey (Dahlin and Loke, 1998).

To plot the data from a 2-D imaging review, the area shaping technique is regularly utilized. In this case, the horizontal location of the point is placed at the mid-point of the set of electrodes used to make that estimation. The vertical area of the plotting point is set at a separation which is relative to the detachment between the terminals.

2.14 Guidelines for Data Inversion

The RES2DINV model is designed to operate, sufficiently, in an automatic and robust manner with minimal input from the user. It has a set of default parameters which guides the inversion process. In most cases the default parameters give reasonable results. The limitation of ingenuinety is common in the inversion of resistivity sounding and other geophysical data. For the same measured data set, there is broad range of models giving rise to the same calculated apparent resistivity values. To reduce the range of possible model, normally some assumptions are made concerning the nature of the subsurface

that can be incorporated into inversion subroutine in almost all surveys. Something is known about the geology of the subsurface in some cases. It is known whether the subsurface bodies of interest have gradational boundaries, such as pollution plumes or bedrock with a thick transitional weathered layer. In such cases the conventional smoothness constrained inversion method (DeGroot-Hedlin and Constable, 1990) gives a model which more closely corresponds with reality. This is the default method used by the RES2DINV program. In others, the subsurface might consist of discrete geological bodies that are internally almost homogeneous with sharp boundaries between different bodies. Examples are igneous intrusive in sedimentary rocks and massive ore bodies for such case, a robust model inversion constrain is more suitable most data sets probably lie between the two extremes of a smoothly varying resistivity and discrete geological bodies with sharp boundaries. Some geological bodies have a predominantly horizontal orientation (for example elementary layers and sills) while others might have a vertical orientation (such as dykes and faults). This information can be incorporated into the inversion process setting the relative weights given to the horizontal and vertical flatness filters if example the structure has a predominantly vertical orientation, such as a dyke, the vertical flatness filter is given an eater weight than the horizontal filter. Another important factor is the quality of the field data. Good quality data usually show a smooth variation of apparent resistivity value in the pseudo section. 1f the data is of poorer quality, with usually high or low apparent resistivity values, here are several things that could be done. The first step is to look at the apparent resistivity pseudosection. If there are sports relatively low or high values, they are likely to be bad datum points. With the RES2DINV program, you can also plot the data in profile form that helps to highlight the bad datum points, and remove them from the data set manually. If the bad datum points are more widespread and random in nation, two types of program inversion parameters that you can modify are: firstly, increase the damping factors. A bigger damping component would produce in smoother general models with less structure, and thus poorer resolution, however it would be less sensitive to uproaring information. The second setting is the robust data constrain option. The

inversion subroutine regularly attempts to decrease the square of the constrast between the measured and determined apparent resistivity values. Data points with a larger difference between the measured and calculated apparent resistivity values are given a greater weight. This normally gives acceptable results if the noise is random in nature. However, in some case, a few bad data points with unusually or high apparent resistivity values (outliers) could distort the results. To diminish the impact of such awful datum points, the robust data constrain causes the program to lessen the absolute difference between estimated and determined apparent resistivity values. The bad datum points are given the same weight as the other data points and thus their effect on the inversion results is considerably reduced.

2.15 DATA PROCESSING AND INVERSION

2.15.1 Inversion of 2D Data Set

The obvious resistivity information got over the arrangement of parallel 2D profile extricated from the 3D information, set were transformed independently utilizing 2D reversal code in both x and y directions that is in-lines and cross-lines (Loke and Barker, l996b). The 2D inversion was done in order to evaluate the nature of the 2D apparent resistivity information. The RES2DINV computer program uses a nonlinear optimization technique which automatically determines a 2D resistivity model of the subsurface for the input apparent resistivity data (Girffiths and Barker, 1993; Loke and Barker, 1996a). The program seperates the subsurface into various rectangular blocks and afterwards ascertain the apparent resistivity values that concur with the measured values using a forward modelling routine. The arrangement of the rectangular blocks is loosely tied to the distribution of the data points in the pseudosections. The inversion routine used by the program is based on the smoothness constrained least squares method (DeGroot-Hedlin and Constable, 1990; Sasaki, 1992). The optimization method then adjusts the resistivity of the model blocks and tries to reduce the difference between the measured and calculate apparent resistivity values using iterative procedure.

CHAPTER THREE

MATERIALS AND METHODS

3.1 Location Study: With the help of aeromagnetic and aero radiometric data obtained from NGSA, the study of the community was carried out for the purpose of reconnaissance study. This proceeded to identify the locations in the community where the study would be carried out.

3.2 Data acquisition: Two forms of data were used: Secondary and Primary data. The Secondary data include the Aeromagnetic data and Aero-radiometric data which were used basically for reconnaissance study. Primary data was acquired within the study area which is suspected to have high potential bitumen deposit.

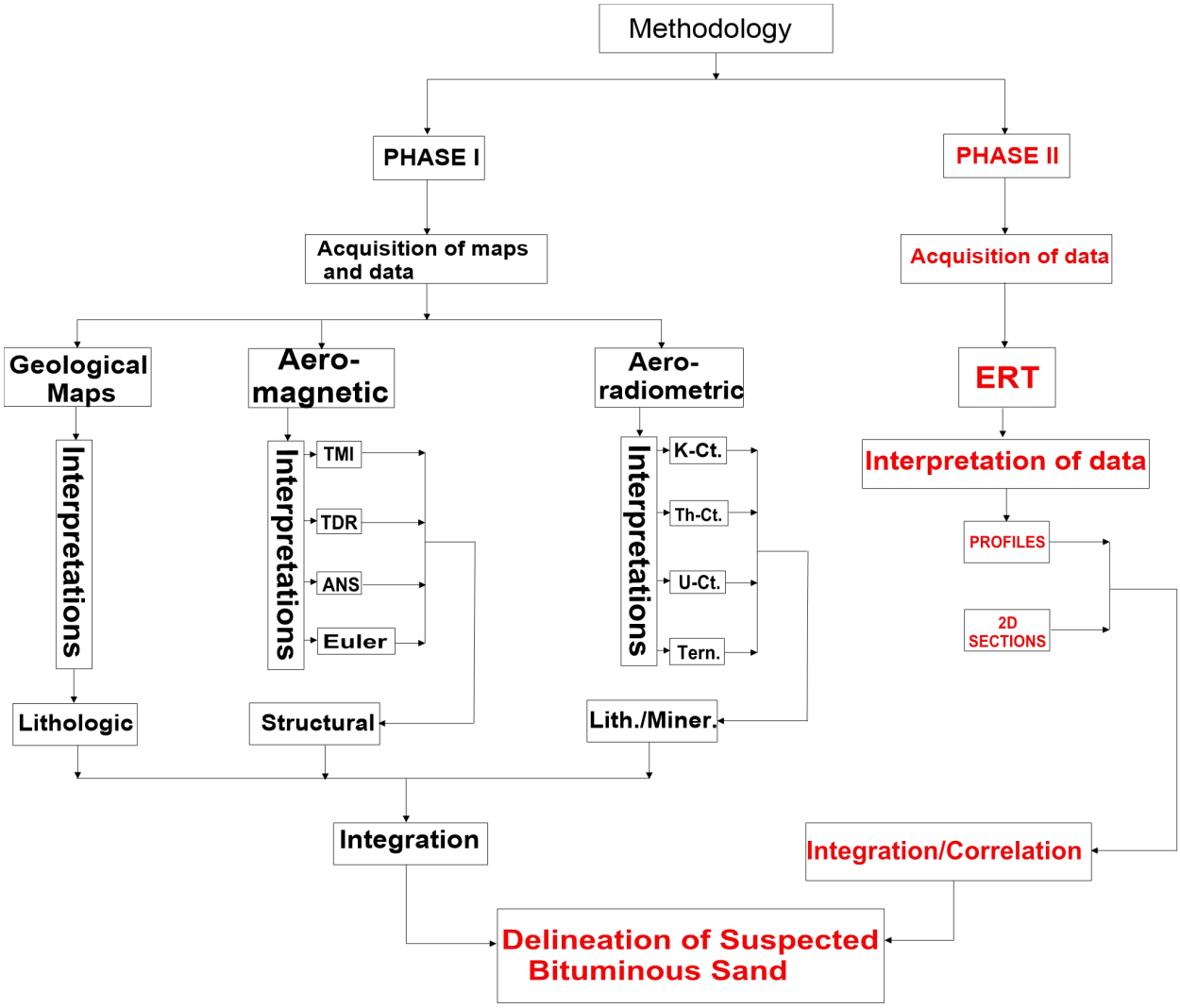

Figure 3.0: Research workflow chat

3.3 Data Specifications

The Airborne geophysical datasets namely aeromagnetic and aero-radiometric were obtained from the Nigeria Geological Survey Agency (NGSA), Abuja. A high resolution airborne data of 1:100,000 sheets 282 were used for this study. As part of a nationwide high resolution airborne geophysical survey aimed at assisting and promoting mineral exploration in Nigeria, aeromagnetic and aero-radiometric data were acquired simultaneously between 2004 and 2008 by Fugro Airborne Survey Limited for the Nigerian Geological Survey Agency (NGSA). The survey was carried out by fixed wing Cessna Caravan aircraft with a flight spacing of 500 meters and a terrain clearance of 80 meters. The flight direction was NW-SE with tie-line spacing of 5000 meters and tie-line direction of NE-SW. IAEA (1991).

The aircraft survey equipment was used to collect the geophysical information (Table 3.1).

S/N	DATA	SOURCE	DESCRIPTION
1	Aeromagnetic data	NGSA	The airborne magnetic data was acquired with Scintrex CS3 Cesium Vapor magnetometer which was flown on a fixed wing Cessna Caravan aircraft with a flight spacing of 500 meters and a terrain clearance of 80 meters.
2	Aeroradiometric data	NGSA	Very high quality aero-radiometric data that cover the study area were acquired from Nigerian Geological Survey Agency, Abuja (NGSA), which carried out airborne radiometric survey simultaneously with airborne magnetic between 2004 and 2008. The aero-radiometric data were acquired at a flight elevation of 80m, line spacing and tie-line spacing were 500m and 5000m respectively.
3	Satellite imagery	USGS	Shuttle Radar Topography Mission Digital Elevation Model (SRTM DEM) based on geographical coverage of longitude 1.70°E – 20.50°E and latitude 3.50°N – 14.10°N was downloaded from http://earthexplorer.usgs.gov/ and clipped to the extent of the study area which falls within longitude 4°5' and 5°45'East of the Greenwich meridian and latitude 7°15' and 8°5' north of the equator.

3.4 Data Processing

Geosoft (Oasis Montaj) and Surfer 10.0 (Golden Software) were the major softwares used to process and enhance the airborne geophysical data. These methods applied were involved in the acquisition of two different Geophysical Airborne data sets (magnetic and radiometric), building of databases (projects), data processing and interpretation. This part presents a summary of the airborne data processing methods. These methods include the orderly editing processes, the gridding method application and taking away of the Earth's magnetic background field.

The Nigeria Geological Survey Agency (NGSA) made some corrections like removing diurnal variations of the magnetic field of the Earth, aircraft heading, instrument variation, lag error between aircraft and the sensor and inconsistencies between flight lines and tie lines. The second phase consists of four procedures:

a) Gridding

b) Estimating the residual magnetic field by subtracting IGRF from total magnetic data measured from the field

c) Any forms of errors from data set was removed through micro-levelling and

d) Integrating the series windows for each different type of data.

Airborne geophysical dataset was enhanced for better interpretation using a series of linear and non-linear filtering.

Mathematically enhanced algorithms were used to evaluate a wide range of processing techniques that can be used to improve the effects of the selected geological host rocks (Milligan and Gunn, 1997; Geosoft Inc., 1995). The discussions below show the effects of some of the applied algorithms.

3.5 Aeromagnetic Data

Even though the magnetic survey has been used extensively in mapping of mineral deposits for decades, modern advancement in acquiring magnetic data, processing and interpretations have amplified the significance of magnetic methods; predominantly the high resolution aeromagnetic survey (Clark, 1997).

The original data in the GDB (Geodata base) format, after having been projected into Longitude and Latitude Coordinate System (using Geosoft software), the geographical coordinates of the study area (also in longitude and latitude) was superimposed to extract the database for this project. The minimum curvature technique was applied using the grid and image tool in gridding the extracted database for both the radiometric and magnetic data. The magmap tool offering a number of utilities

was implemented to assist magnetic-anomaly grid (observed magnetic field less the Definitive International Geomagnetic Reference Field) to be calculated for the right time of year and altitude of the aircraft during survey and apply the following filters.

Magnetic variations in the magnetic field of Earth originate from the iron II oxide concentration in the localized rocks and the geological interpretation of these anomalies are made easier with the help of resulting images and maps (Liu and Mackey, 1998). Once a grid was produced and the necessary filters applied it was displayed as an image using the grid and image tool. Thereafter, the tilt derivative, apparent susceptibility and 3D-Euler deconvolution filters were laid to further lift the dataset.

3.5.1 Analytic Signal Amplitude

The analytic signal amplitude was estimated using the actual (left over) magnetic field. The analytic signals filter is not dependent on the geomagnetic field direction (inclination and declination) of the host body. High analytical signal amplitudes are recorded around areas of large mineral deposits (Liu and Mackey, 1998).The analytic signal grid is computed from the existing derivative grids. It is the square root of the sum of the squares of the derivative in the x, y, and z directions.

Analytic Signal =$\sqrt{\partial x * \partial x + \partial y * \partial y + \partial z * \partial z}$.

To locate the edges of magnetic source bodies, Analytic signal was used particularly where remanence and/or low magnetic latitude complicates interpretation (Geosoft, 2010). This filter gives a representation of the magnetic anomaly of the causative body which depends on the location of the body (horizontal coordinate and depth) and not on its magnetization direction (Debeglia and Corpel, 1997). This technique when applied to the TMI data helps to clearly display the edge extent and contacts between the different formations within an area.

3.5.2 Tilt Derivative

Tilt derivative tool is a generalized local phase tool. When applied to a residual magnetic field, it strengthened the weak magnetic anomalies overshadowed by responses from magnetic structures. A good estimate of location and depth of magnetic sources can be achieved by applying the Tilt angle calculation to a pole reduced grid of magnetic intensity. The tilt derivative method is extensively used in magnetic data processing to delineate both deep-seated and shallow structures. This approach assumes the source to be a buried vertical contact model. The zero contours indicate the location of source edges and the half distance between the – 45^{o} and + 45^{o} contours provides an estimate of the depth to top of the buried contact. The calculation of tilt derivative has an option to calculate the total horizontal derivative of the tilt derivative grid. The tilt derivative and total horizontal derivative are used for mapping shallow basement structures and mineral exploration targets (Geosoft, 2010). Edged detection filters are normally applied to delineate linear features without necessary diminishing the long wavelength anomalies (Oruc and Selim, 2011). For this reason, the Tilt derivative (TDR) filter, (a very good edge detection filter) was applied to bring out short wavelength and reveals the presence of magnetic lineaments.

Tilt derivative is calculated using the relation below:

$$TDR = \tan^{-1}\left(\frac{VDR}{THDR}\right)$$

where VDR and THDR are the first vertical and horizontal derivatives of the total magnetic field intensity (TMI) respectively. For clarity: VDR $= \frac{\partial T}{\partial Z}$, THDR $= \sqrt{\left(\frac{\partial T^2}{\partial x}\right) + \left(\frac{\partial T^2}{\partial y}\right)}$ and HD_TDR $= \sqrt{\left(\frac{\partial TDR^2}{\partial x}\right) + \left(\frac{\partial TDR^2}{\partial y}\right)}$.

3.6 Aero-Radiometric Data

This data helped to map lithology of the area. Most often, a better relationship is recognized in the radiometric data around rocks that are weathered and unweathered. These data when correlated with

that of electrical resistivity tomography, electromagnetic, magnetic and geochemical are usually helpful in the explorations of mineral deposits (Gunn *et al.,* 1997; Shives *et al.,* 2000).

Aero-radiometric method is one of the most rapid for soil chemistry surveying of the uranium, thorium and potassium. This part explains some enhancing techniques of the radiometric data which include ternary, Ratio, Potassium, Thorium and Uranium maps for the study area. The purpose of enhancing the data is to identify and interpret signatures related with the source rocks for potential bitumen.

3.6.1 Total Count (TC), Potassium (K), Thorium (Th) and Uranium (U) Channels

By using the grid and image tool in Geosoft software, the total count image was produced after micro-levelling the entire dataset to get rid of any apparent residual errors. These images were generated by using mini-curvature gridding since the data were collected in grid window. The images were then related with the geological units, patterns and trends.

The potassium image was developed to identify regions of strong potassium concentration.

Thorium is usually considered as a stable element which does not move easily. However, several deposits of gold depict increases in potassium and thorium which suggest that thorium was moved during hydrothermal activities (Silva et al., 2003). Reduction in thorium and increase in potassium shows a signs of alteration for most deposits of ore (Ostrovskiy, 1975). It is for this and many more reasons that led to the developing of the Th image map.

The uranium image especially ratio map of uranium to potassium (U:K) shows good definition in mapping the granitoid rocks which show low uranium but high potassium concentration.

3.6.2 Composite Images and Ratio Maps

The radioelement composite image presents a single display of the three radioelement concentrations. This map suggests to a great extent the lithological differences due to the variations in colour. The uranium, thorium, and potassium maps emphasize regions where the specific radioelement has a total and pretty higher amount (Elawadi *et al.,* 2004).

Uranium, potassium and thorium were represented with blue, red and green respectively in generating the ternary map. In order to minimize the poor signal-to-noise ratio especially in the uranium concentration the blue colour was used. The maps discussed in the chapter four were generated with the relative intensities of colour to represent slight differences caused the rock types. To enhance the contrast of the histogram of potassium, thorium and uranium a histogram was used to present the finest colour differences prior to generating the ternary map.

Nevertheless, for this research, the ternary image generated demonstrated a better outcome.

In order to get rid of lithological differences and variations caused due to soil moisture, non-planar nature of the host rock and errors related with altitude correction, ratio images were as well produced. According to Silva et al. (2003), lithological variations have a tendency to be removed because radioelement amounts normally change as lithology change. For example U/Th and U/K ratios were created for locating the areas where relative amount of uranium are strong.

3.7 Interpretation of Airborne Geophysical Data

The different lithologic units and associated geological structures were deduced from the aeromagnetic and airborne radiometric datasets covering the Agbabu area by considering the signatures that are associated with these features. Usually, lithologic units of sedimentary, metamorphism, igneous and geological processes such as deformational tectonic geological structures (fault, folds and other lineaments) produces distortion on a uniform magnetic and radiometric signal. These deformations thus assist in the interpretation of geological structures and various lithologic units in the study area.

The major geological unit boundaries and structures outlined along with the magnetic signatures and their boundaries coinciding with regions of increasing contrast in intensities of the geophysical data. The major litho-stratigraphic unit of the area and the sequence of geological events (intrusion, deformation) were used to establish the tectonic framework to aid geology and structure mapping.

High magnetic anomalies associated with low K concentrations were used to map metavolcanics. High K concentrations associated with moderate magnetic anomalies were used to map the weathered granitoids. Meta-sedimentary rocks typically have a layered magnetic response, largely composed of linear magnetic anomalies. Planar fracture or discontinuity in geophysical signatures associated with the various lithological units, across which there has been major displacement along regions of weakness as a result of tectonic movement and undulating lineaments resulting from permanent deformation were used to delineate faults and folds respectively. Local separation or discontinuity plane in magnetic signatures about which there are no displacement were used to delineate fractures. Discontinuities that mark distinct terrains which involve rock deformation at the edges of lithologic tectonic units and corresponding to anomalous low Th/K ratio were used to mark shear zones.

Hydrothermally altered zones are often associated with elevated K. The reason is that K becomes more receptive in shear zone due to the breakdown of feldspars, biotite and muscovite in clay minerals. High structural connectivity and areas reflected by low magnetic anomalies were of much importance. In regions where the two coincide and are also marked by faults, fault intersections, fractures and shear zones were used to map alteration zones due to the possibility of hosting hydrothermal fluids as a result of the intense permeability. The integration of hydrothermally altered zones and delineated structures were used to generate potential bitumen zones in the area.

3.8 Field Procedures

Total numbers of five (5) traverses were obtained in the study area close to the existing bitumen. The electrode spacing of 5m was adopted and the profile of 150m length for each traverse. The electrical resistivity data acquisition method used in this study involved setting out Wenner-Schlumberger electrode configurations. Current was sent to the ground through a pair of current electrodes, the injected current flow through the earth and create potential difference across the two potential electrodes. The generated potential difference was calculated with the aid of PASI 16 GL-N Earth

resistivity meter. High integrity data (r.m.s. < 5 %) which approximate the apparent resistivity of the subsurface layers were obtained by integrating the geometric factor of the electrode configuration used.

3.9 Field Equipments

The necessary equipments for data acquisition include: PASI 16 GL-N Earth resistivity meter, electrodes (31 stainless steel metallic electrodes were used. Current was injected into the ground through two current electrodes, the injected current flow through the earth and generates potential difference across two potential electrodes. Cables made up of multi-strand copper wires insulated with polyvinyl chloride (PVC) (these were connected to the electrodes and the resistivity meter. It was used to transmit and receive current), PVC Tape for taking distance measurement, global positioning system (GPS) for location marking and topographical heightening of the traverse points, Hammer to drive the electrodes into the ground to ensure firm contact and spare multi-meter for error detection. The pictures of the field activities showing in **Appendix**

3.10 Wenner-Schlumberger array (array type adopted for this research)

This is a new hybrid between the Wenner-Schlumberger arrays (Pazdirek and Blaha, 1996) arising out of the relatively recent work with electrical imaging surveys. The classical schlumberger array is one of the most commonly used arrays for resistivity sounding survey.

The "n" factor for this array is the ratio of the distance between the C_1 — P_1 (or P_2 — C_2) electrodes to the spacing between the P_1 — P_2 potential pair. The sensitivity pattern for the Schlumberger array is slightly different from the Wenner array with a slight vertical curvature below the center of the array, slightly lower sensitivity values in the regions between the C_1 and P_1 ($P_2$and C_2) also and electrodes. There is a slightly greater concentration of high sensitivity values below the P_1 — P_2 electrodes. This means that this array is moderately sensitive to both horizontal and vertical structures. In areas where both of geological structures are expected this array might be a good compromise between the Wenner and the dipole-dipole-array. The median depth of investigation for this array is about 10% larger than

that for the Wenner array for the same distance between the outer (C_1 and C_2) electrodes. The signal strength for this array is smaller than that for the Wenner array, but it is higher than the dipole-dipole array (Loke, 2014). The Wenner-Schlumberger array has a slightly better horizontal coverage compared with the Wenner array. For the Wenner array each deeper data level has 3 data points less than the previous data level, while for the Wenner- Schlumberger array there is a loss of 2 data points with each deeper data level. The horizontal data coverage is slightly wider than the Wenner array, but narrower than that obtained with the dipole-dipole array.

CHAPTER FOUR

RESULTS AND DISCUSSIONS

Airborne geophysical datasets were employed to interpret the geology structure and alteration zones in the study area. The airborne datasets were used to create high resolution maps that depict main lithology and structural features present in the Agbabu area. These maps were presented in order to identify:

- bitumen deposit zones and
- delineate geological features

Area showing with high signature of the radiometric elements count and coincides with low magnetic intensity and/or high analytic signal are suspected high potential for bitumen deposits. This may occur from alterations or possible invasion by hydrothermal fluids which are capable of containing mineral deposits.

4.1 Interpretation of Magnetic Data

Magnetic variations in the geomagnetic originate from the iron II oxide concentration in the localized rocks and the geological interpretation of these anomalies are made (Silva *et al.,* 2003). The main reason of using the magnetic data is to identify the geological features within the study area.

4.1.1 Total Magnetic Intensity (TMI) Image

The total magnetic intensity map of the study area shown in figure 4.2 was gridded with minimum curvature method and shown with Red-Green-Blue (RGB) colours. The amplitude of a magnetic anomaly relies on magnetization which subsequently corresponds to the magnetic susceptibility of the rocks at specific geographical locations. The amplitude of a magnetic anomaly depends on magnetization which subsequently corresponds to the magnetic susceptibility of the rocks at specific geographical locations. The original Total Magnetic Intensity (TMI) was processed and filtered to enhance weak, small-sized magnetic anomalies from shallow sources and at the same time enhancing

low-amplitude, long-wavelength magnetic anomalies from deeper sources. The total magnetic intensity map is characterized by the presence of high and low magnetic intensity. At low latitude, the rocks formation areas are magnetized in the same direction as the earth of the magnetic field. Therefore, a good number of the high magnetic susceptible regions show low magnetic value while less magnetic susceptible areas also show high magnetic values. Magnetic anomalies are generally high (47.8 – 91.3 nT) around the southern, south-western, western, eastern and north-eastern regions, while the low intensity anomalies (-201.5 – 23.4 nT) occur mainly around the central and south-eastern area where bitumen deposit occur. Aeromagnetic maps reveal major structures such as magnetic dykes, ridges and depressions, linear to curvilinear features and the overall basement characteristics. Figure 4.3 is a contour map of the TMI map shows interval of 10m. Total Magnetic Intensity reveals the rock contacts, structures and trends. The lineament (faults and joints) systems were identified on this image by observing the abrupt changes between the positive and negative magnetic anomalies. The lineament systems are: F1, F2 and F3 with NE-SW, ENE-WSW, and NE-SW trends respectively.

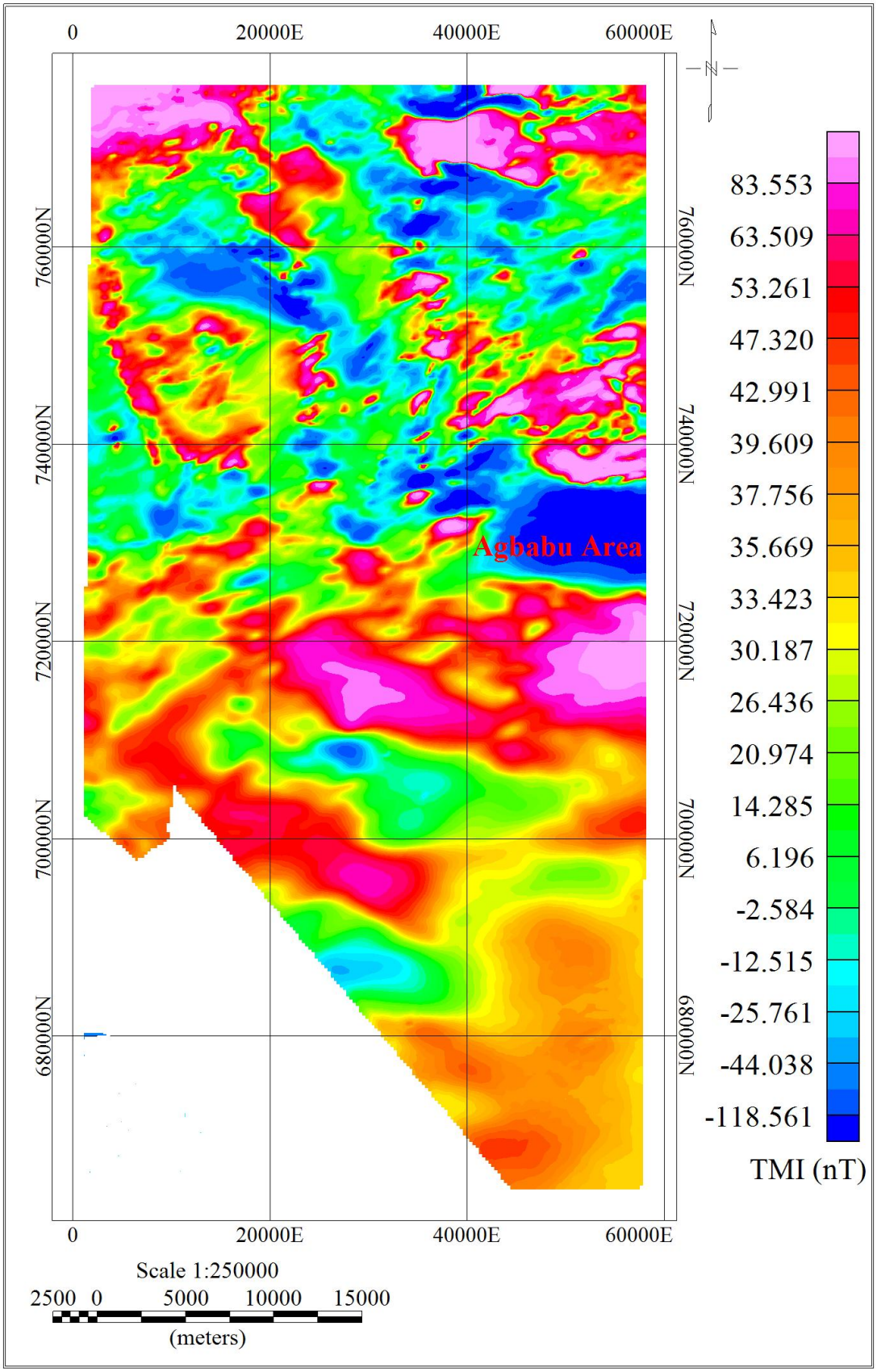

Figure. 4.1: Total Magnetic Intensity Map of Sheet 282 and 296 (Okiti-Pupa and Mahin Sheets)

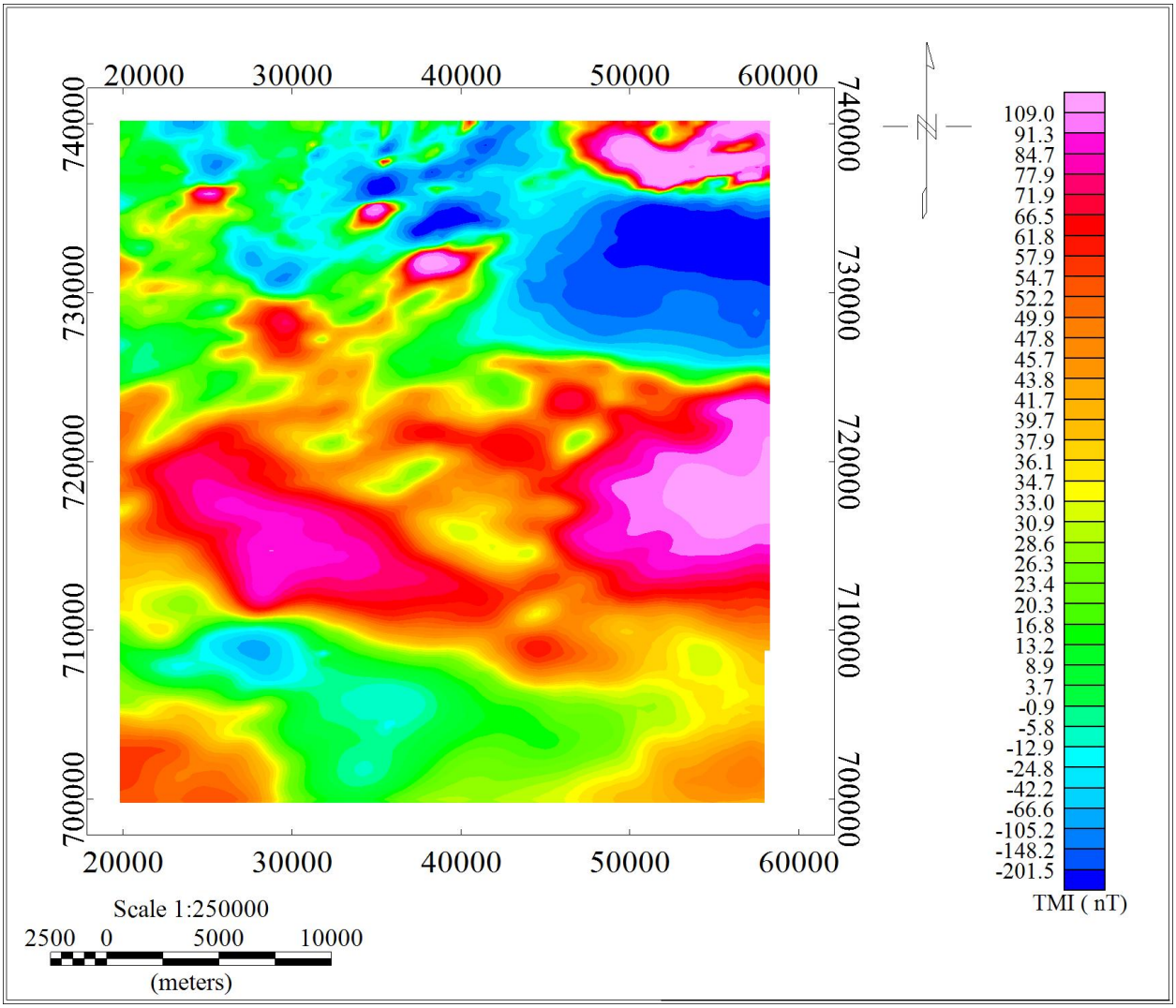

Figure 4.2: Total Magnetic Intensity Map of the study area.

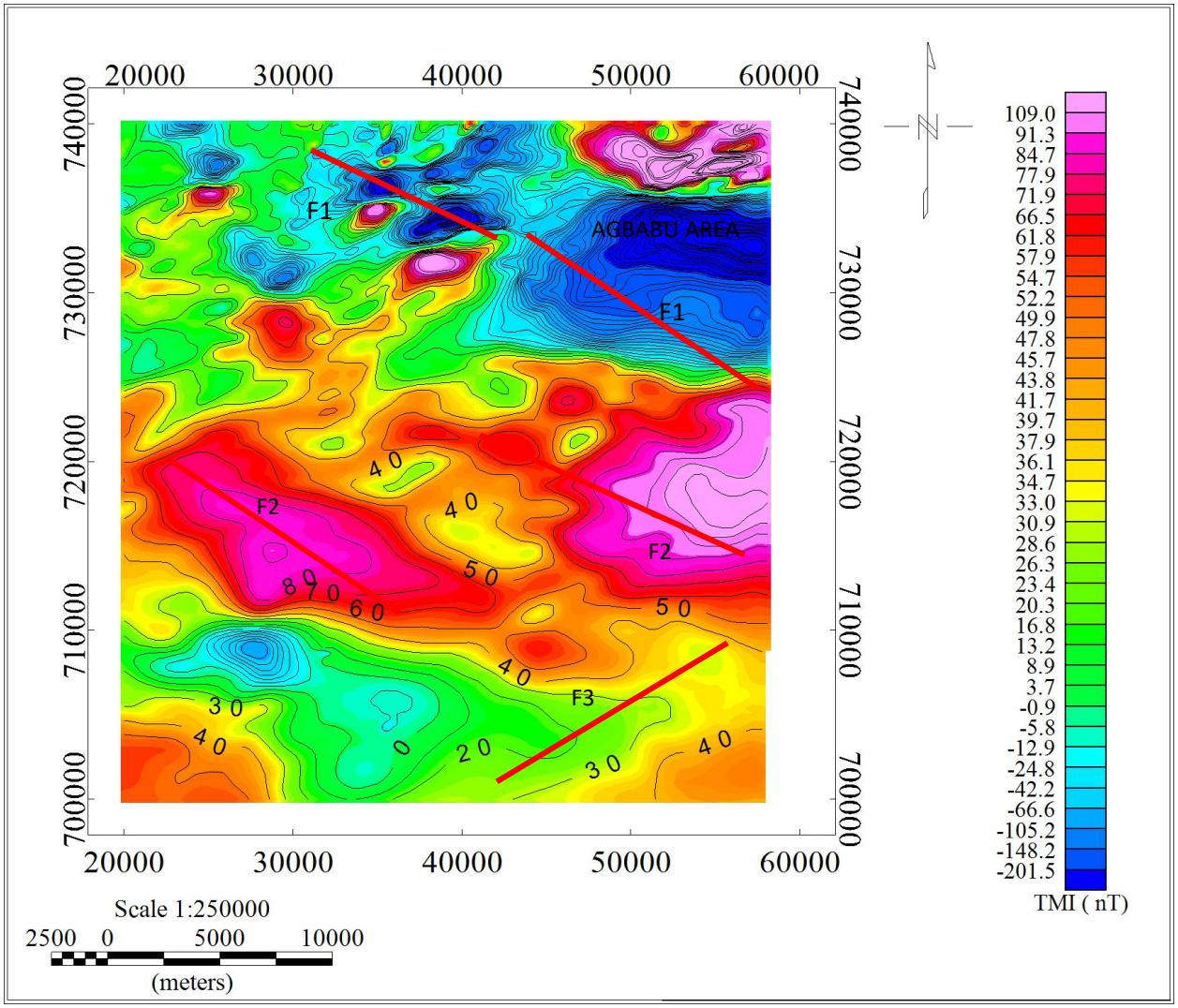

Figure 4.3: Contour Map of the TMI map

4.1.2 Analytic Signal Grid

A significant feature of the analytical signal is that it does not depend on the magnetization field of the source rock. Areas with mineral deposits or concealed geologic features usually show high analytical signal amplitudes. This shows that analytical signal amplitude depends on the magnetic amplitude of the causative body (Nabighian, 1972; Roest and Pilkington, 1993). Figure 4.4 was created from the total magnetic intensity (TMI) by using the analytic signal filter. Applying this filter, the dominant NE-SW trend of geologic features producing magnetic anomalies was clearly mapped and recorded as having low magnetic susceptibilities values.

Analytic signal filter which was connected to the TMI data helps to clearly define the edge of magnetic anomaly sources such as lithological contacts and other concealed geological features within the study area (Debeglia and Corpel, 1997, Oruc and Selim, 2011). The trends of structural features producing magnetic anomalies are generally oriented in an approximately NE-SW direction

These anomalies are caused by deep-crustal, sub-crustal and shallow (intra-basement) subsurface magnetic sources. The variation in the amplitudes of the analytic signal map (figure 4.4) shows the spatial distributions of causative magnetic source bodies within the study area. High amplitudes (0.053 – 0.172 nT) are recorded around the northern, eastern, central and south-eastern part of the study area, while the remaining part exhibit low (-0.088 – 0.027 nT) response.

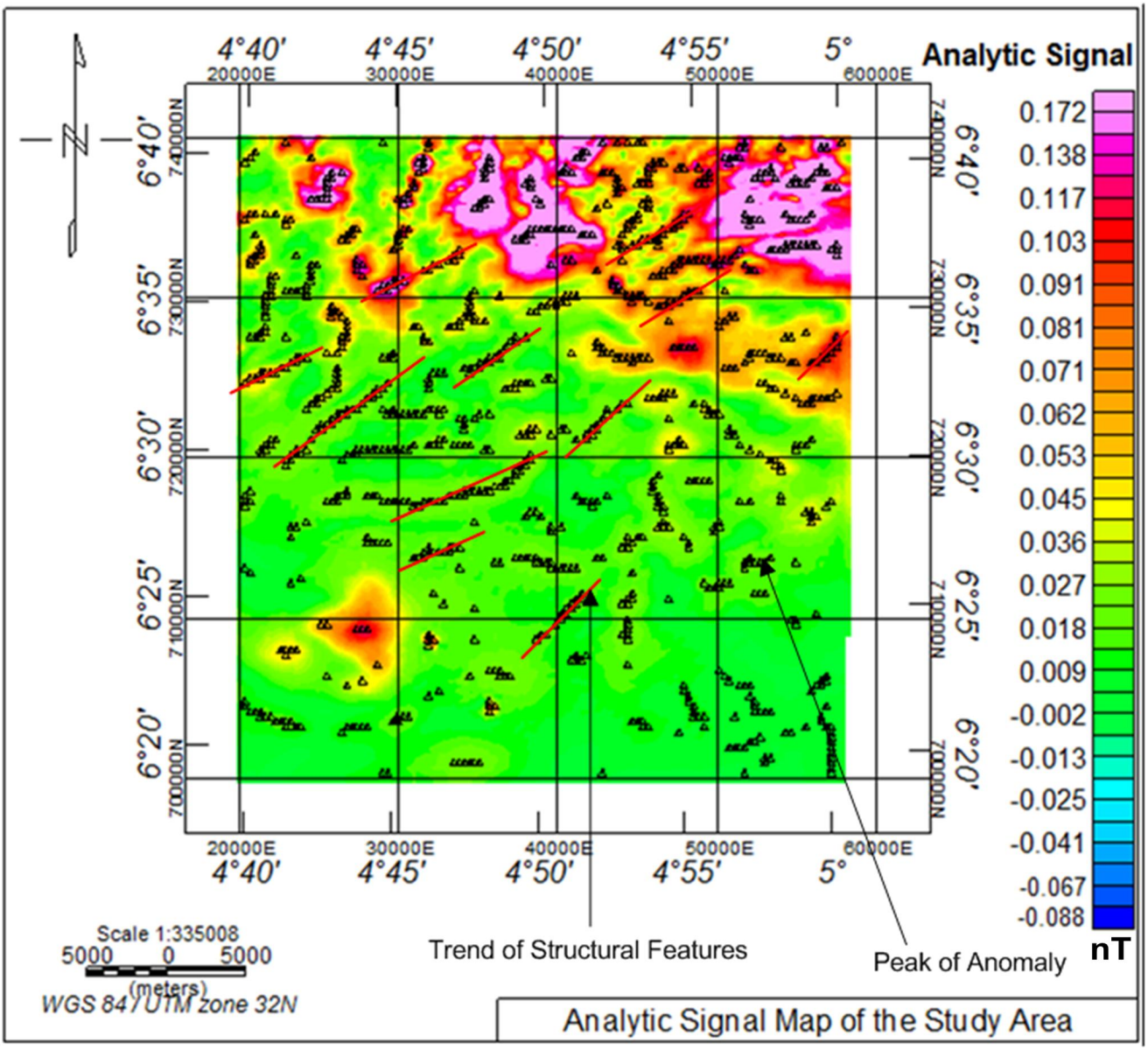

Figure 4.4: Analytic Signal magnetic map

4.1.3 Tilted Derivative (TDR) Map

The structures seen in the analytic map (figure 4.4) as high analytic signal amplitude are now identified in the TDR map (figure 4.5) as low magnetic anomalies. Tilt angle derivative (TDR) locates the edges of formations, using the theory that the zero contours are the edges of the formation (Salem *et al.,* 2007). The TDR shows the presence of large concealed structure suspected to be basement depression which host bitumen deposit where the response is low (-1.4to - 0.4 nT). Tilt Derivatives (TDR) reveal the rock contacts, structures and trends. The lineaments/faults are marked in red ticks while lithological trends are seen in varying trends and arched. The lineaments/faults were classified as Four (4) lineaments (faults and joints) systems were identified on this image by observing the abrupt changes between the positive and negative magnetic anomalies. The lineament systems are: as F1, F2, F3 and F4 trending NNE-SSW (including approximately N-S trend), minor (ENE-WSW and E-W), NE-SW, and NW-SE respectively.

4.1.4. 3D-Euler Deconvolution Map

The peaks of the anomalous bodies are located with an arrow symbols and was further enhanced with the 3D-Euler deconvolution map to determine the depth to top of the magnetic source across the area.

It enhances both weak and strong magnetic anomalies associated with geological structures of the area. It reveals locations and depths to source of magnetic anomalies which ranges from 1703 – 185m within this study area (Figure 4.6). The solutions were produced by selecting structural index of 1.0 for the map. The depth to top of magnetic anomaly within the metasediment (where Agbabu is located) ranges between 841 – 1703m but shallower (185 – 841) within the Basement region. The depth to basement within Agbabu area (1459 – 1703m) is more than the surrounding area.

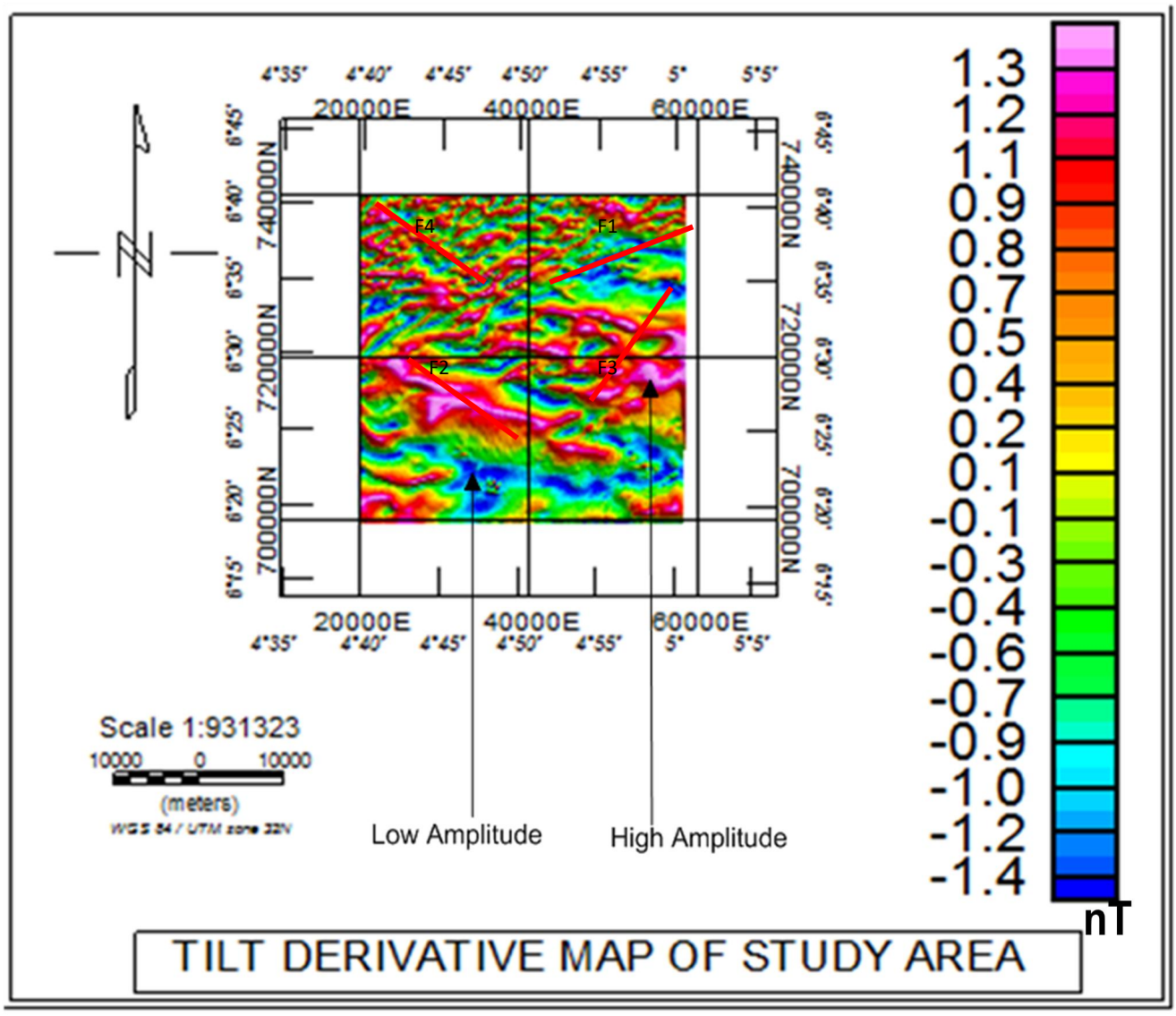

Figure 4.5: Tilt Derivative Map of the study area.

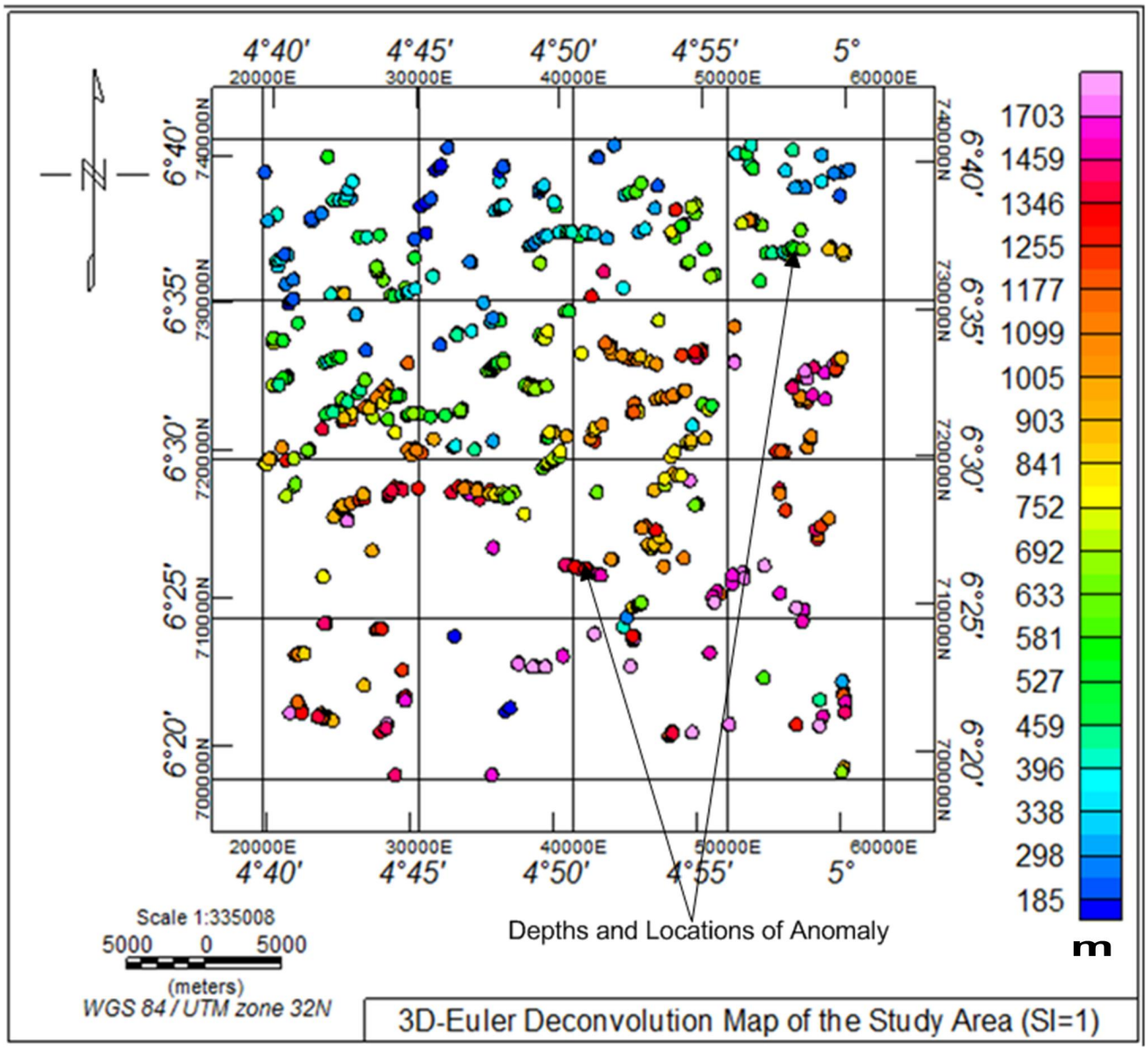

Figure 4.6: 3D-Euler Deconvolution Map of the study area.

4.1.5 3D-Euler and Tilt Derivative Map

The TDR filter enhances geological structures of the area (figure 4.7). In this map, the Euler deconvolution solution was superimposed on the TDR map to visualize their degree of correlation. There is high level of correlation, as most of the Euler solutions fall within areas delineated as having low magnetic response. These are areas suspected to have high potential for deposits of minerals such as bitumen.

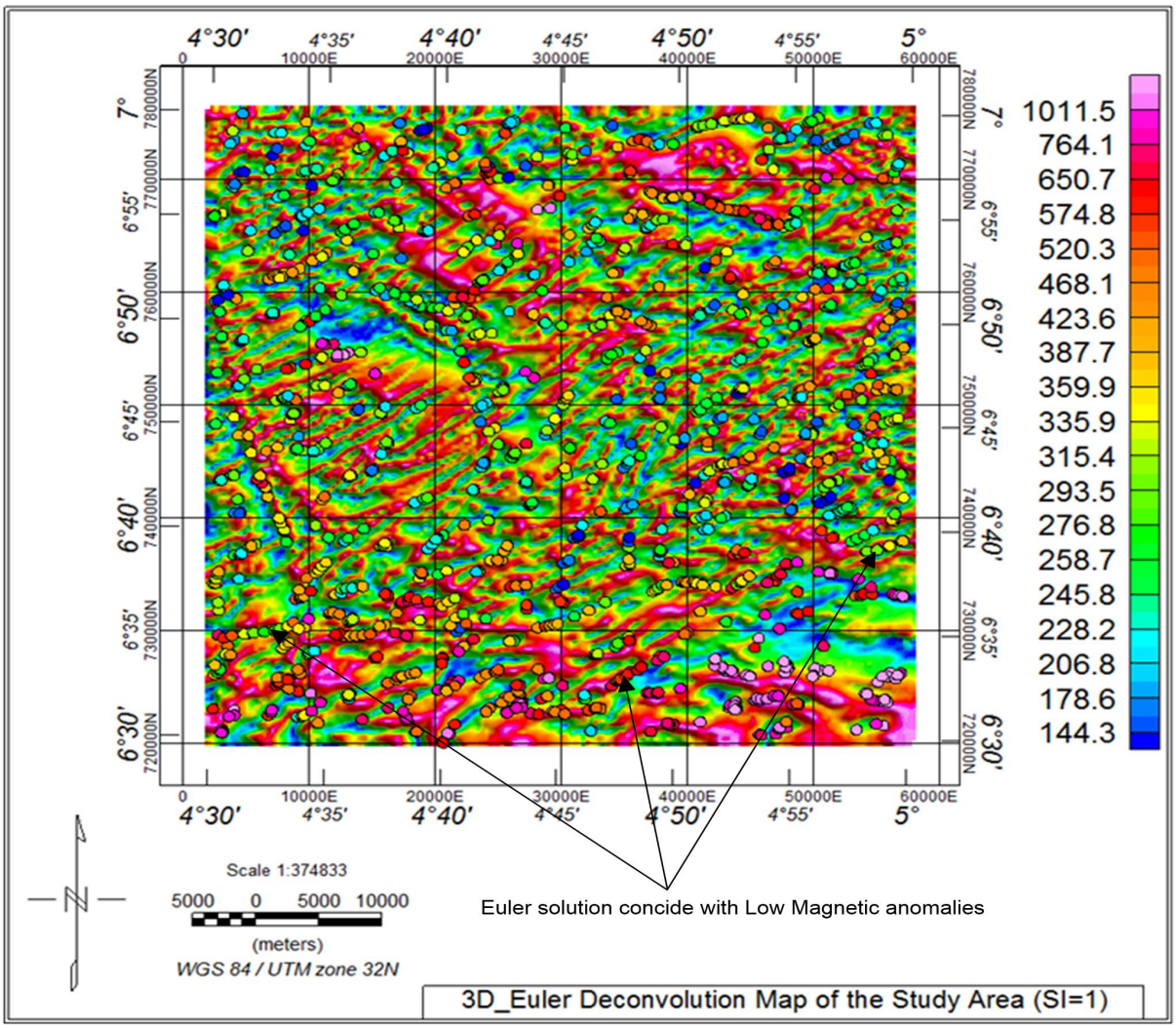

Figure 4.7: 3D_Euler and Tilt Derivative Map

4.2 Interpretation of Radiometric Data

The contrast in the content of the mineral of surface geology can be better explained using the radiometric survey information, which is also useful in outcropping lateral lithologies. Airborne radiometric surveys determine concentration of gamma radiations resulting from the mineral forming rocks (Telford *et al.,* 1990). These gamma radiations consists thorium (Th), potassium (K) and uranium (U) which are present as trace elements in the soil and naturally breakdown to emit the gamma radiations. The gamma ray spectrometer is used to measure the gamma ray emissions; also the individual energy levels of the associated radionuclide are established. This information about the energies of the radionuclide was helpful in the mapping of the lithologies by determining if a spatial correlation exists between the radiometric observations and lithological rocks.

4.2.1 Potassium (K) Channel

The radiometric survey data produced the various potassium (K), uranium (U) and thorium (Th) anomalies. Figure 4.8 shows the potassium concentration map in percent (%). The high % K concentration implies rocks that are highly rich potassium bearing-minerals such as feldspar and on the other hand shows that the rocks are less weathered, as well as with less structural deformities, which include muscovite and biotite (Boadi *et al*., 2013). Conversely, the low % K concentration usually indicates rocks with low potassium bearing-minerals, high weathering and intense meta-morphism, which led to the patches/pockets of high concentration seen in most parts of the southern section of the area. It is wide spread in the felsic breccias of the metasediments (MS), but are weak in mafic metavolcanic (MV) series (Manu, 1993); thus, the weak K anomaly in the metavolcanics (MV). Comparing figure 4.8 to the TMI map (figure 4.2) the K concentrations is generally high (0.6 – 2.5 %) within the Basement complex (i.e. metavolcanic formations) over a wide area in the north, northeastern and northwestern section of the areas, but relatively low (0.0 – 0.6%) within the metasediment (i.e. sedimentary terrain) over a wide areas in the southern and southeastern and

southwestern parts which host the bitumen deposit. The deep-seated fault (F) at the northern part (Agbabu) has contributed immensely to the low % K concentration due to the accumulated fluid (bitumen) of less rich potassium minerals within a likely depression (D) created by the hanging-wall of the fault. The map has also been able to reveal the strike directions of the minerals to be trending generally in NW-SE direction, but some of the rocks still trend NE-SW, NS, NNW-SSE, and there are fewer rocks trending NNE-SSW directions.

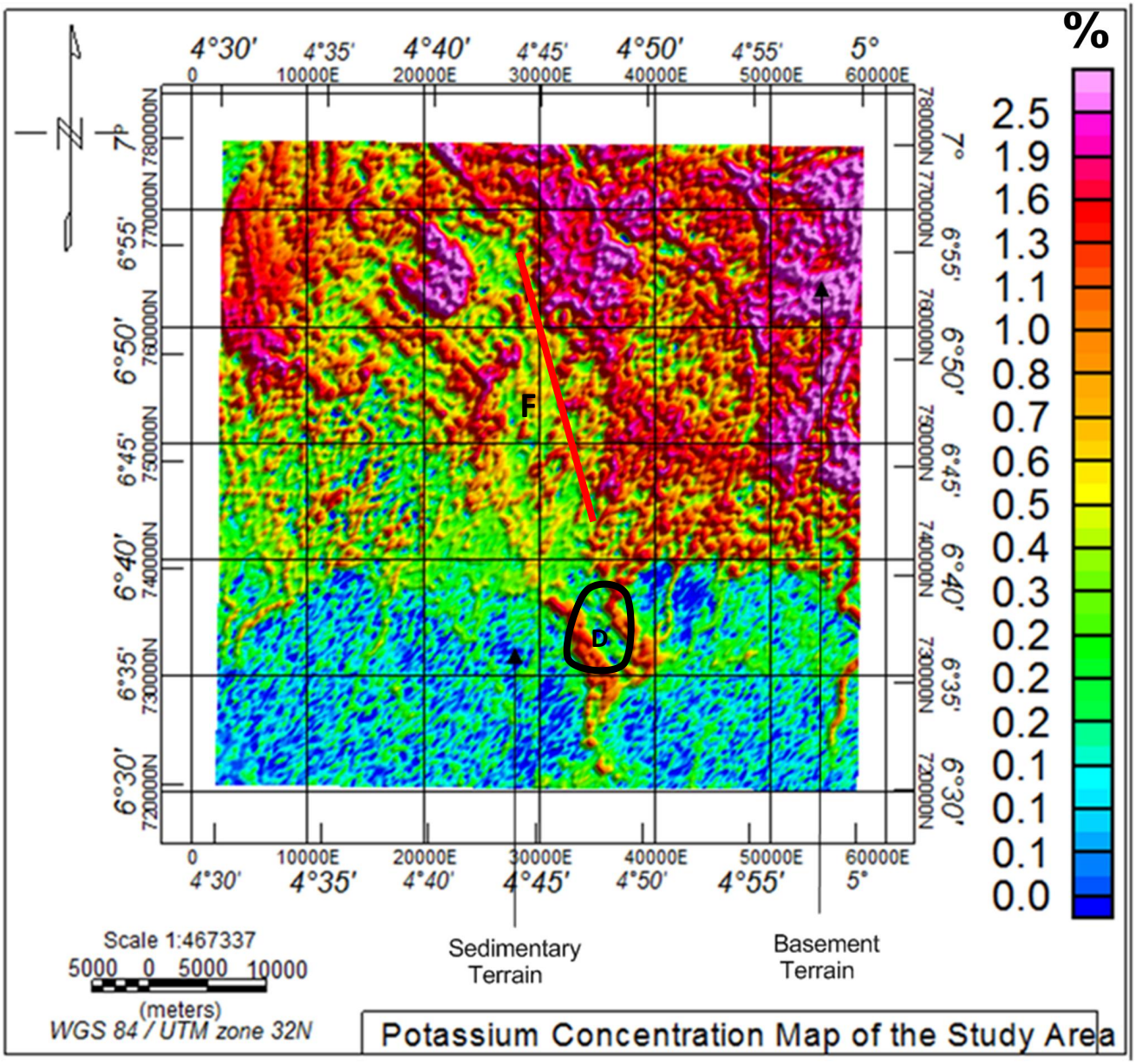

Figure 4.8: Potassium (K) Concentration Map of the Radiometric Data

4.2.2 Thorium (Th) Channel

Anomalies in the thorium data in figure 4.9 shows Thorium (Th) concentration map in parts per million (ppm), helped to separate basement and the sedimentary terrains. The north, northwest and northeast regions of the study area produced the highest thorium concentrations (7.9 – 28.0 ppm) corresponding to rocks bearing-rich thorium minerals such as thorite, zircon etc., and are related partly with the basement regions. The sedimentary basin which is the south, southwest and southeast regions also produced low intensities of immobile and mobile Thorium (Silva *et al.,* 2003). From the map, it can be clearly seen that the southeast region has a very low concentration of thorium (1.8 – 9.2 ppm) which shows the depth to the basement rock is very high. In addition, the low concentration ranged from 1.8 -9. 2 ppm representing intra-basement structures such as faults (F) and lineaments (R-R). Less than 4.0 ppm is considered as very low Th and is attributed to in-filled geologic materials such fluids (Bitumen) that are not thorium-rich, while the yellowish color de-notes the edges of the anomalous bodies. However, the high anomaly on Th map compared with depleted of U map in the northern parts is due to the resistive nature of thorium-rich bearing-minerals to weathering. Interestingly, Th radiation observed in the study area clearly differentiates the lithology, regional lineament, and faults, as well as identifies the degree of weathering and areas rich in thorium bearing-minerals.

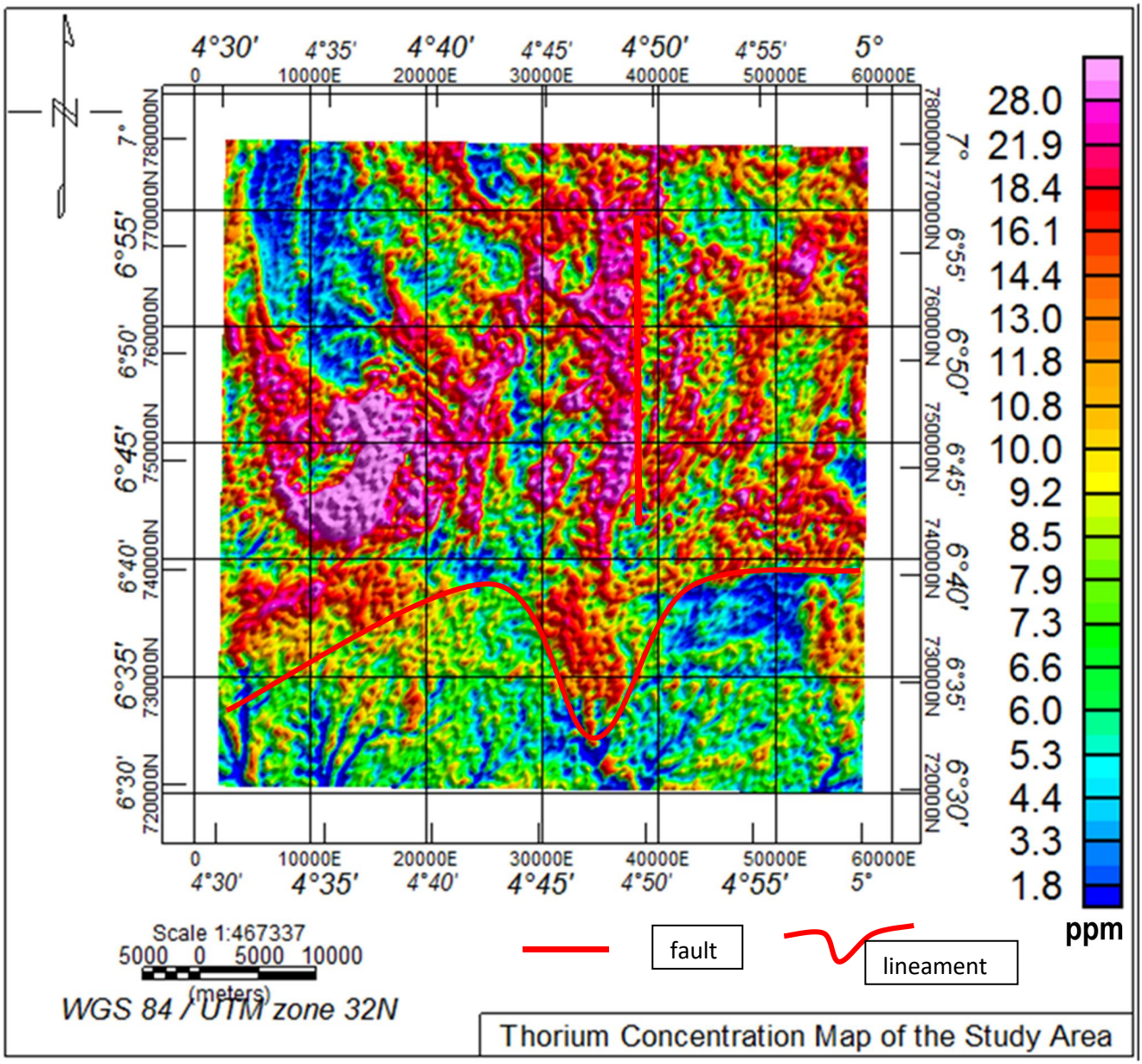

Figure 4.9: Thorium (Th) Concentration Map of the Radiometric Data

4.2.3 Uranium (U) Channel

This channel in figure 4.10 shows the Uranium concentration map of varying concentration in ppm and also emphasis the geological features shown in the Thorium map. The map also shows the boundaries of the basement and the sedimentary basins. The north, northwest and northeast regions (i.e. above the lineament (red line) trend) of the study area produced the higher uranium concentrations (1.9 – 5.1 ppm) and are related partly with the basement rocks within the area. It reveals very high U radiation at the western part, which could also be attributed to radon gas radiating outwardly through the deep-seated WE trending fault. Though one would expect low U concentration because of it susceptible nature to weathering like what we have in the southern half of the lineament, this high radiation level confirms the presence of uranium deposit around western and northeast region. The sedimentary terrain (i.e below this lineament trend, are areas of very low to low (≤ LLD to 0.3 ppm)) which is the south, southwest and southeast regions produced low concentration (0.3 – 1.9ppm) of uranium. It shows the edges of the rich to low uranium bearing-minerals (bitumen) with scattered highs of U concentration denoting in-situ rocks rich in uranium-bearing minerals and some pockets of uranium deposits hosted by some minor faults (Silva *et al.,*2003). From the map produced it can be clearly seen that the southeast region has a very low intensity of uranium which confirmed the depth of the basement rock as very deep around regions suspected to contain the bitumen deposit.

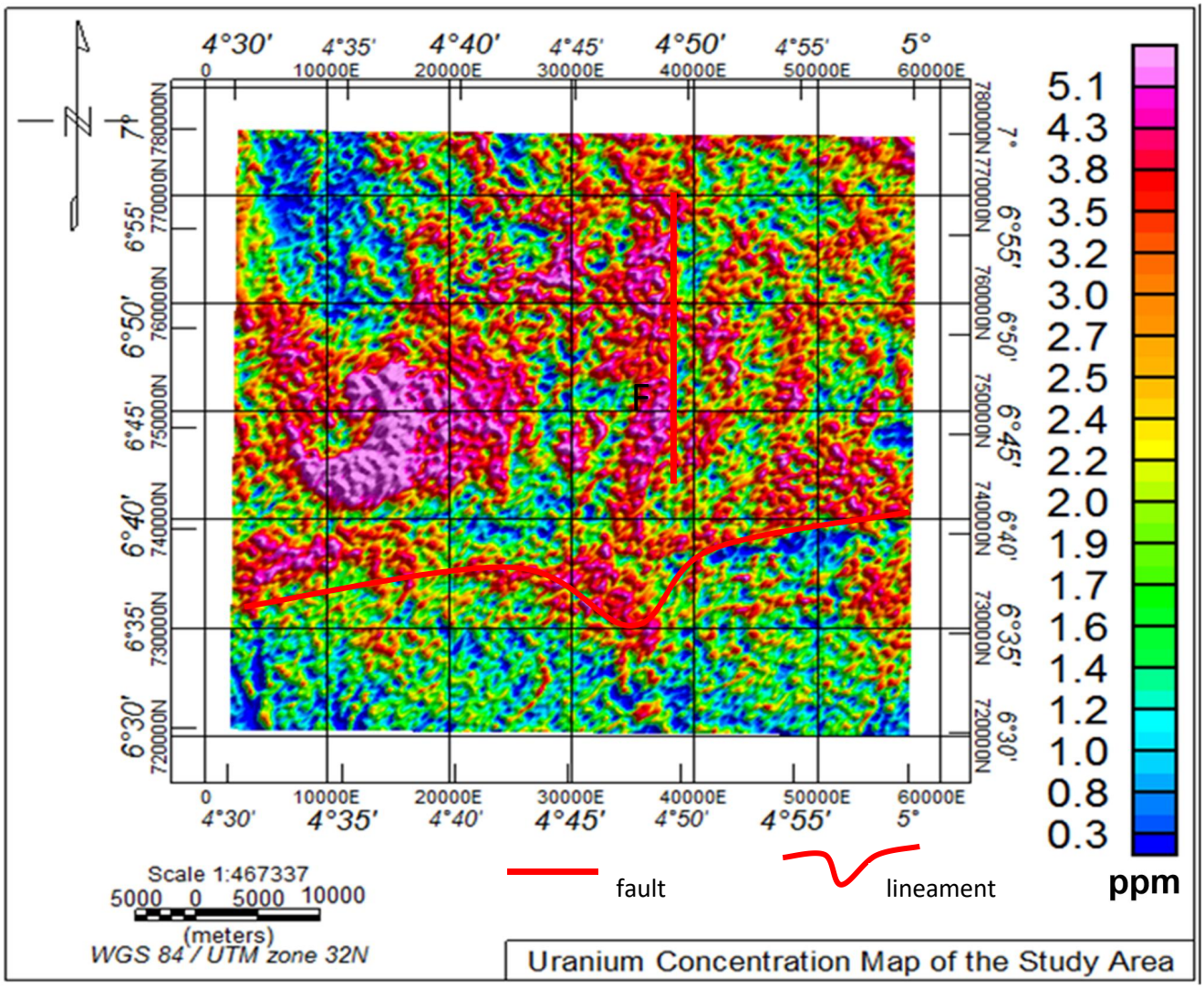

Figure 4.10: Uranium (Th) Concentration Map of the Radiometric Data

4.2.4 Composite Images (Ternary map)

In figure 4.11 consists of colours produced from the individual concentrations of the gamma radiations and corresponds to slight differences in the relative amounts of the three components. Ternary images from radiometric data are an excellent tool for mapping and delineating lithological boundaries in an area Silva et al., (2003). The ternary image figure 4.11 is a composite image produced from the concentrations of these gamma radiations and corresponds to variations in the relative of the three radioelements. Variation of radioelement signature on the ternary map corresponds to changes in the geological formation. Magnetite and quartz-rich rocks appear darker than the surrounding rocks, indicating lower concentrations in K, U and Th. The whitish areas in the ternary image indicate high concentration of potassium, thorium and uranium resulting from felsic volcanic rocks. The yellowish region indicates area with high count of potassium and thorium but low uranium count, the magenta colour shows areas with high potassium and uranium count but weak thorium count. This dark/light areas which coincides with magnetic anomalies (litho-contacts) is attributed to some geologic processes such as weathering, alteration and shearing of rocks within these areas. The aerial extent of bitumen in the study area was carved out with red boundary line. It reveals area or region of the study area containing large or significant quantities of bitumen deposit. The location of two old exploratory wells (Well 1 and Well 2) within the study area was identified by blue symbols. The image was also used to map out the sedimentary and basement boundary indicated by yellow boundary lines with the basement region towards the north above and sedimentary region towards the south below. The map also indicates towns/ villages as well as roads in the area of study.

The area suspected to contain bitumen deposit on this map appeared dark due to two main reasons:

- The area falls within the metasediments which is noted to have contain little or no amount of radioelements; and also
- Bitumen which has the highest percentage by volume of materials within the rock matrix is non-radioactive, thus the area appear dark on the map.

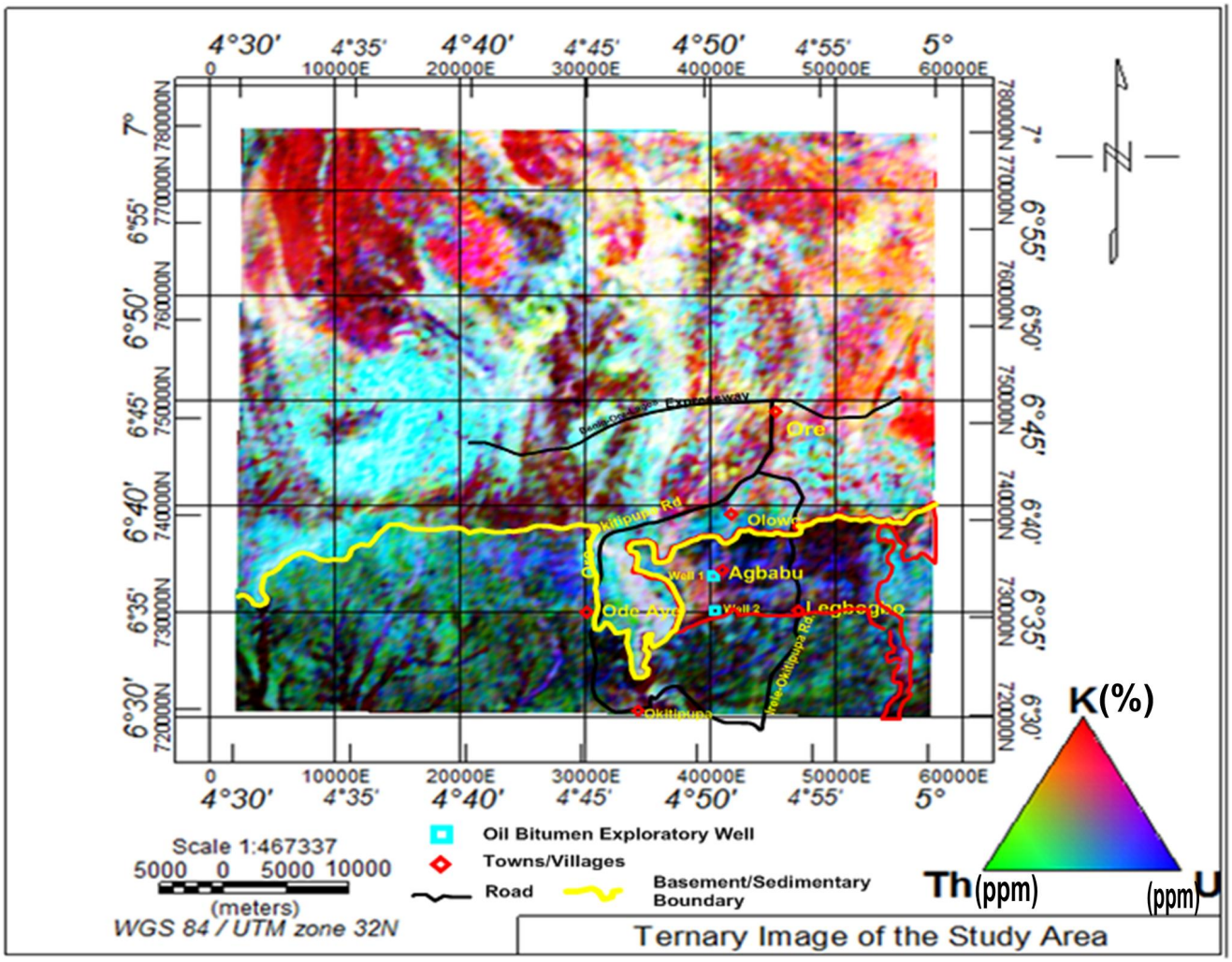

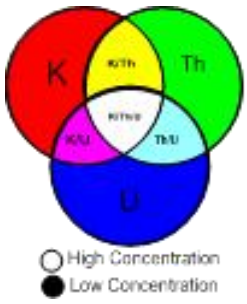

Figure 4.11 Ternary Map showing some aerial features

4.3 2D Resistivity Forward Modelling and Inversion

Obtaining the 2-Dimensional geoelectrical resistivity data set, inverting or modelling the data set is necessary to get the desired subsurface resistivity images or distribution. The process of estimating geophysical model parameters of a multi layered and heterogeneous earth model from observed field data is known as inversion. The experimental observation can be predicted (forward modeling problem) using the laws of physics relating the model parameter to the pragmatic statistical. The choice of the model parameters is largely dependent on the nature of the geophysical problem to be solved. The relationship between the observed data and the model parameters is a non-linear, ill-conditioned and largely under-determined inverse problem. Standard modelling and inversion techniques for linear inverse problems cannot be employed successfully for such non-linear inverse problems. In solving non-linear inverse problems, an initial model (a skilled quess model) is usually modified in an iterative procedure so that the difference between the model response and the observed data values can be minimized. The model parameters are then updated using a linearized interactive adjustment procedure. Conventional approaches are based on a cumulative least-squares errors and cumulative least-absolute deviation.

4.4 Data Input And Format

To interpret the data from a 2-D imaging survey, a 2-D model for the sub-surface which consists of a large number of rectangular blocks is usually used. A computer program is then use to determine the resistivity of the blocks so that the calculated apparent resistivity values agree with the measured values from the field survey. The computer program RES2DINV will automatically subdivide the subsurface into a number of blocks, and it then uses a least-square inversion scheme to determine the appropriate resistivity value for each block. The location of the electrodes and apparent resistivity values must be entered into a number of blocks, and it then uses a least-squares inversion scheme to determine the appropriate resistivity value for each block. The location of the electrodes and apparent resistivity values must be entered into text file which can be read by the RES2DINV program (Loke

and Barker, 1996a). The program manual gives a detailed description of the data format used. As an example, part of an example data fi1e Wenner-Schlumberger Digital Audio Tape (DAT) is shown below with some comments:-

Data in File				**Comments**
Wenner-Schlumberger				; Name of survey line
5.0				; Smallest electrode spacing
7				; Array type (W-S = 7)
167				; Total no of measurements
0				; Type of x-location for datum point (1 for mid-pt)
0				; Flag for W-S data (enter 0 resistivity data only)
0	5	1	135.106	; The x-location, electrode spacing, ρa value
5	5	1	125.68	; The same information for other (data pt)
10	5	1	135.106	
15	5	1	141.39	
20	5	1	163.384	
25	5	1	150.816	
30	5	1	144.532	
35	5	1	166.526	
40	5	1	172.81	
45	5	1	157.1	
50	5	1	172.81	
55	5	1	204.23	

60	5	1	251.36
65	5	1	267.07
70	5	1	270.212

4.7 Discussion of Results

This method was carried out with the aim of revealing the geo-electric layers and its characteristics (thicknesses and resistivity) and also to investigate the depth to top of bitumen deposit within the study area.

4.7.1 Traverse One

Three subsurface geo-electric layers are shown beneath this traverse. These include the sandy soil, bitumen and aquiferous zone.

The inverted 2-D resistivity section shows the image of the subsurface to a depth of 17.3m as shown in Fig. 4.12C. The length of this traverse is 150 m and oriented in an approximately N – S direction. The first layer of Fig. 4.12C designated with green and yellow colour has resistivity values in the range of 75 - 210Ωm. It can be seen from this profile that the topsoil which varies between 0- 3.88m in depth with thickness of 3.88m could probably consist of sandy soil. The second geo-electric layer of Fig. 4.12C has resistivity in the range of 200 - 700Ωm which is indicated by brown, deep brown, red and purple. This formation occurs at a depth of 3.88m – 13.4m between lateral distances 52m -53m, 63m-72m, 84m-107m and 121m-132m could possibly be accumulated of bitumen. Evidently, the profile length of 84m- 107m has a sharp increase of resistivity (500 - 700Ωm) which could now indicate possible accumulation of bitumen. The third layer of Fig. 4.12C has a low resistivity from 10 – 74.3Ωm. It has a thickness of about 3.9m and could be a possible aquiferous zone.

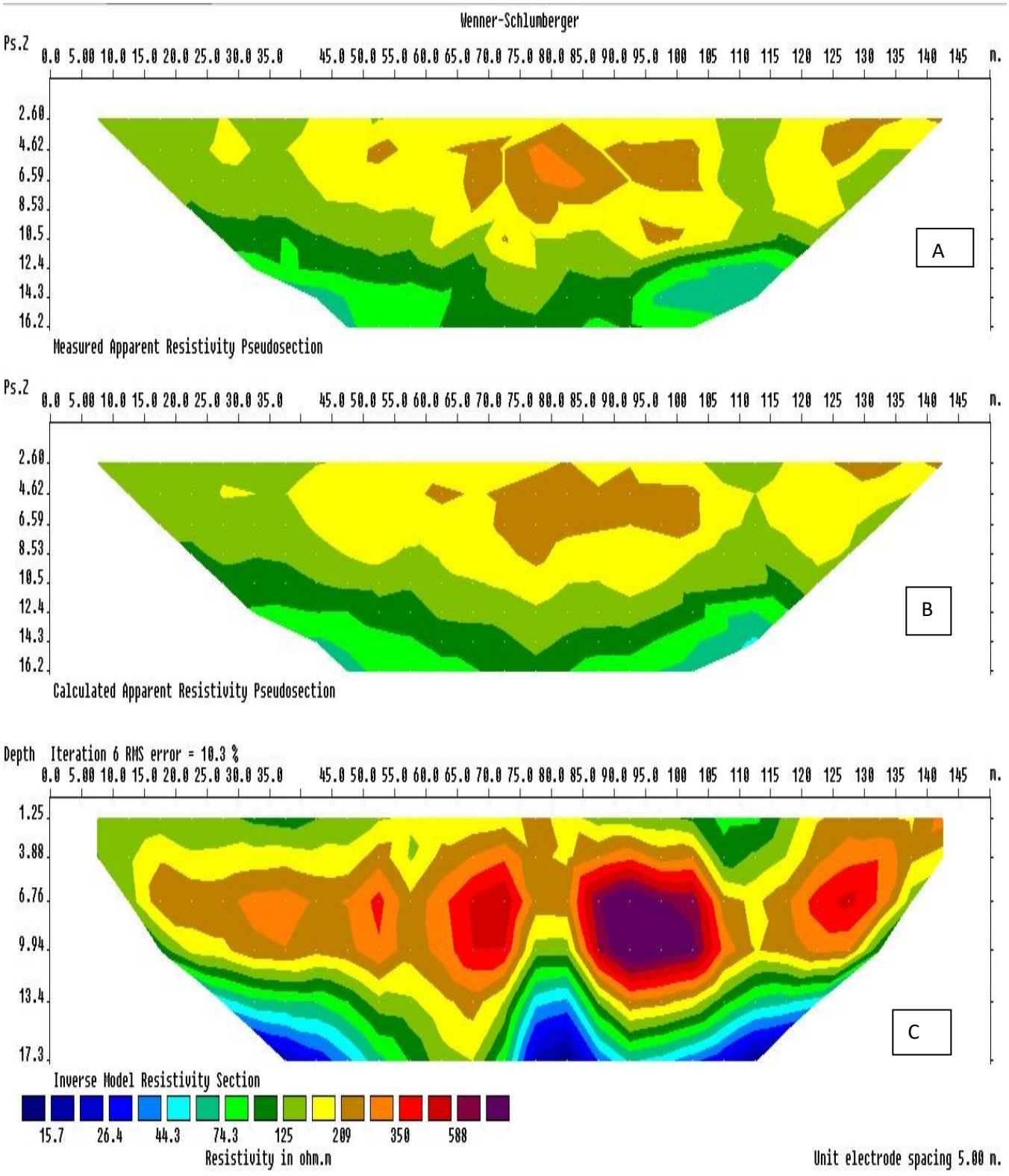

Figure 4.12: Inverted 2D-Resistivity Section along Traverse one

4.7.2 Traverse Two

Three subsurface geo-electric layers were delineated beneath this traverse. These include the sandy soil, bitumen and aquiferous zone.

The inverted 2-D resistivity section shows the image of the subsurface to a depth of 17.3m as shown in Fig. 4.13C. The length of this traverse is 150m and oriented in an approximately N–S direction. The first layer of Fig. 4.13C has an increase resistivity values ranging from 166 - 495Ωm designated with brown, deep brown, red and purple. This formation occurs at a depth of 0 – 13.4m between lateral distances 30m -40m, 60-85m and 98m-132m could possibly be accumulated of bitumen. Evidently, the profile length of 30m - 40m and 60m-85m having a sharp increase of resistivity (371 – 495Ωm) which could now indicate possible accumulation of bitumen. The second geo-electric layer of Fig. 4.13C designated with yellow, deep green and light green colour has undulating thickness between 2.15 and 3.9m down the profile with resistivity values between 74.4- 166Ωm could probably consist of sandy soil. The third geo-electric layer of Fig. 4.13C designated with light blue and deep blue colour extends to a depth from15.3-17.3m along a lateral distances 30m-40m and 85m-110m has a low resistivity from 10 – 50Ωm. It has a thickness of about 2m could possibly serve as a perched aquifer.

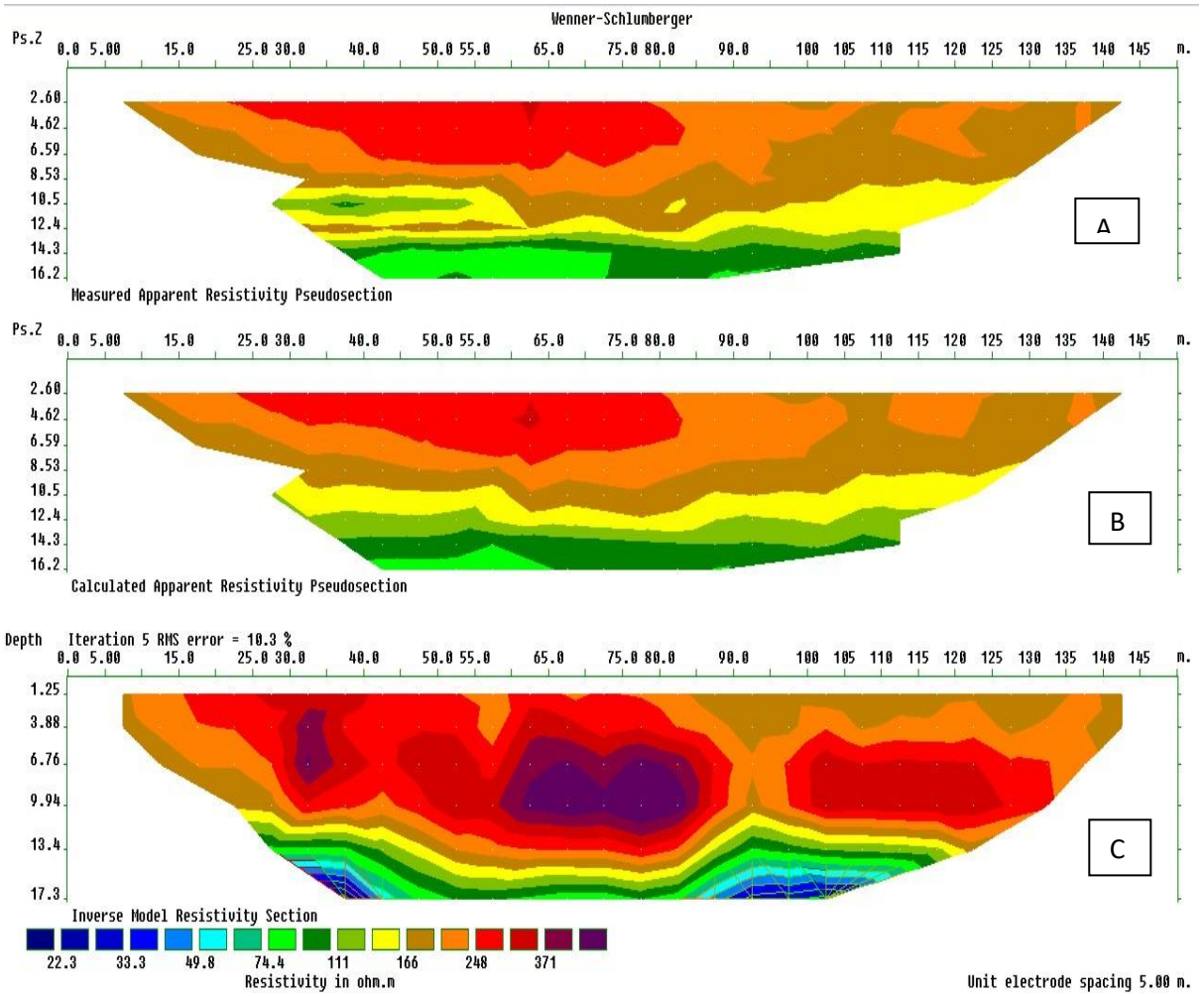

Figure 4.13: Inverted 2D-Resistivity Section along Traverse Two

4.7.3 Traverse Three

Three subsurface geo-electric layers were delineated beneath this traverse. These include the sandy soil, bitumen and aquiferous zone.

The inverted 2-D resistivity section shows the image of the subsurface to a depth of 17.3m as shown in Fig.4.14C. The length of this traverse is 150m and oriented in an approximately W–E direction. The first layer of Fig. 4.14C has an increase resistivity values ranging from 127 - 515Ωm designated with red and purple. This formation occurs at a depth of 0 – 13.4m between lateral distances 8m-125m could possibly be accumulated of bitumen. Evidently, the profile length of 8m -77m and 105m-117m having a sharp increase of resistivity (321 - 515Ωm) which could now indicate possible accumulation of bitumen. The second geo-electric layer of Fig. 4.14C designated with brown yellow and green colour has undulating depth varies from 1.25 - 17.3m down the profile with resistivity values between 7.78- 127Ωm could indicate the presence of sandy soil of varying porosity and permeability. The third geo-electric layer of Fig. 4.14C designated with light blue and deep blue colour extends to a depth from13.4m-17.3m along a lateral distances 65m-80m having a low resistivity from 0 – 7.78Ωm. It has a thickness of about 3.9m which could possibly serve as a perched aquifer. The three traverses show similar features at depth 13.4m. This correlation could indicate the presence of possible accumulation of bitumen at this depth.

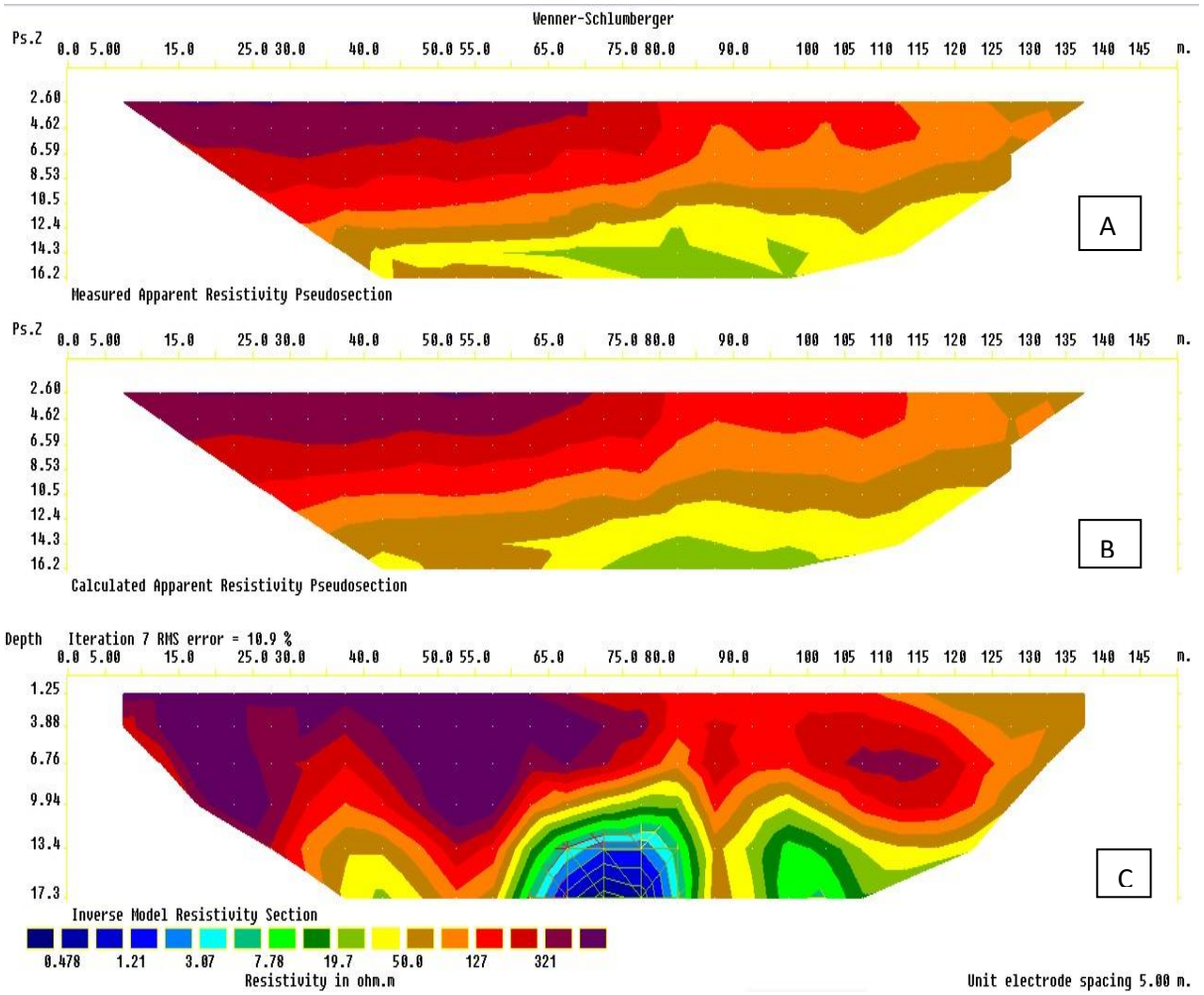

Figure 4.14: Inverted 2D-Resistivity Section along Traverse Three

4.7.4 Traverse Four

Three subsurface geo-electric layers were delineated beneath this traverse. These include the sandy soil, bitumen and aquiferous zone.

The inverted 2-D resistivity section shows the image of the subsurface to a depth of 17.3m as shown in Fig.4.15C. The length of this traverse is 150m and oriented in an approximately N–S direction. The first layer of Fig. 4.15C has an increase resistivity values ranging from 107 - 465Ωm designated with red and purple colour. This formation occurs at a depth of 9.94m along a lateral distances 17.5m-142.5m could possibly be accumulated of bitumen. This formation occurs at a depth of 0-9.94m. Evidently, the lateral profile length having a sharp increase of resistivity (286 - 465Ωm) could now indicate possible accumulation of bitumen. The second geo-electric layer of Fig. 4.15C designated with brown, yellow and green colour has undulating along lateral distance 35m-55m. It has resistivity values between 5.61- 107Ωm could probably consist of sandy soil. This formation has a depth varying from 9.94m- 17.3m with thickness of 7.36m. The third geo-electric layer of Fig. 4.15C designated with light blue and deep blue colour extends to a depth from13.34m-17.3m along a lateral distances 34m-53m having a low resistivity from 0 – 5.61Ωm. It has a thickness of about 3.9m which could possibly host a large volume of underground water resources.

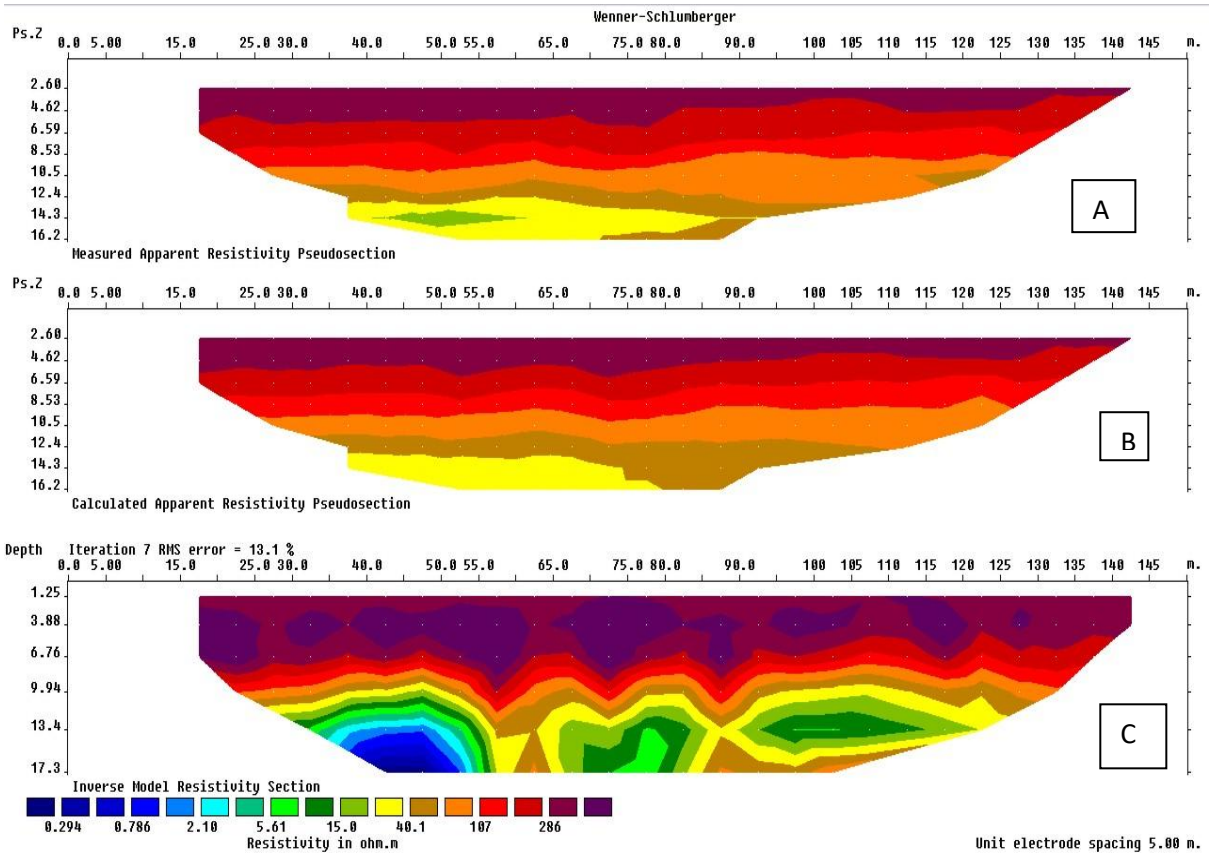

Figure 4.15: Inverted 2D-Resistivity Section along Traverse Four

4.7.5 Traverse Five

Three subsurface geo-electric layers were delineated beneath this traverse. These include the sandy soil, bitumen and aquiferous zone.

The inverted 2-D resistivity section shows the image of the subsurface to a depth of 17.3m (Fig. 4.16C). The length of this traverse is 150m and oriented in an approximately N - S direction. The first layer of Fig. 4.16C has an increase resistivity values ranging from 211 - 745Ωm designated with red and purple colour. This formation occurs at a depth of 9.94m along a lateral distances 12.5m-137.5m could possibly be accumulated of bitumen. It has a thickness ranging from 0-9.94m. Evidently, the lateral profile length having a sharp increase of resistivity (478 - 745Ωm) could now indicate possible accumulation of bitumen. The second geo-electric layer of Fig. 4.16C designated with brown, yellow and green colour has undulating along lateral distance 47m-67m, 78m-62m and 105m 115m. It has resistivity values between 18.1- 211Ωm could probably consist of sandy soil. This formation has a thickness varying from 8.35m-17.3m. The third geo-electric layer of Fig. 4.16C designated with light blue and deep blue colour extends to a depth from13.4m-17.3m along a lateral distances 34m- 53m having a low resistivity from 1m – 8.2Ωm. It has a thickness of about 3.9m which could possibly host a large volume of underground water resources.

Traverse 4 and 5 having correlation of the same depth of 9.94m that could possibly be accumulated of bitumen.

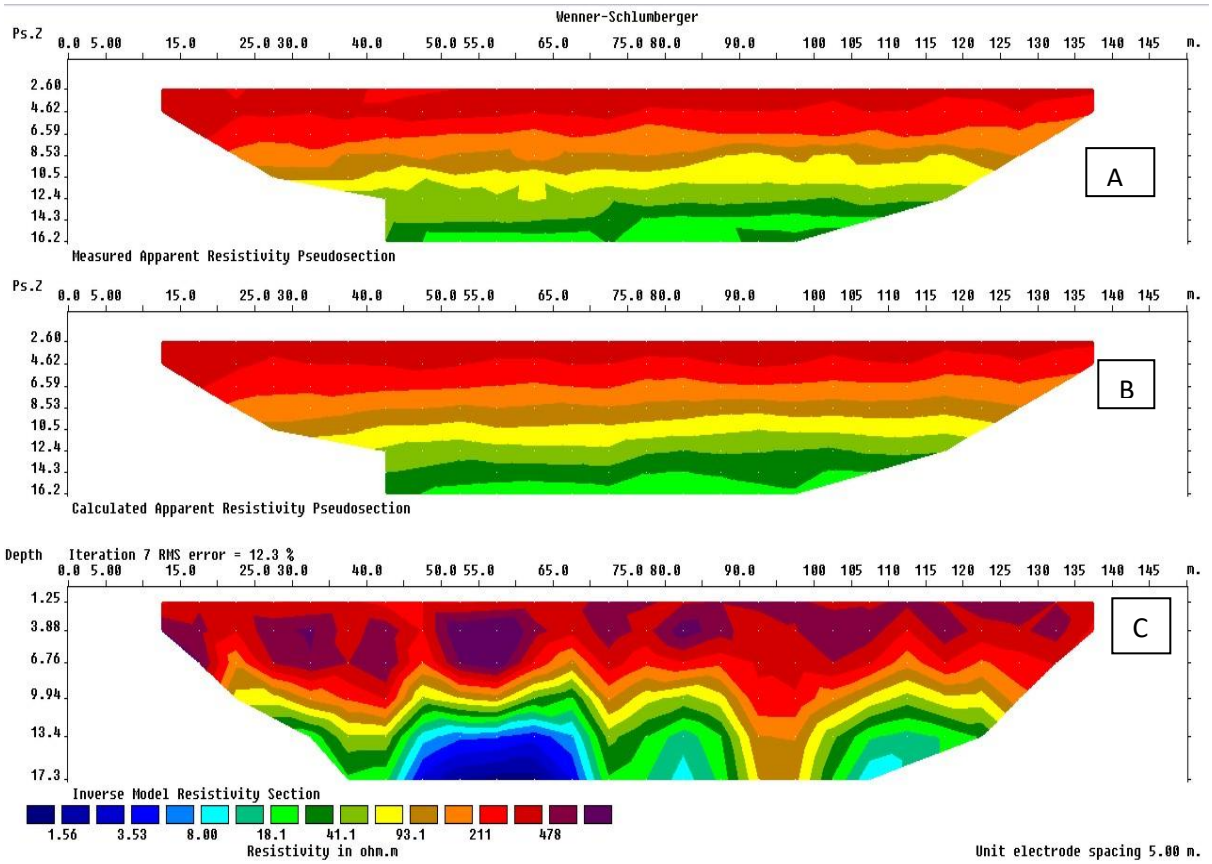

Figure 4.16: Inverted 2D-Resistivity Section along Traverse Five

The inverted 2D resistivity interpretation has shown that occurrence of bitumen was found between the depths of 13.4m and 9.93m for Traverses 1,2,3 ; and Traverses 4,5 respectively and these corroborated by boreholes shown below with a depth of about 18m.

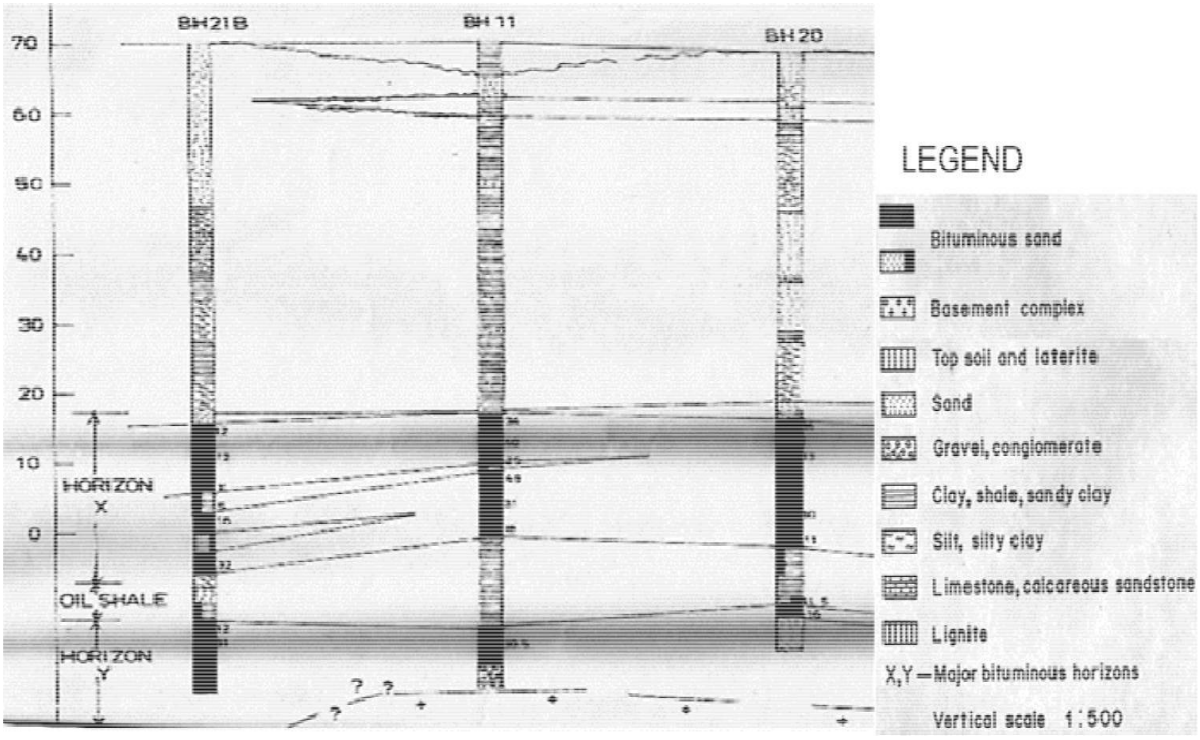

Figure 4.17: Lithofacies / bitumen saturation comparing panel of the study area (Modified after GCU, Uni. of Ile-Ife, 1980)

CHAPTER FIVE

FINDINGS, CONTRIBUTION TO KNOWLEDGE, CONCLUSION AND SUGGESTION FOR FURTHER STUDY

5.1 Findings

The findings of the study are as follows:

1. Airborne radiometric survey revealed the concentration of radioelements - thorium (Th), potassium (K) and uranium (U) at Agbabu area of Southwestern Nigeria.
2. Aeromagnetic survey identified rock boundaries, lineaments trend and depth (841 – 1703m) to source of causative body of magnetic anomaly at Agbabu area of Southwestern Nigeria.
3. The airborne magnetic maps of the study area revealed good contrast between geological structures.
4. 2-Dimensional electrical resistivity survey revealed the geoelectrical parameters of rock materials at a depth of between 9.94m and 13.4m at Agbabu area of Southwestern Nigeria.
5. The coordinates of the airborne surveys agreed perfectly with the values of ERT indicating the reliability of this type of joint geophysical investigation.

5.2 Contribution to Knowledge

This work has added to knowledge in this ways:

1. This research has shown that the occurrence of bitumen was found between the depths of 13.4m and 9.93m for Traverses 1,2,3 ; and Traverses 4,5 respectively corroborated by boreholes with a depth of about 18m.
2. This study proves the effectiveness of integrated geophysical methods in mapping the occurrence of bitumen within the study area.

5.3 Conclusion

This study has shown that the combined used of aeromagnetic and aero-radiometric with electrical imaging gives one of the best prospecting methods for the investigation of bitumen deposits within the study area. Rock boundaries, lineaments trend, depth to source of causative body of magnetic anomaly and concealed geological features were delineated. Aero-radiometric images reveal spatial distribution of concentration of radioelement across the study area. The interpretations of radiometric datasets revealed the spatial variation of potassium (K), thorium (Th) and uranium (U) radioelement concentrations to be as high as (0.6 – 2.5%), (7.9 – 28.0 ppm) and (1.9 – 5.1 ppm) respectively within the basement complex, but as low (0.0 – 0.6%), (1.8 – 9.2ppm) and (0.3 – 1.9ppm) respectively within the sedimentary terrain. In this study, the ground-truthing (second phase) survey helps to confirm and validate the occurrence of bitumen deposit within the survey area. The electrode configuration (Wenner-Schlumberger) adopted helps to image the subsurface geo-electric layers and evaluated the rock properties (resistivity and thickness). 2-D Electrical Resistivity imaging reveals the spatial distribution and the presence of bitumen at the surveyed area. Bitumen bearing horizon was seen occurring from the surface to infinity given an indication that it was at a shallow occurrence which can easily seep to the surface location with a mean depth of 10.1m within the study area. The inverted 2D-resistivity sections show images of the subsurface to a depth of 17.3m and reveal three to three geo-electric layers. This integrated approach is helpful in mapping both surface and concealed subsurface geological features thereby narrowing down search for bitumen deposit within the area.

5.4 Suggestions for Further Studies

The suggestions for further studies are:

1. To validate and confirm potentially viable economic deposit for pollution study.
2. Using other geophysical method like gravity, seismic to confirm the authenticity of the result obtained.
3. This study will provide information that will guide mining engineers on drilling operation in the study area.

REFERENCES

Adegoke, O.S., Ako, B.D., and Enu, E.I., (1980). Geotechnical Investigation of the Ondo State bitumen sands. Rept. Consultancy Unit Obafemi Awolowo University. Ile Ife. pp: 257.

Agagu, O.K., (1985). A geological guide to Bituminous Sediments in South-Western Nigeria: Unpublished Report, Department of Geology, University of Ibadan.

Airo, M.L.(2002). Aeromagnetic and Aero-radiometric Response to Hydrothermal Alteration. Surveys in Geophysics, 23, 273302. http://dx.doi.org/10.1023/A:1015556614694

Airo, M.L., and Loukola-Ruskeeniemi, K, (2003). Characteristerization of sulfide deposits by airborne magnetic and gamma-ray response in eastern Finland. Ore Geology Reviews 24, 67-84

Aisabokhae, J., Adamu, A., Oresajo, B., (2018). Analytic signal, depth and multispectral interpretation of areas within the Continental Terminal, North-western Nigeria https://dx.doi.org/10.4314/jasem.v22i5.9 Appl. Sci.Environ. Manage. Vol. 22 (5) 669 – 673.

Ako, B.D., Alabi, A.O., Adegoke, O.S., Enu, E.I., (1983). Application of Resistivity Sounding in the Exploration for Nigeria Tar Sand, Energy and Exploitation © Graham and Trotman Limited 2 (2): 155-164.

Akinmosin, A., Omosanya, K.O., Ariyo, S.O., Folorunsho, A.F., Aiyeola, S.O., (2011). Structural control for Bitumen Seepages in Imeri, South-western, Nigeria. International Journal of Basic and Applied Sciences IJBAS-IJENS

Vol: 11 No: 01, 93-103.

Amenyoh, T., Wemegah, D.D., Menyeh, A., and Danuor, S.K., (2009). The use of landsat and aeromagnetic data in the interpretation of geological structures in the Nangodi Belt. Master's thesis, University of Cape Coast.

Amigun, J.O., Adelusi, A.O., and Ako, B. D., (2012).The application of integrated geophysical methods in oil sand exploration in Agbabu area of Southwestern Nigeria. International Research Journal of Geology and Mining (IRJGM) (2276-6618) Vol. 2(9) pp. 243-253.

Ansari, A.H., and Alamdar, K., (2009). Reduction to the pole of magnetic anomalies using analytic signal.World Applied Sciences Journal, 7(4):pp. 405–409.

Appiah, H., (1991). Geology and mine exploration trends of Prestea Goldfields, Ghana. Journal of African Earth Sciences (and the Middle East), 13(2): pp. 235–241.

Bauman, P., (2005). 2-D Resistivity Surveying for Hydrocarbon-A Primer. CSEG Recorder, April, pp. 25-33.

Beard, L.P., and Goitom, B., (2000). Some problems in interpreting low latitude Magnetic surveys 6thEAGE /EEG Meeting.

Bhattacharya D., Joshi G.B and Sharma R., (2011).Uranium Mineralisation Associated with Felsic Volcanismat Mohar, Shivpuri District, Madhya Pradesh .Journal Geological Society of India, 78, pp 55-62

Boadi, B., Wemegah, D.D., and Preko, K., (2013). Geological and Structural Interpretation of the Konongo Area of the Ashanti Gold Belt of Ghana from Aeromagnetic and Radiometric data. International Research Journal

of Geology and Mining (IRJGM) (2276-6618), 3(3), pp. 124-135.

Case, J.E., and Sikora, R.F., (1984). Geologic Interpretation of Gravity and Magnetic Data in the Salida Region, Colorado. US Geological Survey Open-File Report, 46, 84-372

Charbonneau, B., (1991). Geochemical evolution and radioactive mineralogy of the Fort Smith radioactive belt, Northwest Territories, Canada. In Primary Radioactive Minerals (The textural patterns of radioactive mineral paragenetic associations), pp. 21–48. Theophrastus Publications.

Chopin, G.R., (1988). Humics and radionuclide migration. Radiochima Acta, 44/45: pp. 23–28

Christensen, N. B. (1989): AC resistivity sounding. *First Break*, **7(1)**, p. 447-452.

Clark, D.A., (1997). Magnetic properties of rocks and minerals. AGSO Journal of Australian Geology and Geophysics, 17(2)

Clark, D.A., and Emerson, D.W., (1991). Notes on rock magnetic characteristics in applied Geophysical studies. Exploration Geophysics, pp. 22:547–555

Cooley, J. W. and Tukey, J. W. (1965). An algorithm for the machine calculation of complex Fourier series. Math. Comput., 19(90):297–301.

Cristall, J., Farquharson, C., Oldenburg, D., (2004). Airborne Electromagnetic Inversion Applied to Oil Sand: Expanded Abstract, Can. Soc. Expl. Geophysics. Annual Meeting as cited by Douglas R. Schmitt in Heavy and Bituminous Oils: Can Alberta Save the World Preview, October 2005. 25p.

Dahlin, T., (1996). 2D resistivity surveying for environmental and engineering applications. First Break, 14, 275-284.

Dahlin,T. and Loke, M.H., (1998). Resolution of 2D Wenner resistivity imaging as assessed by numerical modelling, Journal of Applied Geophysics, **38**, 237-249.

Dalan, R.A., (2006). A geophysical approach to buried site detection using down-hole susceptibility and soil magnetic techniques. Archaeological Prospection 13, pp. 182 206

Darnley, A.G., (1996). Uranium exploration data and global geochemical baselines: The need for coordinated action. In Uranium Exploration Data and Techniques Applied to the Preparation of Radioelement Maps. IAEA-TECDOC-980.

Davies, J.H., Davies, D.R., (2010). Earth's surface heat flux. Solid Earth 1(1), 5-24

Dearing J.A., (1994). Environmental magnetic susceptibility, using the Bartington MS2 system

Debeglia, N., and Corpel, J., (1997). Automatic 3-D Interpretation of Potential Field Data Using Analytic Signal Derivatives. Geophysics, 62, 87-96. http://dx.doi.org/10.1190/1.1444149

Ground Water", Geological. Survey of Canada, Special, pp. 960.

DeGroot-Hedlin, C. and Constable, S., (1990). Occam's inversion to generate smooth, two dimensional models form magnetotelluric data. Geophysics, 55, 1613-1624

Dickson, B.L. and Scott, K.M., (1997). Interpretation of aerial gamma ray surveys-

adding the geochemical factors. AGSO Journal of Australian Geology and Geophysics,17(2): pp.187–200.

Elawadi, E., Ammar, A., and Elsirafy, A., (2004). Mapping surface geology using airborne gammaray spectrometric survey data - A case study. Proceedings of SEGJ international symposium. Nuclear Materials Authority of Egypt, Airborne Exploration Dept.

Enu, E.I., (1985). Textural characteristic of the Nigeria Tar Sands. Sedimentary geology. V. 44, pp 65-81.

Fertl, W.H., (1983). Gamma-ray spectral logging: a new evaluation frontier. World Oil,pp. 79–91.

Nigeria Geological Survey Agency (NGSA), 2009. Geo-logical map of Nigeria prepared by Nigeria Geologi-cal Survey Agency, 31, Shetima Mangono Crescent Utako District, Garki, Abuja, Nigeria.

Geological Consultancy Unit (GCU), University of Ile – Ife (1980). Geotechnical Investigation of the Ondo State Bituminous Sands. Vol. 1, Folio 15. Unpublished

Gwynn, J. W, and Hanson, F. V., 2009. Annotated Bibliography of Utah Tar Sand Deposits, Open-file Report 503 Utah Geological Survey p.1 – 4.

Geosoft Inc., (1996): OASIS montaj Version 4.0 User Guide, Geosoft Incorporated, Toronto

Grant, F., and Martin, L., (1966). Interpretation theory in applied Geophysics. New York: McGraw-Hill Book Co.

Grant, F. S. (1985). Aeromagnetic, geology of an ore environment, Magnetite in igneous, sedimentary and metamorphic rocks. An overview of Geoexploration. 23: pp. 303–33.

Gregory, A.F., and Horwood, J.L., (1961). A laboratory study of gamma-ray spectra at the surface of rocks. Department of Energy, Mines and Resources, Ottowa. Mines Branch Research Report R85.

Griffiths, D.H and Turnbull, J., (1985). A multi-electrode array for resistivity surveying. First Break 3 (No. 7), 16-20

Griffiths D.H., Turnbull J. and Olayinka A.I., (1990). Two – dimensional resistivity mapping with a computer- controlled array. First Break 8, 121-129.

Griffiths D. H., and Barker R.D., (1993). Two- dimensional resistivity imaging and modeling in areas of complex geology. Journal of Applied Geophysics, 29, 211-226.

Gunn, P. J., Minty, B.R.S., and Milligan, P., (1997). The airborne gamma-ray spectrometric response over arid Australian terrains. Exploration, 97: pp. 733–740.

Harrison, R.J., Dunin-Borkowski, R.E., Kasama, T., Simpson, E.T., and Feinberg, J. M., (2007). Properties of rocks and minerals. Magnetic properties of rocks and mineral. University of Cambridge, Cambridge, UK

IAEA, (International Atomic Energy Agency) 1991, Airborne gamma ray spectrometer surveying, International Atomic Energy Agency, Technical Report Series, 323.

IAEA, (International Atomic Energy Agency) 2003, Guidelines for radioelement mapping using gamma ray spectrometry data, Vienna.

IAEA, (International Atomic Energy Agency) 2003, The use of gamma rays data to define the natural radiation Environment, Vienna.

ICRU, (1994). Gamma ray Spectrometry in the Environment, ICRU Report 53. International Commission on Radiation Units And Measurements, Bethesda, USA.

Inglis, D.R., (1955). Theories of the Earth's Magnetism Rev. Mod. Physics. 27, pp. 212– 248

Jones, H.A., and Hockey, R.D., (1964). "The Geology of Part of South-western Nigeria". Geol. Surv. Nigeria Bull. 31: 87.

Keating, P.B., (1995) A simple Technique to Identify Magnetic Anomalies Due to Kimberlite Pipes. Exploration and Mining Geology, 4, 121-125.

Kearey, P., Brooks, M., and Hill, I., (2002). An introduction to geophysical Exploration third Edition. TJ International. Pp. 2-160

Krishnaswami, S. (1999). Thorium encyclopedia of geochemistry, Kluwer Academic Publishers, London pp. 712.

Langmuir, D. and Hermans, J. S. (1980). The mobility of thorium in natural waters at low temperatures. Geochimica et Cosmochimica Acta, 44: pp. 1753–1766.

Li, Y., and Oldenburg D.W., (1992). Approximate inverse mapping in DC resistivity problems. Geophysical Journal International 109, 343-362.

Liu, S., and Mackey, T., (1998). Using images in a geological interpretation of magnetic data. AGSO Research Newsletter 28

Loke, M.H., (2004): Tutorial 2D and 3D Electrical Imaging Surveys. Available at www.geoelectrical.com, 128pp

Loke, M.H., and Barker, R.D., (1996a). Least-Squares Deconvolution of Apparent Resistivity Pseudosections. Geophysics, 60, p 1682-1690.

Loke, M.H., and Barker, R.D., (1996b). Practical Techniques for 3D resistivity surveys and data inversion. Geophysical Prospecting, 44,499-523.

Manu, J., (1993). Gold deposits of Birimian greenstone belts in Ghana: Hydrothermal alteration and thermodynamics. Verlag Mainz, Wissenchaftsverlag, Aachen Herstellung: Fotodruck Mainz GmbH Susterfeldstr. 83. 52072 Aachen.

Milligan, P. R. and Gunn, P. J. (1997). Enhancement and presentation of airborne Geophysical data. AGSO Journal of Australian Geology and Geophysics, 17(2):64–74.

Milsom J., (2003). Field Geophysics, the geological field guide series. Third edition. John Wiley & Sons Ltd, The Atrium, Southern Gate, Chichester, pp. 71

Minty, B.R.S., (1996). The fundamentals of airborne gamma-ray spectrometry. AGSO Journal of Australian Geology and Geophysics, 17(2): pp. 39–50.

Nabighian, M.N., (1972). The analytical signal of two-dimensional magnetic bodies with polygonal cross-section: its properties and use for automated anomaly interpretation. Geophysics, 37(3): pp. 507–517.

Nicolet, J.P., and Erdi-Krausz, G., (2003). Guidelines for radioelement mapping using gamma ray spectrometry data

Obiora, D.N., Ossai, M.N.,and Okwoli,E., (2015). A case study of aeromagnetic data

interpretation. International Journal of Physical Sciences 10(17), 503-519.

Odunaike, R.K., Laoye, J.A., Fasunwon, O.O., Ijeoma, G.C., Akinyemi. L.P., (2010). Geophysical mapping of the occurence of shallow oil sands in Idiopopo at Okitipupa area, South-western, Nigeria. Afr. J. Environ. Sci. Technol. Vol. 4 (1) pp. 034-044.

Omatsola, M.E., and Adegoke, O.S., (1981). "Tectonic Evolution and Cretaceous Stratigraphy of the Dahomey Basin". J. Min. Geol. 18 (1): 130-137.

Oruc, B., and Selim, H., (2011). Interpretation of magnetic data in the Sinop area of Mid Black Sea, Turkey, using tilt derivative, Euler deconvolution, and discrete wavelet transform. *Journal of Applied Geophysics, 74*, 194–204.

Ostrovskiy, E.A., (1975). Antagonism of radioactive elements in wellrock alteration fields and its use in aerogamma spectrometric prospecting. International Geological Review, 17: pp. 461–8.

Pazdirek, O. and Blaha, V., (1996). Examples of resistivity imaging using ME-100 resistivity field acquisition system. EAGE 58th Conference and Technical Exhibition Extended Abstracts, Amsterdam.

Paterson, N.R, (1990). Curie temperature. In James, D. E. (ed.), The Encyclopedia of solid Earth Geophysics, pp. 166–173. New York: Van Nostrand Reinhold

Paterson, N.R. and Reeves, C.V.,(1985). Application of Gravity and Magnetic Surveys. The State of the Art in 1985. Geophysics, 50, 2558-2594. https://doi.org/10.1190/1.1441884

Plumlee, G.S., Smith, K.S., Ficklin, W.H., and Briggs, P.H., (1992). Geological and geochemical controls on the composition of mine drainages and natural drainages in mineralized areas. Proceedings, 7th International Water-Rock Interaction Conference. Park City, Utah, July, 1992. pp. 419–422

Plummer, C.C., McGeary, D., and Carlson, D.H., (2001). Physical Geology. New York: McGraw Hill, 8th edition.

Rajagopalan, S., (2003). Exploration Geophysics, 34(No. 4): pp. 257–262.

Rajesh, V.J., Yokoyama, K., Santosh, M., Arai, S., Oh, C.W., and Kim, S.W., (2006). Zirconolite and Baddeleyite in an Ultramafic Suite from Southern India: Early Ordovician Carbonatite-Type Melts Associated with Extensional Collapse of the Gondwana Crust.

Reeves, C.V., (1989). Aeromagnetic interpretation and rock magnetism. First Break, 7: pp.275–286

Reynolds, J.M., (1997). An introduction to Applied and Environmental Geophysics, John Wiley & Ltd. Bans Lane, Chichester. pp. 124-132

Rivas, J., (2009). Gravity and Magnetic Methods. jarivas@lageo.com.sv

Roest, W.R., and Pilkington, M., (1993). Identifying remanent magnetization effects in magnetic data.Geophysics, 58: pp. 653–659.

Salem, A., Williams, S., Fairhead, J., Ravat, D., and Smith, R., (2007). Tilt-depth method: a simple depth estimation method using first-order magnetic derivatives. *The Leading Edge , 26*, 1502-1505.

Sasaki, Y., (1992). Resolution of resistivity tomography inferred from numerical simulation. Geophysical Prospecting, 40, 453-464.

Shives, R., Charbonneau, B., and Ford, K,. (2000). The detection of potassic alteration by gamma-ray spectrometry-recognition of alteration related to mineralization. Geophysics-Wisconsin. The Tulsa-Society of Exploration Geophysicists, 65(6): pp. 2001–2011.

Silva, A.M., Pires, A.C.B., McCafferty, A., Moraes, R.A.V., and Xia, H., (2003). Application of airborne geophysical data to mineral exploration in the uneven exposed terrains of the Rio Das Velhas greenstone belt. Revista Brasileira de Geociências, 33(2):17–28.

Stratton, J. A. (1941): *Electromagnetic Theory*. McGraw-Hill, New York.

Studemeister, P.A., (1983). The redox state of iron: a powerful indicator of hydrothermal alteration. Geoscience Canada, 10: pp. 189–194.

Stummer, P., Maurer, H. and Green, A. (2004): Experimental design: electrical resistivity data sets that provides optimum subsurface information. *Geophysics*, **69**, p. 120-139.

Telford, W.M., Geldart, L.P., and Sheriff, R.E., (1990). Applied Geophysics. Cambridge University Press, second edition.

Wemegah, D.D., Menyeh, A., and Danuor, S.K., (2009). Magnetic Susceptibility Characterization of mineralized and non mineralized rocks of the Subenso Concession of Newmont Ghana Gold Limited. In Ghana Science

Association Biennial Conference, UCC.

Wedepohl, K.K., (Exec. Ed) (1978). Handbook of Geochemistry, Volume 2, Part 5, Berlin, Heidelberg, New York

Whitham, K., (1960). Measurement of the geomagnetic elements. In Methods and techniques in Geophysics 1, S. K. Runcorn. pp. 134–48.

Wilford, J.R., Bierwirth, P.N., and Craig, M.A., (1997). Application of Airborne Gamma ray Spectrometry in Soil/Regolith Mapping and Applied Geomorphology. AGSO Journal of Australian Geology and Geophysics, 17(2):201-216.

Appendix 1: Data Obtained from Nigerian Geological Survey Agency (NGSA)

Aeromagnetic Data

X	Y	Z
46600	664900	40.43204
46700	664900	40.25464
46800	664900	40.037
46900	664900	39.83871
47000	664900	39.67297
47100	664900	39.57393
47200	664900	39.57814
47300	664900	39.66404
47400	664900	39.73962
47500	664900	39.71819
47600	664900	39.58039
47700	664900	39.36911
47800	664900	39.13695
47900	664900	38.92344
48000	664900	38.75645

48100	664900	38.64536
48200	664900	38.57877
48300	664900	38.5532
48400	664900	38.56657
48500	664900	38.54591
48600	664900	38.35194
48700	664900	38.01152

Aero-radiometric Data

X	Y	Z
48400	720300	0.101114
48500	720300	0.085264
48600	720300	0.088991
48700	720300	0.118732
48800	720300	0.142644
48900	720300	0.124779
49000	720300	0.073414
49100	720300	0.022989

49200	720300	0.006631
49300	720300	0.032642
49400	720300	0.070418
49500	720300	0.09607
49600	720300	0.095902
49700	720300	0.097107
49800	720300	0.100937
49900	720300	0.108695
50000	720300	0.107435
50100	720300	0.094047
50200	720300	0.072381

Appendix 2: Data acquired from Electrical Resistivity Tomography (ERT) survey

2D ELECTRICAL RESISTIVITY

IMAGING FIELD DATA

REPORT SHEET

	ARRAY TYPE	**WENNER-SCHLUMBBERGER**	**DATE**	**15/06/2018**	
	INSTRUMENT USED	PASI 16GL-N	STATE	ONDO	
	LOCATION	Traverse 1	L.G.A	ODIGBO	
	LINE NUMBER	TR 1			
	OBSERVER	Funmi			

LAT. 06˚59'23" LONG. 004˚49'25.6" Elev. 12.9m

Electrode Location a = 5, n = 1, k = 31.42

C1	P1	P2	C2	R (Ω)	ρ (Ωm)
0	5	10	15	4.3	135.106

5	10	15	20	4	125.68
10	15	20	25	4.3	135.106
15	20	25	30	4.5	141.39
20	25	30	35	5.2	163.384
25	30	35	40	4.8	150.816
30	35	40	45	4.6	144.532
35	40	45	50	5.3	166.526
40	45	50	55	5.5	172.81
45	50	55	60	5	157.1
50	55	60	65	5.5	172.81
55	60	65	70	6.5	204.23
60	65	70	75	8	251.36
65	70	75	80	8.5	267.07
70	75	80	85	8.6	270.212
75	80	85	90	6.3	197.946
80	85	90	95	5.9	185.378
s85	90	95	100	5.5	172.81
90	95	100	105	5.6	175.952

95	100	105	110	5.5	172.81
100	105	110	115	5	157.1
105	110	115	120	4.2	131.964
110	115	120	125	5.3	166.526
115	120	125	130	6.4	201.088
120	125	130	135	6.6	207.372
125	130	135	140	7.2	226.224
130	135	140	145	6.4	201.088
135	140	145	150	6.9	216.798
Electrode Location a = 5, n = 2, k = 94.25					
C1	P1	P2	C2	R (Ω)	ρ (Ωm)
0	10	15	25	1.4	131.95
5	15	20	30	1.6	150.8
10	20	25	35	1.6	150.8
15	25	30	40	1.8	169.65
20	30	35	45	1.7	160.225
25	35	40	50	1.7	160.225
30	40	45	55	1.9	179.075

35	45	50	60	1.9	179.075
40	50	55	65	2.4	226.2
45	55	60	70	2.1	197.925
50	60	65	75	2.2	207.35
55	65	70	80	2.3	216.775
60	70	75	85	2.2	207.35
65	75	80	90	3.1	292.175
70	80	85	95	2.6	245.05
75	85	90	100	2.2	207.35
80	90	95	105	2.3	216.775
85	95	100	110	4.6	433.55
90	100	105	115	2.4	226.2
95	105	110	120	1.7	160.225
100	110	115	125	1.6	150.8
105	115	120	130	1.9	179.075
110	120	125	135	3.3	311.025
115	125	130	140	2.5	235.625
120	130	135	145	1.7	160.225

125	135	140	150	1.7	160.225
Electrode Location a = 5, n = 3, k = 188.50					
C1	P1	P2	C2	R (Ω)	ρ (Ωm)
0	15	20	35	0.754	142.129
5	20	25	40	0.706	133.081
10	25	30	45	0.802	151.177
15	30	35	50	0.809	152.4965
20	35	40	55	0.814	153.439
25	40	45	60	0.868	163.618
30	45	50	65	0.971	183.0335
35	50	55	70	0.997	187.9345
40	55	60	75	2.2	414.7
45	60	65	80	0.925	174.3625
50	65	70	85	1.2	226.2
55	70	75	90	1.1	207.35
60	75	80	95	1.4	263.9
65	80	85	100	1.6	301.6
70	85	90	105	0.765	144.2025

75	90	95	110	1.1	207.35
80	95	100	115	1.2	226.2
85	100	105	120	1.2	226.2
90	105	110	125	0.778	146.653
95	110	115	130	0.772	145.522
100	115	120	135	0.99	186.615
105	120	125	140	0.99	186.615
110	125	130	145	0.773	145.7105
115	130	135	150	0.836	157.586
Electrode Location a = 5, n = 4, k = 314.16					
C1	P1	P2	C2	R (Ω)	ρ (Ωm)
0	20	25	45	0.384	120.6374
5	25	30	50	0.413	129.7481
10	30	35	55	0.419	131.633
15	35	40	60	0.435	136.6596
20	40	45	65	0.484	152.0534
25	45	50	70	0.486	152.6818
30	50	55	75	0.517	162.4207

35	55	60	80	0.508	159.5933
40	60	65	85	0.54	169.6464
45	65	70	90	0.673	211.4297
50	70	75	95	0.553	173.7305
55	75	80	100	0.836	262.6378
60	80	85	105	0.602	189.1243
65	85	90	110	0.605	190.0668
70	90	95	115	0.64	201.0624
75	95	100	120	0.567	178.1287
80	100	105	125	0.133	41.78328
85	105	110	130	0.564	177.1862
90	110	115	135	0.482	151.4251
95	115	120	140	0.539	169.3322
100	120	125	145	0.622	195.4075
105	125	130	150	0.499	156.7658
Electrode Location a = 5, n = 5, k = 471.24					
C1	P1	P2	C2	R (Ω)	ρ (Ωm)
0	25	30	55	0.226	106.5002

5	30	35	60	0.233	109.7989
10	35	40	65	0.199	93.77676
15	40	45	70	0.253	119.2237
20	45	50	75	0.277	130.5335
25	50	55	80	0.291	137.1308
30	55	60	85	0.282	132.8897
35	60	65	90	0.381	179.5424
40	65	70	95	0.29	136.6596
45	70	75	100	0.456	214.8854
50	75	80	105	0.336	158.3366
55	80	85	110	0.329	155.038
60	85	90	115	0.315	148.4406
65	90	95	120	0.395	186.1398
70	95	100	125	0.486	229.0226
75	100	105	130	0.103	48.53772
80	105	110	135	0.19	89.5356
85	110	115	140	0.103	48.53772
90	115	120	145	0.25	117.81

95	120	125	150	0.302	142.3145
Electrode Location a = 5, n = 6, k = 659.73					
C1	P1	P2	C2	R (Ω)	ρ (Ωm)
0	30	35	65	0.124	81.80652
5	35	40	70	0.142	93.68166
10	40	45	75	0.151	99.61923
15	45	50	80	0.159	104.8971
20	50	55	85	0.174	114.793
25	55	60	90	0.163	107.536
30	60	65	95	0.188	124.0292
35	65	70	100	0.169	111.4944
40	70	75	105	0.216	142.5017
45	75	80	110	0.245	161.6339
50	80	85	115	0.191	126.0084
55	85	90	120	0.204	134.5849
60	90	95	125	0.207	136.5641
65	95	100	130	0.079	52.11867
70	100	105	135	0.122	80.48706

75	105	110	140	0.101	66.63273
80	110	115	145	0.093	61.35489
85	115	120	150	0.115	75.86895
Electrode Location a = 5, n = 7, k = 879.65					
C1	P1	P2	C2	R (Ω)	ρ (Ωm)
0	35	40	75	0.173	152.1795
5	40	45	80	0.071	62.45515
10	45	50	85	0.086	75.6499
15	50	55	90	0.134	117.8731
20	55	60	95	0.094	82.6871
25	60	65	100	0.102	89.7243
30	65	70	105	0.129	113.4749
35	70	75	110	0.15	131.9475
40	75	80	115	0.156	137.2254
45	80	85	120	0.126	110.8359
50	85	90	125	0.122	107.3173
55	90	95	130	0.113	99.40045
60	95	100	135	0.076	66.8534

65	100	105	140	0.131	115.2342
70	105	110	145	0.179	157.4574
75	110	115	150	0.066	58.0569
Electrode Location a = 5, n = 8, k = 1131.12					
C1	P1	P2	C2	R (Ω)	ρ (Ωm)
0	40	45	85	0.031	35.06472
5	45	50	90	0.061	68.99832
10	50	55	95	0.078	88.22736
15	55	60	100	0.07	79.1784
20	60	65	105	0.086	97.27632
25	65	70	110	0.037	41.85144
30	70	75	115	0.089	100.6697
35	75	80	120	0.101	114.2431
40	80	85	125	0.068	76.91616
45	85	90	130	0.08	90.4896
50	90	95	135	0.087	98.40744
55	95	100	140	0.063	71.26056
60	100	105	145	0.077	87.09624

65	105	110	150	0.067	75.78504

2D ELECTRICAL RESISTIVITY

IMAGING FIELD DATA

REPORT SHEET

	ARRAY TYPE	**WENNER-SCHLUMBERGER**	**DATE**	**15/06/2018**	
	INSTRUMENT USED	PASI 16GL-N	STATE	ONDO	
	LOCATION	Traverse 2	L.G.A	ODIGBO	
	LINE NUMBER	Tr 2			
	OBSERVER	Funmi			

LAT. 06˚59'58'' LONG. 004˚49'27.5'' Elev. 15.0m

Electrode Location a = 5, n = 1, k = 31.42

C1	P1	P2	C2	R (Ω)	ρ (Ωm)
0	5	10	15	6.2	194.804

5	10	15	20	6.7	210.514
10	15	20	25	7.5	235.65
15	20	25	30	8	251.36
20	25	30	35	9.2	289.064
25	30	35	40	9.2	289.064
30	35	40	45	9.4	295.348
35	40	45	50	8.8	276.496
40	45	50	55	8.7	273.354
45	50	55	60	8.8	276.496
50	55	60	65	8.4	263.928
55	60	65	70	10	314.2
60	65	70	75	8.7	273.354
65	70	75	80	9.1	285.922
70	75	80	85	8	251.36
75	80	85	90	7.4	232.508
80	85	90	95	6.6	207.372
85	90	95	100	6.6	207.372
90	95	100	105	6.4	201.088

95	100	105	110	6.4	201.088
100	105	110	115	6.6	207.372
105	110	115	120	6.3	197.946
110	115	120	125	6.3	197.946
115	120	125	130	6.7	210.514
120	125	130	135	7.1	223.082
125	130	135	140	5.8	182.236
130	135	140	145	6.6	207.372
135	140	145	150	5.8	182.236
Electrode Location a = 5, n = 2, k = 94.25					
C1	P1	P2	C2	R (Ω)	ρ (Ωm)
0	10	15	25	2	188.5
5	15	20	30	2.1	197.925
10	20	25	35	2.2	207.35
15	25	30	40	2.4	226.2
20	30	35	45	2.6	245.05
25	35	40	50	2.7	254.475
30	40	45	55	2.7	254.475

35	45	50	60	2.7	254.475
40	50	55	65	2.9	273.325
45	55	60	70	2.5	235.625
50	60	65	75	3.2	301.6
55	65	70	80	2.8	263.9
60	70	75	85	2.9	273.325
65	75	80	90	3	282.75
70	80	85	95	2.7	254.475
75	85	90	100	2.4	226.2
80	90	95	105	2.3	216.775
85	95	100	110	2.4	226.2
90	100	105	115	2.2	207.35
95	105	110	120	1.9	179.075
100	110	115	125	2.2	207.35
105	115	120	130	2.3	216.775
110	120	125	135	3	282.75
115	125	130	140	1.8	169.65
120	130	135	145	2	188.5

125	135	140	150	2.2	207.35
Electrode Location a = 5, n = 3, k = 188.50					
C1	P1	P2	C2	R (Ω)	ρ (Ωm)
0	15	20	35	0.899	169.4615
5	20	25	40	0.917	172.8545
10	25	30	45	1.1	207.35
15	30	35	50	1.1	207.35
20	35	40	55	1.2	226.2
25	40	45	60	1.4	263.9
30	45	50	65	1.5	282.75
35	50	55	70	1.1	207.35
40	55	60	75	1.1	207.35
45	60	65	80	1.5	282.75
50	65	70	85	1.3	245.05
55	70	75	90	1.4	263.9
60	75	80	95	1.3	245.05
65	80	85	100	1.3	245.05
70	85	90	105	1.1	207.35

75	90	95	110	1.2	226.2
80	95	100	115	0.983	185.2955
85	100	105	120	0.698	131.573
90	105	110	125	1	188.5
95	110	115	130	0.998	188.123
100	115	120	135	1.3	245.05
105	120	125	140	1.1	207.35
110	125	130	145	0.659	124.2215
115	130	135	150	0.98	184.73
Electrode Location a = 5, n = 4, k = 314.16					
C1	P1	P2	C2	R (Ω)	ρ (Ωm)
0	20	25	45	0.461	144.8278
5	25	30	50	0.462	145.1419
10	30	35	55	0.622	195.4075
15	35	40	60	0.622	195.4075
20	40	45	65	0.618	194.1509
25	45	50	70	0.58	182.2128
30	50	55	75	0.635	199.4916

35	55	60	80	0.59	185.3544
40	60	65	85	0.724	227.4518
45	65	70	90	0.695	218.3412
50	70	75	95	0.745	234.0492
55	75	80	100	0.707	222.1111
60	80	85	105	0.624	196.0358
65	85	90	110	0.594	186.611
70	90	95	115	0.665	208.9164
75	95	100	120	0.785	246.6156
80	100	105	125	0.606	190.381
85	105	110	130	0.542	170.2747
90	110	115	135	0.56	175.9296
95	115	120	140	0.53	166.5048
100	120	125	145	0.563	176.8721
105	125	130	150	0.52	163.3632
Electrode Location a = 5, n = 5, k = 471.24					
C1	P1	P2	C2	R (Ω)	ρ (Ωm)
0	25	30	55	0.258	121.5799

5	30	35	60	0.262	123.4649
10	35	40	65	0.216	101.7878
15	40	45	70	0.252	118.7525
20	45	50	75	0.211	99.43164
25	50	55	80	0.262	123.4649
30	55	60	85	0.314	147.9694
35	60	65	90	0.408	192.2659
40	65	70	95	0.391	184.2548
45	70	75	100	0.405	190.8522
50	75	80	105	0.398	187.5535
55	80	85	110	0.342	161.1641
60	85	90	115	0.388	182.8411
65	90	95	120	0.391	184.2548
70	95	100	125	0.351	165.4052
75	100	105	130	0.347	163.5203
80	105	110	135	0.307	144.6707
85	110	115	140	0.309	145.6132
90	115	120	145	0.211	99.43164

95	120	125	150	0.288	135.7171
Electrode Location a = 5, n = 6, k = 659.73					
C1	P1	P2	C2	R (Ω)	ρ (Ωm)
0	30	35	65	0.268	176.8076
5	35	40	70	0.28	184.7244
10	40	45	75	0.257	169.5506
15	45	50	80	0.272	179.4466
20	50	55	85	0.268	176.8076
25	55	60	90	0.199	131.2863
30	60	65	95	0.251	165.5922
35	65	70	100	0.237	156.356
40	70	75	105	0.221	145.8003
45	75	80	110	0.263	173.509
50	80	85	115	0.265	174.8285
55	85	90	120	0.215	141.842
60	90	95	125	0.193	127.3279
65	95	100	130	0.208	137.2238
70	100	105	135	0.228	150.4184

75	105	110	140	0.208	137.2238
80	110	115	145	0.216	142.5017
85	115	120	150	0.348	229.586
Electrode Location a = 5, n = 7, k = 879.65					
C1	P1	P2	C2	R (Ω)	ρ (Ωm)
0	35	40	75	0.107	94.12255
5	40	45	80	0.103	90.60395
10	45	50	85	0.088	77.4092
15	50	55	90	0.094	82.6871
20	55	60	95	0.086	75.6499
25	60	65	100	0.115	101.1598
30	65	70	105	0.135	118.7528
35	70	75	110	0.142	124.9103
40	75	80	115	0.172	151.2998
45	80	85	120	0.065	57.17725
50	85	90	125	0.121	106.4377
55	90	95	130	0.112	98.5208
60	95	100	135	0.072	63.3348

65	100	105	140	0.122	107.3173
70	105	110	145	0.108	95.0022
75	110	115	150	0.116	102.0394
Electrode Location a = 5, n = 8, k = 1131.12					
C1	P1	P2	C2	R (Ω)	ρ (Ωm)
0	40	45	85	0.073	82.57176
5	45	50	90	0.06	67.8672
10	50	55	95	0.083	93.88296
15	55	60	100	0.077	87.09624
20	60	65	105	0.061	68.99832
25	65	70	110	0.077	87.09624
30	70	75	115	0.08	90.4896
35	75	80	120	0.104	117.6365
40	80	85	125	0.096	108.5875
45	85	90	130	0.077	87.09624
50	90	95	135	0.053	59.94936
55	95	100	140	0.104	117.6365
60	100	105	145	0.058	65.60496

65	105	110	150	0.064	72.39168

2D ELECTRICAL RESISTIVITY

IMAGING FIELD DATA

REPORT SHEET

	ARRAY TYPE	**WENNER-SCHLUMBERGER**	**DATE**	**15/06/2018**		
	INSTRUMENT USED	PASI 16GL-N	STATE	ONDO		
	LOCATION	Traverse 3	L.G.A	ODIGBO		
	LINE NUMBER	Tr 3				
	OBSERVER	Funmi				

LAT. 06˚59'42'' LONG. 004˚49'30.8'' Elev. 14.6m

Electrode Location a = 5, n = 1, k = 31.42

C1	P1	P2	C2	R (Ω)	ρ (Ωm)

0	5	10	15	13.7	430.454
5	10	15	20	15.8	496.436
10	15	20	25	17.2	540.424
15	20	25	30	15.9	499.578
20	25	30	35	17.1	537.282
25	30	35	40	14.7	461.874
30	35	40	45	16.8	527.856
35	40	45	50	16.2	509.004
40	45	50	55	16.7	524.714
45	50	55	60	16.9	530.998
50	55	60	65	15.8	496.436
55	60	65	70	15.4	483.868
60	65	70	75	12.3	386.466
65	70	75	80	8.9	279.638
70	75	80	85	7.6	238.792
75	80	85	90	5.2	163.384
80	85	90	95	3.8	119.396
85	90	95	100	4.7	147.674

90	95	100	105	4.7	147.674
95	100	105	110	4.4	138.248
100	105	110	115	4.9	153.958
105	110	115	120	3.9	122.538
110	115	120	125	3	94.26
115	120	125	130	2.8	87.976
120	125	130	135	2.1	65.982
125	130	135	140	2.4	75.408
130	135	140	145	1.6	50.272
135	140	145	150	1.3	40.846
Electrode Location a = 5, n = 2, k = 94.25					
C1	P1	P2	C2	R (Ω)	ρ (Ωm)
0	10	15	25	3.5	329.875
5	15	20	30	4.1	386.425
10	20	25	35	4.1	386.425
15	25	30	40	4.1	386.425
20	30	35	45	3.7	348.725
25	35	40	50	4.2	395.85

30	40	45	55	4.2	395.85
35	45	50	60	3.7	348.725
40	50	55	65	4	377
45	55	60	70	3.7	348.725
50	60	65	75	8.5	801.125
55	65	70	80	2.8	263.9
60	70	75	85	2.9	273.325
65	75	80	90	2.7	254.475
70	80	85	95	1.8	169.65
75	85	90	100	1.3	122.525
80	90	95	105	16	1508
85	95	100	110	1.5	141.375
90	100	105	115	1.3	122.525
95	105	110	120	1.6	150.8
100	110	115	125	1.7	160.225
105	115	120	130	1.1	103.675
110	120	125	135	1.1	103.675
115	125	130	140	0.876	82.563

120	130	135	145	0.938	88.4065
125	135	140	150	0.702	66.1635
Electrode Location a = 5, n = 3, k = 188.50					
C1	P1	P2	C2	R (Ω)	ρ (Ωm)
0	15	20	35	1.6	301.6
5	20	25	40	1.6	301.6
10	25	30	45	1.1	207.35
15	30	35	50	1.8	339.3
20	35	40	55	1.6	301.6
25	40	45	60	1.5	282.75
30	45	50	65	1.4	263.9
35	50	55	70	1.5	282.75
40	55	60	75	1.4	263.9
45	60	65	80	1.3	245.05
50	65	70	85	1	188.5
55	70	75	90	0.991	186.8035
60	75	80	95	1.1	207.35
65	80	85	100	0.796	150.046

70	85	90	105	0.582	109.707
75	90	95	110	0.661	124.5985
80	95	100	115	0.646	121.771
85	100	105	120	0.596	112.346
90	105	110	125	0.639	120.4515
95	110	115	130	0.547	103.1095
100	115	120	135	0.472	88.972
105	120	125	140	0.453	85.3905
110	125	130	145	0.38	71.63
115	130	135	150	0.48	90.48
Electrode Location a = 5, n = 4, k = 314.16					
C1	P1	P2	C2	R (Ω)	ρ (Ωm)
0	20	25	45	0.727	228.3943
5	25	30	50	0.772	242.5315
10	30	35	55	0.675	212.058
15	35	40	60	0.736	231.2218
20	40	45	65	0.606	190.381
25	45	50	70	0.606	190.381

30	50	55	75	0.681	213.943
35	55	60	80	0.608	191.0093
40	60	65	85	0.603	189.4385
45	65	70	90	0.527	165.5623
50	70	75	95	0.448	140.7437
55	75	80	100	0.411	129.1198
60	80	85	105	0.079	24.81864
65	85	90	110	0.268	84.19488
70	90	95	115	0.311	97.70376
75	95	100	120	0.415	130.3764
80	100	105	125	0.306	96.13296
85	105	110	130	0.329	103.3586
90	110	115	135	0.252	79.16832
95	115	120	140	0.216	67.85856
100	120	125	145	0.205	64.4028
105	125	130	150	0.191	60.00456
Electrode Location a = 5, n = 5, k = 471.24					
C1	P1	P2	C2	R (Ω)	ρ (Ωm)

0	25	30	55	0.367	172.9451
5	30	35	60	0.342	161.1641
10	35	40	65	0.316	148.9118
15	40	45	70	0.322	151.7393
20	45	50	75	0.312	147.0269
25	50	55	80	0.274	129.1198
30	55	60	85	0.256	120.6374
35	60	65	90	0.198	93.30552
40	65	70	95	0.188	88.59312
45	70	75	100	0.159	74.92716
50	75	80	105	0.19	89.5356
55	80	85	110	0.109	51.36516
60	85	90	115	0.106	49.95144
65	90	95	120	0.113	53.25012
70	95	100	125	0.116	54.66384
75	100	105	130	0.122	57.49128
80	105	110	135	0.135	63.6174
85	110	115	140	0.111	52.30764

90	115	120	145	0.095	44.7678
95	120	125	150	0.085	40.0554
Electrode Location a = 5, n = 6, k = 659.73					
C1	P1	P2	C2	R (Ω)	ρ (Ωm)
0	30	35	65	0.178	117.4319
5	35	40	70	0.106	69.93138
10	40	45	75	0.122	80.48706
15	45	50	80	0.19	125.3487
20	50	55	85	0.058	38.26434
25	55	60	90	0.259	170.8701
30	60	65	95	0.203	133.9252
35	65	70	100	0.104	68.61192
40	70	75	105	0.066	43.54218
45	75	80	110	0.123	81.14679
50	80	85	115	0.046	30.34758
55	85	90	120	0.06	39.5838
60	90	95	125	0.053	34.96569
65	95	100	130	0.068	44.86164

70	100	105	135	0.065	42.88245
75	105	110	140	0.081	53.43813
80	110	115	145	0.063	41.56299
85	115	120	150	0.057	37.60461
Electrode Location a = 5, n = 7, k = 879.65					
C1	P1	P2	C2	R (Ω)	ρ (Ωm)
0	35	40	75	0.069	60.69585
5	40	45	80	0.052	45.7418
10	45	50	85	0.041	36.06565
15	50	55	90	0.097	85.32605
20	55	60	95	0.069	60.69585
25	60	65	100	0.017	14.95405
30	65	70	105	0.031	27.26915
35	70	75	110	0.07	61.5755
40	75	80	115	0.0074	6.50941
45	80	85	120	0.032	28.1488
50	85	90	125	0.035	30.78775
55	90	95	130	0.041	36.06565

60	95	100	135	0.03	26.3895
65	100	105	140	0.041	36.06565
70	105	110	145	0.045	39.58425
75	110	115	150	0.041	36.06565
Electrode Location a = 5, n = 8, k = 1131.12					
C1	P1	P2	C2	R (Ω)	ρ (Ωm)
0	40	45	85	0.04	45.2448
5	45	50	90	0.055	62.2116
10	50	55	95	0.054	61.08048
15	55	60	100	0.064	72.39168
20	60	65	105	0.052	58.81824
25	65	70	110	0.043	48.63816
30	70	75	115	0.017	19.22904
35	75	80	120	0.073	82.57176
40	80	85	125	0.022	24.88464
45	85	90	130	0.025	28.278
50	90	95	135	0.022	24.88464
55	95	100	140	0.027	30.54024

60	100	105	145	0.014	15.83568
65	105	110	150	0.029	32.80248

2D ELECTRICAL RESISTIVITY

IMAGING FIELD DATA

REPORT SHEET

	ARRAY TYPE	**WENNER-SCHLUMBERGER**	**DATE**	**15/06/2018**		
	INSTRUMENT USED	PASI 16GL-N	STATE	ONDO		
	LOCATION	Traverse 4	L.G.A	ODIGBO		
	LINE NUMBER	Tr 4				
	OBSERVER	Funmi				

LAT. 06˚59'10'' LONG. 004˚49'29.7'' Elev. 13.5m

Electrode Location a = 5, n = 1, k = 31.42

C1	P1	P2	C2	R (Ω)	ρ (Ωm)

0	5	10	15	11.8	370.756
5	10	15	20	14.9	468.158
10	15	20	25	12	377.04
15	20	25	30	12.1	380.182
20	25	30	35	12.4	389.608
25	30	35	40	11	345.62
30	35	40	45	10.4	326.768
35	40	45	50	10.4	326.768
40	45	50	55	10.8	339.336
45	50	55	60	11.7	367.614
50	55	60	65	11.8	370.756
55	60	65	70	12	377.04
60	65	70	75	11.6	364.472
65	70	75	80	13.5	424.17
70	75	80	85	12	377.04
75	80	85	90	12	377.04
80	85	90	95	12.2	383.324
85	90	95	100	11.8	370.756

90	95	100	105	11.1	348.762
95	100	105	110	10.9	342.478
100	105	110	115	10.9	342.478
105	110	115	120	12	377.04
110	115	120	125	11.4	358.188
115	120	125	130	11.4	358.188
120	125	130	135	10.8	339.336
125	130	135	140	9.9	311.058
130	135	140	145	10.4	326.768
135	140	145	150	10.4	326.768
Electrode Location a = 5, n = 2, k = 94.25					
C1	P1	P2	C2	R (Ω)	ρ (Ωm)
0	10	15	25	4.3	405.275
5	15	20	30	3.5	329.875
10	20	25	35	3.2	301.6
15	25	30	40	3.7	348.725
20	30	35	45	3.7	348.725
25	35	40	50	4	377

30	40	45	55	3.8	358.15
35	45	50	60	4	377
40	50	55	65	4	377
45	55	60	70	3.7	348.725
50	60	65	75	3.7	348.725
55	65	70	80	3.3	311.025
60	70	75	85	3.5	329.875
65	75	80	90	3.8	358.15
70	80	85	95	2.9	273.325
75	85	90	100	2.9	273.325
80	90	95	105	2.9	273.325
85	95	100	110	2.8	263.9
90	100	105	115	2.4	226.2
95	105	110	120	2.7	254.475
100	110	115	125	3.1	292.175
105	115	120	130	1.8	169.65
110	120	125	135	2.2	207.35
115	125	130	140	3	282.75

120	130	135	145	2.4	226.2
125	135	140	150	2.3	216.775
Electrode Location a = 5, n = 3, k = 188.50					
C1	P1	P2	C2	R (Ω)	ρ (Ωm)
0	15	20	35	1.4	263.9
5	20	25	40	1.2	226.2
10	25	30	45	1.3	245.05
15	30	35	50	1.2	226.2
20	35	40	55	1.1	207.35
25	40	45	60	1.1	207.35
30	45	50	65	1.1	207.35
35	50	55	70	1.1	207.35
40	55	60	75	1.1	207.35
45	60	65	80	1.1	207.35
50	65	70	85	1	188.5
55	70	75	90	1.4	263.9
60	75	80	95	1.4	263.9
65	80	85	100	1.3	245.05

70	85	90	105	1.2	226.2
75	90	95	110	1.2	226.2
80	95	100	115	1.1	207.35
85	100	105	120	1	188.5
90	105	110	125	0.88	165.88
95	110	115	130	0.89	167.765
100	115	120	135	0.54	101.79
105	120	125	140	0.763	143.8255
110	125	130	145	0.943	177.7555
115	130	135	150	0.867	163.4295
Electrode Location a = 5, n = 4, k = 314.16					
C1	P1	P2	C2	R (Ω)	ρ (Ωm)
0	20	25	45	0.511	160.5358
5	25	30	50	0.473	148.5977
10	30	35	55	0.497	156.1375
15	35	40	60	0.344	108.071
20	40	45	65	0.461	144.8278
25	45	50	70	0.421	132.2614

30	50	55	75	0.562	176.5579
35	55	60	80	0.455	142.9428
40	60	65	85	0.389	122.2082
45	65	70	90	0.524	164.6198
50	70	75	95	0.563	176.8721
55	75	80	100	0.563	176.8721
60	80	85	105	0.403	126.6065
65	85	90	110	0.329	103.3586
70	90	95	115	0.3	94.248
75	95	100	120	0.327	102.7303
80	100	105	125	0.375	117.81
85	105	110	130	0.355	111.5268
90	110	115	135	1	314.16
95	115	120	140	0.411	129.1198
100	120	125	145	0.334	104.9294
105	125	130	150	0.374	117.4958
Electrode Location a = 5, n = 5, k = 471.24					
C1	P1	P2	C2	R (Ω)	ρ (Ωm)

0	25	30	55	0.173	81.52452
5	30	35	60	0.252	118.7525
10	35	40	65	0.171	80.58204
15	40	45	70	0.195	91.8918
20	45	50	75	0.206	97.07544
25	50	55	80	0.117	55.13508
30	55	60	85	1.44	678.5856
35	60	65	90	0.151	71.15724
40	65	70	95	0.255	120.1662
45	70	75	100	0.191	90.00684
50	75	80	105	0.171	80.58204
55	80	85	110	0.162	76.34088
60	85	90	115	0.162	76.34088
65	90	95	120	0.117	55.13508
70	95	100	125	0.171	80.58204
75	100	105	130	0.151	71.15724
80	105	110	135	0.162	76.34088
85	110	115	140	0.142	66.91608

90	115	120	145	0.09	42.4116
95	120	125	150	0.109	51.36516
Electrode Location a = 5, n = 6, k = 659.73					
C1	P1	P2	C2	R (Ω)	ρ (Ωm)
0	30	35	65	0.266	175.4882
5	35	40	70	0.072	47.50056
10	40	45	75	0.073	48.16029
15	45	50	80	0.091	60.03543
20	50	55	85	0.086	56.73678
25	55	60	90	0.061	40.24353
30	60	65	95	0.061	40.24353
35	65	70	100	0.072	47.50056
40	70	75	105	0.088	58.05624
45	75	80	110	0.091	60.03543
50	80	85	115	0.097	63.99381
55	85	90	120	0.096	63.33408
60	90	95	125	0.121	79.82733
65	95	100	130	0.056	36.94488

70	100	105	135	0.029	19.13217
75	105	110	140	0.056	36.94488
80	110	115	145	0.121	79.82733
85	115	120	150	0.088	58.05624
Electrode Location a = 5, n = 7, k = 879.65					
C1	P1	P2	C2	R (Ω)	ρ (Ωm)
0	35	40	75	0.028	24.6302
5	40	45	80	0.027	23.75055
10	45	50	85	0.021	18.47265
15	50	55	90	0.012	10.5558
20	55	60	95	0.044	38.7046
25	60	65	100	0.028	24.6302
30	65	70	105	0.03	26.3895
35	70	75	110	0.047	41.34355
40	75	80	115	0.033	29.02845
45	80	85	120	0.077	67.73305
50	85	90	125	0.044	38.7046
55	90	95	130	0.044	38.7046

60	95	100	135	0.062	54.5383
65	100	105	140	0.021	18.47265
70	105	110	145	0.027	23.75055
75	110	115	150	0.128	112.5952
Electrode Location a = 5, n = 8, k = 1131.12					
C1	P1	P2	C2	R (Ω)	ρ (Ωm)
0	40	45	85	0.021	23.75352
5	45	50	90	0.046	52.03152
10	50	55	95	0.032	36.19584
15	55	60	100	0.032	36.19584
20	60	65	105	0.028	31.67136
25	65	70	110	0.028	31.67136
30	70	75	115	0.038	42.98256
35	75	80	120	0.041	46.37592
40	80	85	125	0.04	45.2448
45	85	90	130	0.06	67.8672
50	90	95	135	0.099	111.9809
55	95	100	140	0.012	13.57344

60	100	105	145	0.0088	9.953856
65	105	110	150	0.015	16.9668

2D ELECTRICAL RESISTIVITY

IMAGING FIELD DATA

REPORT SHEET

	ARRAY TYPE	**WENNER-SCHLUMBERGER**	**DATE**	**15/06/2018**		
	INSTRUMENT USED	PASI 16GL-N	STATE	ONDO		
	LOCATION	Traverse 5	L.G.A	ODIGBO		
	LINE NUMBER	Tr 5				
	OBSERVER	Funmi				

LAT. 06˚59'37'' LONG. 004˚49'26.8'' Elev. 13.7m

Electrode Location a = 5, n = 1, k = 31.42

C1	P1	P2	C2	R (Ω)	ρ (Ωm)

0	5	10	15	7	219.94
5	10	15	20	12	377.04
10	15	20	25	11.4	358.188
15	20	25	30	9.5	298.49
20	25	30	35	11.6	364.472
25	30	35	40	11.7	367.614
30	35	40	45	11.8	370.756
35	40	45	50	8.7	273.354
40	45	50	55	12.2	383.324
45	50	55	60	6.6	207.372
50	55	60	65	10.9	342.478
55	60	65	70	11.2	351.904
60	65	70	75	10.6	333.052
65	70	75	80	11	345.62
70	75	80	85	13.6	427.312
75	80	85	90	13.1	411.602
80	85	90	95	13.2	414.744
85	90	95	100	14.6	458.732

90	95	100	105	14.6	458.732
95	100	105	110	12	377.04
100	105	110	115	12	377.04
105	110	115	120	14.2	446.164
110	115	120	125	11.2	351.904
115	120	125	130	11.8	370.756
120	125	130	135	13.8	433.596
125	130	135	140	12.4	389.608
130	135	140	145	11.2	351.904
135	140	145	150	15.2	477.584
Electrode Location a = 5, n = 2, k = 94.25					
C1	P1	P2	C2	R (Ω)	ρ (Ωm)
0	10	15	25	3.9	367.575
5	15	20	30	2.7	254.475
10	20	25	35	3.6	339.3
15	25	30	40	3.7	348.725
20	30	35	45	3.4	320.45
25	35	40	50	3.7	348.725

30	40	45	55	3.7	348.725
35	45	50	60	4.2	395.85
40	50	55	65	4	377
45	55	60	70	3.8	358.15
50	60	65	75	3.4	320.45
55	65	70	80	3.6	339.3
60	70	75	85	4.1	386.425
65	75	80	90	3.1	292.175
70	80	85	95	3.2	301.6
75	85	90	100	3.3	311.025
80	90	95	105	3.3	311.025
85	95	100	110	3.2	301.6
90	100	105	115	2.8	263.9
95	105	110	120	3.4	320.45
100	110	115	125	3.3	311.025
105	115	120	130	2.7	254.475
110	120	125	135	2.7	254.475
115	125	130	140	3.4	320.45

120	130	135	145	2.5	235.625
125	135	140	150	2.3	216.775
Electrode Location a = 5, n = 3, k = 188.50					
C1	P1	P2	C2	R (Ω)	ρ (Ωm)
0	15	20	35	1.9	358.15
5	20	25	40	1.4	263.9
10	25	30	45	1.2	226.2
15	30	35	50	1.4	263.9
20	35	40	55	1.4	263.9
25	40	45	60	1.2	226.2
30	45	50	65	0.8	150.8
35	50	55	70	1.1	207.35
40	55	60	75	1.1	207.35
45	60	65	80	0.966	182.091
50	65	70	85	1.2	226.2
55	70	75	90	1.1	207.35
60	75	80	95	0.84	158.34
65	80	85	100	1	188.5

70	85	90	105	1.1	207.35
75	90	95	110	1.1	207.35
80	95	100	115	1.1	207.35
85	100	105	120	1.2	226.2
90	105	110	125	1	188.5
95	110	115	130	1.2	226.2
100	115	120	135	1.1	207.35
105	120	125	140	1	188.5
110	125	130	145	1	188.5
115	130	135	150	0.974	183.599
Electrode Location a = 5, n = 4, k = 314.16					
C1	P1	P2	C2	R (Ω)	ρ (Ωm)
0	20	25	45	0.586	184.0978
5	25	30	50	1.9	596.904
10	30	35	55	0.607	190.6951
15	35	40	60	0.411	129.1198
20	40	45	65	0.403	126.6065
25	45	50	70	0.482	151.4251

30	50	55	75	0.411	129.1198
35	55	60	80	0.386	121.2658
40	60	65	85	0.521	163.6774
45	65	70	90	0.411	129.1198
50	70	75	95	0.411	129.1198
55	75	80	100	0.448	140.7437
60	80	85	105	0.407	127.8631
65	85	90	110	0.302	94.87632
70	90	95	115	0.249	78.22584
75	95	100	120	0.325	102.102
80	100	105	125	0.265	83.2524
85	105	110	130	0.341	107.1286
90	110	115	135	0.329	103.3586
95	115	120	140	0.271	85.13736
100	120	125	145	0.375	117.81
105	125	130	150	0.45	141.372
Electrode Location a = 5, n = 5, k = 471.24					
C1	P1	P2	C2	R (Ω)	ρ (Ωm)

0	25	30	55	0.218	102.7303
5	30	35	60	0.314	147.9694
10	35	40	65	0.213	100.3741
15	40	45	70	0.175	82.467
20	45	50	75	0.135	63.6174
25	50	55	80	0.186	87.65064
30	55	60	85	0.165	77.7546
35	60	65	90	0.137	64.55988
40	65	70	95	0.182	85.76568
45	70	75	100	0.161	75.86964
50	75	80	105	0.171	80.58204
55	80	85	110	0.142	66.91608
60	85	90	115	0.112	52.77888
65	90	95	120	0.144	67.85856
70	95	100	125	0.155	73.0422
75	100	105	130	0.155	73.0422
80	105	110	135	0.162	76.34088
85	110	115	140	0.15	70.686

90	115	120	145	0.149	70.21476
95	120	125	150	0.159	74.92716
Electrode Location a = 5, n = 6, k = 659.73					
C1	P1	P2	C2	R (Ω)	ρ (Ωm)
0	30	35	65	0.19	125.3487
5	35	40	70	0.261	172.1895
10	40	45	75	0.067	44.20191
15	45	50	80	0.077	50.79921
20	50	55	85	0.068	44.86164
25	55	60	90	0.088	58.05624
30	60	65	95	0.098	64.65354
35	65	70	100	0.084	55.41732
40	70	75	105	0.067	44.20191
45	75	80	110	0.077	50.79921
50	80	85	115	0.071	46.84083
55	85	90	120	0.074	48.82002
60	90	95	125	0.071	46.84083
65	95	100	130	0.065	42.88245

70	100	105	135	0.06	39.5838
75	105	110	140	0.077	50.79921
80	110	115	145	0.066	43.54218
85	115	120	150	0.067	44.20191
Electrode Location a = 5, n = 7, k = 879.65					
C1	P1	P2	C2	R (Ω)	ρ (Ωm)
0	35	40	75	0.027	23.75055
5	40	45	80	0.051	44.86215
10	45	50	85	0.079	69.49235
15	50	55	90	0.019	16.71335
20	55	60	95	0.05	43.9825
25	60	65	100	0.072	63.3348
30	65	70	105	0.025	21.99125
35	70	75	110	0.042	36.9453
40	75	80	115	0.029	25.50985
45	80	85	120	0.027	23.75055
50	85	90	125	0.028	24.6302
55	90	95	130	0.027	23.75055

60	95	100	135	0.025	21.99125
65	100	105	140	0.028	24.6302
70	105	110	145	0.028	24.6302
75	110	115	150	0.042	36.9453
Electrode Location a = 5, n = 8, k = 1131.12					
C1	P1	P2	C2	R (Ω)	ρ (Ωm)
0	40	45	85	0.036	40.72032
5	45	50	90	0.059	66.73608
10	50	55	95	0.016	18.09792
15	55	60	100	0.016	18.09792
20	60	65	105	0.053	59.94936
25	65	70	110	0.018	20.36016
30	70	75	115	0.025	28.278
35	75	80	120	0.012	13.57344
40	80	85	125	0.016	18.09792
45	85	90	130	0.02	22.6224
50	90	95	135	0.028	31.67136
55	95	100	140	0.028	31.67136

60	100	105	145	0.018	20.36016
65	105	110	150	0.016	18.09792

PICTURES OF RESEARCH ACTIVITIES

Plate 1: Setting of equipment on the survey field.

Plate 2: Men and equipment on the survey field

Plate 3: Connecting up the wire to the current electrode

Plate 4: Recording the reading from the PASI Terremeter 16GL-N Model

Plate 5: Showing bitumen at the surface of the earth.

Plate 6: The Villager and I at the bitumen location

Plate 7: Standing at another well bitumen location

Plate 8: Taking of reading with the PASI Terremeter